Understanding the Molecular and Cellular Functions of Odd-Skipped Related 1 in Outflow Tract Development

Menglan Xiang

UNDERSTANDING THE MOLECULAR AND CELLULAR FUNCTIONS OF
ODD-SKIPPED RELATED 1 IN OUTFLOW TRACT DEVELOPMENT

by

Menglan Xiang

Bachelor of Science
Huazhong University of Science and Technology, 2013

A Dissertation

Submitted to the Graduate Faculty

of the

University of North Dakota

in partial fulfillment of the requirements

for the degree of

Doctor of Philosophy

Grand Forks, North Dakota

August
2019

This dissertation, submitted by Menglan Xiang in partial fulfillment of the requirements for the Degree of Doctor of Philosophy from the University of North Dakota, has been read by the Faculty Advisory Committee under whom the work has been done and is hereby approved.

_____
Ke K. Zhang, Chairperson

_____
Linglin Xie, Co-Chairperson

_____
Scott H. Garrett

_____
Colin K. Combs

_____
Wen-Chen Hu

This dissertation is being submitted by the appointed advisory committee as having met all of the requirements of the School of Graduate Studies at the University of North Dakota and is hereby approved.

_____
Christopher Nelson
Associate Dean of the School of Graduate Studies

4/24/19
_____
Date

PERMISSION

Title   Understanding the molecular and cellular functions of *Odd-skipped related 1* in outflow tract development

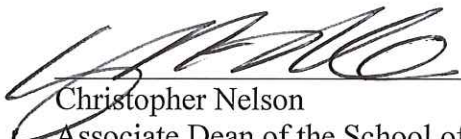Department   Biochemistry and Molecular Biology

Degree   Doctor of Philosophy

In presenting this dissertation in partial fulfillment of the requirements for a graduate degree from the University of North Dakota, I agree that the library of this University shall make it freely available for inspection. I further agree that permission for extensive copying for scholarly purposes may be granted by the professor who supervised my dissertation work or, in his absence, by the Chairperson of the department or the dean of the School of Graduate Studies. It is understood that any copying or publication or other use of this dissertation or part thereof for financial gain shall not be allowed without my written permission. It is also understood that due recognition shall be given to me and to the University of North Dakota in any scholarly use which may be made of any material in my dissertation.

Menglan Xiang
April 10, 2019

TABLE OF CONTENTS

LIST OF FIGURES

LIST OF TABLES

ACKNOWLEDGEMENTS

I would like to thank the various individuals who have made this work possible. First and foremost, I would like to thank my mentor Dr. Kurt Zhang for training me to become a better scientist. His knowledge has broadened my horizon in many areas and his encouragement of independent thinking has allowed me to search for and pursue my scientific interests. I especially could not be more appreciative of his support during difficult times. I am also grateful to my co-mentor, Dr. Linglin Xie for her guidance and motivation. Her encouragement on taking proactive attitude towards problem-solving has made a deep impact on me and her insight on my dissertation is greatly appreciated. I would like to thank Dr. Colin Combs, Dr. Scott Garrett and Dr. Don Sens for their advice and continued support throughout my graduate career and the completion of this work, and Dr. Wen-Chen Hu for his support and valuable feedback. I am grateful to Dr. Min Wu for reading and commenting on this work.

I would like to recognize my colleagues who have offered me guidance in my research. I would like to thank Jiangyuan Li, Henghui Cheng and Lin Liu for their contribution to this study. I am grateful to Yi Yang, Brent Weichel and Kaitlin Clarke for sharing their knowledge in bioinformatics and programming, Qiang Fu, Jielin Liu, and Jie Wu for their experience and assistance in the wet lab, and Peter Duea and Hokyi Lai for their input on data interpretation and algorithm design. I could not ask for more supportive teammates.

ABSTRACT

The cardiac outflow tract (OFT) is a transient conduit that connects the embryonic heart chambers to the vascular network. Transcription factor *Osr1* promotes the proliferation and cell cycle progression of second heart field (SHF), an essential cell population that contribute to the developing OFT. In this study, we investigated the role of *Osr1* in OFT development on cellular and molecular levels using a systems biology approach. We observed OFT rotation and elongation defects, as well as double-outlet right ventricle and overriding aorta as a result of SHF-specific deletion of *Osr1*. Using genetic inducible fate mapping, we showed that *Osr1*-expressing SHF cells migrate to the pulmonary trunk, however the cell lineage is ectopically distributed in the aorta, in addition to the pulmonary trunk, in *Osr1* knockout embryos. To understand the molecular mechanism that leads to the aberrant localization of the Osr1 cell lineage, we performed transcriptional profiling of the isolated Osr1$^+$ SHF population which showed *Osr1*-dependent expression of genes involved in tight junctions, cell adhesions, tissue connectivity and movement. Using *in vivo* and *in vitro* transcription factor binding assays, qRT-PCR as well as immunohistochemistry, we demonstrated that cell surface receptor *Pdgfrb* is a novel transcription target of *Osr1*. Furthermore, we showed that the *Drosophila Pdgfrb* homolog *Pvr* is required for the alignment and organization of *Odd*-expressing pericardial cells in the *Drosophila* larvae, demonstrating that the *Osr1-Pdgfrb* function is evolutionarily conserved.

The heart is derived from two progenitor pools: first heart field (FHF) and second heart field (SHF). The SHF is a heterogeneous population and consists of subregions anterior SHF (aSHF) and posterior SHF (pSHF). Although being adjacent to each other and of similar cell types, their cell fates significantly differ. In this study, we investigated how epigenetic mechanisms shape the transcriptional profiles of the cardiac progenitor populations. Using Assay for Transposase Accessible Chromatin with high-throughput sequencing, we found that tissue-specific accessible regions are enriched with corresponding cardiac transcription factor binding motifs. Using whole-genome bisulfite sequencing, we showed that hypermethylation correlates with inhibited gene expression for tissue-specific markers. Thus this study addressed a multi-tier regulatory mechanism for cardiac progenitor cells.

CHAPTER I

INTRODUCTION

1.1   The Mechanistic Basis of Cardiac Outflow Tract Development

Cardiac outflow tract (OFT) is the transient ventricular outlet that develops into the aorta and pulmonary trunk during embryogenesis. The formation of OFT is an intricate process that involves interactions among cell types originating from multiple sources. Aberrations of this process lead to OFT defects, which constitute approximately 30% of congenital heart diseases. This section reviews the major types of OFT defects and their implications, the cell lineages that contribute to OFT and the key molecular regulators that control OFT development in a spatiotemporal manner.

1.1.1   Major Types of Structural Outflow Tract Defects

Congenital heart diseases (CHDs) are structural anomalies of the heart or major blood vessels that arise during embryonic development. They affect 8 per 1000 live births in the United States, 6.9 per 1000 in Europe and 9.3 per 1000 in Asia and are the leading noninfectious cause of mortality in infants (Benjamin et al., 2018). The severity of CHDs often varies, ranging from minor lesions that can resolve spontaneously, more severe forms that require surgical procedures to major malformations that result in prenatal death. Due to advancements in medical treatment, the survival rate of CHDs has increased substantially over the past several decades and it is estimated that there were 1.4 million adults living with CHDs in the United States in 2010 (Gilboa et al., 2016).

The cardiac outflow tract (OFT) is a transient conduit that connects the embryonic heart chambers to the vascular network. OFT defects, also referred to as conotruncal heart defects, include a spectrum of disease types and constitute approximately 30% of CHDs (Benjamin et al., 2018). The structural defects are detrimental to the establishment of separate systemic and pulmonary circulations.

Persistent truncus arteriosus (PTA) consists of a common arterial trunk arising from the ventricular part of the heart. It is the most severe type of OFT defect, resulting from complete or partial failure of the formation of the septum, which normally divides the embryonic OFT into the aortic and pulmonary trunks (Collet and Edwards, 1949). The common trunk may originate from the left ventricle, right ventricle, or override a ventricular septal defect, receiving blood from both ventricles that supplies the coronary, pulmonary and systemic circulations (Adachi et al., 2009; Collet and Edwards, 1949). PTA usually requires neonatal surgical repair to prevent cyanosis and pulmonary failure (Neeb et al., 2013).

In transposition of the great arteries (TGA), the aorta arises from the right ventricle and the pulmonary trunk arises from the left ventricle, a misalignment of both arteries with their corresponding ventricles. TGA is associated with heterotaxy, which refers to abnormal left-right patterning (Ramsdell, 2005). TGA is commonly concurrent with atrial or ventricular septal defects, which are essentially a rescue mechanism to allow for a mixture of oxygenated and deoxygenated blood to be circulated in the body (Martins and Castela, 2008). TGA has a high birth prevalence, composing 5-7% of all CHDs (Martins and Castela, 2008), and surgical treatment is required soon after birth.

Double outlet right ventricle (DORV) describes the phenomenon where well-defined aortic and pulmonary trunks both arise from the right ventricle. It is caused by OFT alignment defects and is often concurrent with other CHDs such as ventricular septal defects (Obler et al., 2008). DORV is detrimental to the health because deoxygenated blood from the right ventricle is circulated in the body via systemic circulation and surgical procedures are also required to correct this defect.

Overriding aorta (OA) is defined as the aorta positioning directly above a ventricular septal defect. The misaligned aorta supplies the body with a mixture of oxygenated and deoxygenated blood received from the left and right ventricles. It is also one of the four defects of Tetralogy of Fallot, a rare and complex CHD. Interestingly, OA, DORV, and TGA all arise from rotation failure, with increasing severity of misalignment, which implies a common pathogenesis for these defects (Neeb et al., 2013).

Aside from the major OFT defects mentioned above, other anomalies of the great arteries and veins include patent ductus arteriosus, valvular pulmonic or aortic stenosis, coarctation of aorta, aberrant subclavian artery, persistent left superior vena cava, and anomalous pulmonary venous connection (Benjamin et al., 2018; Neeb et al., 2013). Due to the emphasis of this dissertation, they will not be discussed here.

1.1.2 Cell Lineages in Outflow Tract Morphogenesis

The morphogenesis of OFT is a complex process that involves the interplay of multiple cell lineages under precise spatiotemporal control. During early development, cardiomyocytes derive from the mesoderm, the middle germ layer formed through gastrulation. At the third week of human development, or embryonic day (E) 8 in mice,

cardiomyocytes undergo migration to form the cardiac crescent, also referred to as first heart field (FHF), which subsequently fuses at the midline to generate the primitive heart tube (Buckingham et al., 2005; Kelly and Buckingham, 2002). In the meantime, an extra-cardiac progenitor population originated from the splanchnic mesoderm, known as the second heart field (SHF) invades the resident FHF cells and contributes to the arterial and venous poles of the elongating heart tube. The heart tube then undergoes rightward looping and is segmented into the atrium, atrioventricular canal (AVC), ventricle and OFT (Buckingham et al., 2005; Lin et al., 2012). The atrial and ventricular chambers are further divided into the left and right atria and the left and right ventricles respectively, via a process known as atrioventricular septation. Several mesenchymal tissues including AVC endocardial cushions, mesenchymal cap and the dorsal mesenchymal protrusion contribute to this process, which eventually gives rise to a four-chambered heart (Anderson et al., 2003; Mommersteeg et al., 2006; Moorman et al., 2003; Snarr et al., 2007; Wessels et al., 2000). Concurrently, endocardial cells at AVC and OFT cushions undergo endothelial-mesenchymal transition (EndoMT) and form the atrioventricular and semilunar valves to ensure directional blood flow (de Lange et al., 2004; Okamoto et al., 2010; Restivo et al., 2006).

The primitive OFT is situated at the arterial pole during cardiac looping, connecting the ventricle with the aortic sac. Fate-mapping studies in chick and mouse have demonstrated that during heart tube elongation, new myocardium is differentiated from SHF progenitor cells in the splanchnic and pharyngeal mesoderm beneath the floor of the foregut and progressively added to the arterial pole, incorporating into first the conal, or proximal OFT, and later the truncal, or distal OFT (Kelly et al., 2001; Mjaatvedt

et al., 2001; Waldo et al., 2001). SHF also gives rise to the vascular smooth muscle at the base of the aorta and pulmonary trunk (Verzi et al., 2005; Waldo et al., 2005a). Furthermore, *Mef2c*-expressing SHF descendants contribute to the endocardium of OFT (Verzi et al., 2005) (Figure 1B). Another cell lineage essential for OFT elongation is the cardiac neural crest (CNC), which is a subset of the migratory neural crest originating from the lower hindbrain. CNC cells migrate from the dorsal neural tube to the OFT via caudal pharyngeal arches (Hutson and Kirby, 2003; Lin et al., 2012; Neeb et al., 2013). During OFT elongation, CNC restricts the proliferation of and facilitates the deployment of SHF to the OFT myocardium (Figure 1A). In CNC-ablated chick embryos, SHF fails to migrate into the OFT and stops at the junction of the OFT and the ventral pharynx. As a result, the embryos display diminished OFT length and inner curvature, as well as misalignment with the pharyngeal arch arteries (Waldo et al., 2005b; Yelbuz et al., 2002).

The OFT subsequently undergoes remodeling, in which a single cylindrical lumen is separated into the aorta and pulmonary trunk via OFT septation. During the colonization of OFT, a group of CNC cells first form a condensed mesenchyme, giving rise to the aorticopulmonary septum that divides the aortic sac and truncal OFT into aortic and pulmonary channels (Waldo et al., 1998). The OFT then undergoes conotruncal transition, forming an angle at the junction of the conal and truncal OFT lumen which initially is located midway between the base of the ventricles and the divided aortic sac, but later moves closer to the heart (Waldo et al., 1998). CNC further invades proximally and populates the truncal endocardial cushions, which then fuse and muscularize, elongating the OFT septum craniocaudally (Lin et al., 2012; Neeb et al., 2013; Waldo et al., 1998). By contrast, the mesenchymal conal cushions are derived from

endocardium via EndoMT. The conal cushions then fuse with additional contribution from the ingrowing myocardium and scattered CNC cells, forming the conal septum (Lin et al., 2012; Rana et al., 2007; Waldo et al., 1998) (Figure 1C).

Concomitant with septation, OFT undergoes counterclockwise rotation where the myocardial wall of the OFT rotates before and during formation of the great arteries, placing the pulmonary trunk in an anterior position and the aorta in a posterior position (Bajolle et al., 2006). Completion of septation is marked by convergence of OFT and ventricular septa, resulting in proper alignment of the ventricles to the arteries (Lin et al., 2012). OFT misalignment due to rotation failure may cause a spectrum of cardiac anomalies such as PTA, TGA and DORV (Bajolle et al., 2006; Neeb et al., 2013). After OFT septation, the truncal OFT endocardial cushions further remodel into the mature aortic and pulmonary semilunar valves at the junction of conal and truncal regions of OFT (Lin et al., 2012; Neeb et al., 2013). Together these ensure directional blood flow and the establishment of the systemic and pulmonary circulations.

1.1.3 Hedgehog Signaling in Outflow Tract Formation

The multi-step and multi-lineage nature of OFT formation requires a precise orchestration of the simultaneous and sequential occurrence of cellular events. Advances in gene targeting approaches have led to the discovery of signaling molecules, structural genes and transcription factors comprising the intricate regulatory network for heart development. Hh signaling pathway is one of the key regulators of embryonic development. During OFT formation, Hh signaling maintains SHF proliferation and migration (Dyer and Kirby, 2009; Dyer et al., 2010). Fate mapping studies have shown that Hh-receiving SHF cells, marked by Hh effector *Gli1*, migrate from the pharyngeal

mesoderm into the pulmonary artery between E9.5 and E11.5. Specifically, the Hh-receiving cells first enter the OFT, then further populate the pulmonary region, establishing a continuum of cells from the pharyngeal mesoderm to the OFT. Finally, the population is incorporated into the OFT endocardial cushions and pulmonary artery wall (Hoffmann et al., 2009).

Shh, one of the ligands of the Hh pathway, provides guidance cues for CNC migration and localization and is required for the survival of SHF and CNC (Goddeeris et al., 2007; Smoak et al., 2005). Deficiency in Hh signaling leads to OFT elongation and septation defects, arch artery defects and right ventricle hypoplasia (Dyer and Kirby, 2009; Goddeeris et al., 2007; Smoak et al., 2005). On the molecular level, Shh is a mediator of the downstream signal transducers within the Hh pathway. Shh is required for the expression of its inhibitory receptors Ptch1 and Ptch2 as well as Gli1, an intracellular effector of the Hh signaling in the pharyngeal arches (Dyer et al., 2010; Smoak et al., 2005). Additionally, Hh signaling forms interactions with major cardiac transcription factors and pathways to regulate heart development in a dynamic fashion. Literature suggests that Isl1, Gata4 and Tbx5 lie upstream of Hh signaling whereas Nkx2.5 and Tbx1 act as its downstream targets. Isl1, a marker of the SHF progenitor population, is required for Shh expression. Ablation of Smo, an activating membrane receptor of Hh signaling in Isl1-expressing cells results in various OFT abnormalities such as elongation defects and PTA, as well as reduced expression of Nrp2, a neuropilin receptor of VEGF and semaphorin signaling required for cardiovascular development, in the OFT (Cai et al., 2003; Lin et al., 2006). Tbx5 and Gata4 promotes atrial septation possibly through direct interaction with Hh signaling facilitator Gas1 and effector Gli1, respectively (Xie et al.,

7

2012; Zhou et al., 2017). Loss of *Ptch1* upregulates *Nkx2.5*, an transcription factor essential for both FHF and SHF whereas loss of *Smo*, which is inhibited by *Ptch1*, leads to reduced expression *Nkx2.5* that is concomitant with cardiac looping failure (Zhang et al., 2001). Interestingly, conflicting results have been reported for the effect of Hh signaling on *Tbx1*, a causative gene of the DiGeorge Syndrome. Initial studies demonstrated that *Shh* is required to induce *Tbx1* expression in the pharyngeal arches at E9.5 and E10.5, possibly through *Foxa2* (Garg et al., 2001; Yamagishi et al., 2003), however another study found no difference in *Tbx1* expression between *Shh* mutants *wildtype* littermates (Goddeeris et al., 2007). A positive feedback relationship between Hh and Wnt signaling within the SHF is inferred from evidence showing *β-catenin*-dependent *Shh* expression in *Isl1*-expressing cells and *Smo*-dependent expression of *β-catenin*, *Lef1* and *Axin2* in *Mef2c*-expressing cells between E9.5 and E10.5 (Briggs et al., 2016; Lin et al., 2007).

1.1.4 Platelet-Derived Growth Factor Signaling in Heart Development

The platelet-derived growth factor (PDGF) pathway plays critical roles in embryonic development, cell migration, and angiogenesis. Specifically, the cell surface receptors for PDGF, *Pdgfra* and *Pdgfrb*, have been implicated into the intricate molecular network that governs heart development (Van den Akker et al., 2008; Bax et al., 2010; Bloomekatz et al., 2017; Peng et al., 2017). *Pdgfra* modulates cardiomyocyte migration towards the midline during heart tube assembly (Bloomekatz et al., 2017). *Pdgfra* is also expressed in the SHF progenitor cells and has been shown to downregulate *Nkx2.5* and *Wt1* during SHF development (Bax et al., 2010). On the other hand, *Pdgfrb* is expressed in atrioventricular cushion mesenchymal cells and is a direct downstream target of TGFβ

signaling (Peng et al., 2017). *Pdgfb* knockout embryos display a common pulmonary artery branching off the pulmonary trunk, instead of individual left and right pulmonary arteries in *wildtype* embryos. In addition, the majority of mutant embryos show DORV with dextropositioning of the ascending aorta and ventricular septal defect as well as atrioventricular valve malformation and hypoplastic compact myocardium, concomitant with decreased myocardial proliferation (Van den Akker et al., 2008). Mutation of either *Pdgfra* and *Pdgfrb* gives rise to atrioventricular septal defects, and hypoplasia of the valves or compact myocardium (Van den Akker et al., 2008; Bax et al., 2010). In addition, PDGFRα and PDGFRβ form heterodimers in regulating craniofacial mesenchyme development (Fantauzzo and Soriano, 2016).

1.2 *Osr1* is an Essential Regulator of Heart Development

Odd-skipped (*Odd*) was initially discovered in *Drosophila* as a pair-rule gene required for segmentation. In the mouse, *Odd-skipped related 1* (*Osr1*) is a transcription factor crucial for the development of various organs including the heart, kidney, lung, etc., and homozygous mutation of *Osr1* has proven to be embryonic lethal. Despite various studies on the role of *Osr1* in heart development, the mechanisms by which *Osr1* regulates molecular and cellular events remain unknown. This section reviews the expression pattern of *Odd* during *Drosophila* and of *Osr1* during mouse embryogenesis as well as the pathologic phenotypes in the mutant embryos. Additional focus on the localization and migration of *Osr1*-expressing cells in mouse heart development, the molecular pathways that interact with *Osr1*, and its association with human congenital heart diseases will also be discussed.

1.2.1 *Odd* in *Drosophila* Segmentation

Odd in *Drosophila* encodes a transcription factor of 392 amino acids and contains four tandem Cys-Cys/His-His zinc finger repeats (Coulter et al., 1990). It was initially identified as one of the genes in the pair-rule class required for *Drosophila* segmentation, a developmental process marked by transformation of a single field of the embryo into homologous repetitive units called segments. Pair-rule genes are responsible for bi-segmental patterning. They comprise the middle regulatory level of the spatial organization hierarchy, following the gap gene class, which divides the embryos into groups of contiguous segments, and preceding the segment polarity gene class, which controls the basic structures of individual segments. In *Odd* mutants, defects are found in denticle bands in odd-numbered abdominal segments and in the mesothorax, as well as in anal and labial structures (Coulter and Wieschaus, 1988; Nüsslein-volhard and Wieschaus, 1980).

In *Drosophila*, *Odd* is first expressed in syncytial blastoderms at nuclear division cycle 13. As cellularization proceeds, *Odd* expression domain expands and evolves into seven primary stripes separated by gaps. Subsequently during gastrulation, *Odd* is expressed in eight secondary stripes complementary to the primary stripes, resulting in a pattern of uniform expression in every segment (Coulter et al., 1990). Although pattern deletions in *Odd* mutants are relatively less severe than that in other pair-rule mutants, embryos that lack *Odd* exhibit additive or restored phenotype in specific structures when combined with mutations of other segmentation genes such as *even-skipped*, *engrailed* or *wingless*, suggesting that the function of *Odd* as an activator or repressor is dependent on the local context which involves interactions with genes in parallel or hierarchical fashion

(Coulter and Wieschaus, 1988; Coulter et al., 1990; Le-Drean et al., 1998). Difference in phenotypes observed in response to stage-specific induction of ectopic *Odd* expression shows that *Odd* regulation is also time-sensitive (Le-Drean et al., 1998).

1.2.2   *Osr1* in Mouse Development

A decade after the discovery of *Odd* in *Drosophila*, its homolog was cloned and characterized in the mouse, termed *Odd-skipped related 1* (*Osr1*) (So and Danielian, 1999). The mouse *Osr1* encodes a 266-amino-acid protein that contains three Cys-Cys/His-His zinc finger domains which highly resembles Odd in *Drosophila* (So and Danielian, 1999). *Osr1* is first expressed in the nascent intermediate mesoderm at E7.5. At E8.5, neurulation initiates and *Osr1* expression is found on either side of the neural plate, extending from caudal to the cardiac crescent to the tail end of the embryo. By E9.5, *Osr1* expression is shifted towards the posterior half of the embryo including the dorsal atrial myocardium, lung bud mesenchyme, fore- and hindgut endoderm and the caudal somites. By E10.5, *Osr1* is expressed in the branchial arches, the trunk caudal to the branchial arches, forebrain as well as the ectodermal mesenchyme in fore- and hindlimb buds. At E11.5, the expression range of *Osr1* further expands to all three branchial arches and increased expression is found in the limb buds and ventral embryonic trunk. At E12.5, *Osr1* expression is newly established in the mouth region, and as limbs continue to develop, *Osr1* is localized to interdigital and proximal limb areas, although expression throughout the rest of the embryo is diminished (Figure 2) (So and Danielian, 1999; Wang et al., 2005).

Following the spatiotemporal characterization of the *Osr1* expression pattern, several transgenic lines were generated and primary as well as stem cell cultures of *Osr1-*

expressing cells were used to study the functional roles of *Osr1* and the molecular events in which it is involved in early embryogenesis (Lan et al., 2011; Mae et al., 2013; Mugford et al., 2008; Taguchi et al., 2014; Vallecillo-García et al., 2017; Wang et al., 2005). The importance of *Osr1* is evidenced by developmental defects of various organs in homozygous *Osr1* mutants and death *in utero* as a result. Mice heterozygous for the *Osr1* null allele are normal and fertile, however, majority of *Osr1*$^{-/-}$ mutants die between E11.5 and E12.5 due to circulation distress mainly caused by lack of primary atrial and ventricular septum, dilated atria, hypoplasia of venous valves, and malformed atrioventricular junction. Additionally, *Osr1*$^{-/-}$ mutants completely fail to develop the metanephric kidneys and gonads, which are derivatives of the intermediate mesoderm (Wang et al., 2005). Analysis of *Osr1*$^{-/-}$ embryos that survived through later stages revealed that they also exhibit abnormal cartilage formation in synovial joints (Gao et al., 2011) and neural crest (Liu et al., 2013), defects in limb muscles (Vallecillo-García et al., 2017), and defects in the respiratory system including lung lobes, tracheas, and pulmonary arteries (Han et al., 2017).

1.2.3   *Osr1* in Heart Development and Disease

1.2.3.1 *Odd* in *Drosophila* heart development. The developmental processes of the heart and the underlying molecular mechanisms are highly conserved between *Drosophila* and vertebrates (Ahmad, 2017; Tao and Schulz, 2007). In both *Drosophila* and vertebrate embryos, the heart originates from bilateral rows of mesodermal cells that migrate and ultimately fuse to form a heart tube at the midline. Unlike undergoing looping and septation, forming a four-chambered heart as in vertebrates, the *Drosophila* heart remains tubular (Ahmad, 2017). The *Drosophila* heart consists of two major cell

types: cardioblasts, which form the contractile tube of the heart, and the non-muscular pericardial cells, which flank the cardioblasts. *Odd* marks a subpopulation of pericardial cells that flank the dorsal midline and are in close physical contact to the cardioblasts. Within a hemisegment, *Odd*-pericardial cells develop from three heart progenitors within the dorsal mesoderm. Among the three progenitors, two divide asymmetrically, each producing one *Odd*-pericardial cell and one cardioblast, a process mediated by *sanpodo* and *numb*. The third progenitor divides symmetrically to produce two *Odd*-pericardial cells (Ward and Skeath, 2000).

1.2.3.2 *Osr1* in heart development in the mouse model. In the developing mouse heart, *Osr1* gene activity begins as early as E9.5 and is maintained through E13.5. *In situ* hybridization and X-gal staining of the β-galactosidase fusion protein encoded from the *Osr1* locus revealed that *Osr1* is expressed sequentially in the dorsal atrial myocardium, the developing atrial septum, SHF, dorsal mesenchymal protrusion, cardinal vein, left leaflet of venous valves, outflow tract mesenchyme, and parietal pericardium (Wang et al., 2005; Xie et al., 2012; Zhou et al., 2015). Genetic inducible fate mapping using tamoxifen-induced CreER^{T2} recombinase encoded from the *Osr1* locus showed that *Osr1*-expressing cells from as early as E8.0 to E11.0 contribute to structures in the mature heart including the atrial wall, the core of the dorsal mesenchymal protrusion, and the mesenchymal cap of the atrial septum (Mugford et al., 2008; Zhou et al., 2015), suggesting that the role of *Osr1* in heart development may lie in providing early cues to the cells from the intermediate mesoderm, prompting them to undergo migration, lineage specification and eventually acquire cardiac cell properties.

Despite widespread distribution of *Osr1* expression during development and the various defects observed in knockout embryos, initial studies did not identify molecular evidence for *Osr1* regulation of heart development. Whereas *Osr1*$^{-/-}$ embryos show severely dilated atria, lack of septum primum and hypoplastic venous valves at E11.5, the location and magnitude of the expression of cardiac transcription factors *Pitx2*, *Nkx2.5*, *Gata4*, *Tbx5* and *Tbx18* remain unchanged compared to their *wildtype* littermates (Wang et al., 2005). On the other hand, *Osr1* expression is induced by *Tbx5* in a cardiac-derived mouse cell line (Plageman and Yutzey, 2006), indicating that *Osr1* might be involved in a novel molecular pathway in the developing heart. Indeed, subsequent studies found that *Osr1* expression is dependent on *Gata4* and *Shh*, and is a downstream target of *Tbx5* in E9.5 posterior SHF (Xie et al., 2012; Zhou et al., 2017). Surprisingly, *Osr1* ablation results in a reduction of several other components of the Hedgehog pathway, including *Smo*, a transmembrane receptor and *Gli1*, a transcription factor linking the signaling cascade to its downstream genes (Zhou et al., 2015). Further investigation found that the requirement of *Osr1* for atrial septation might be due to its essential roles in regulating the proliferation and cell cycle progression, but not the survival of posterior SHF progenitor cells (Zhou et al., 2015). In addition, germline compound haploinsufficiency of *Osr1* and *Tbx5* results in increased incidence of atrial septal defect compared to *Tbx5* heterozygotes (Zhou et al., 2015). This demonstrates an additive effect of *Osr1* and *Tbx5* that is reminiscent of the additive phenotypes in double mutants of *Odd* and several other pair-rule genes during *Drosophila* segmental patterning (Coulter and Wieschaus, 1988).

1.2.3.3 *OSR1* mutation and congenital heart defects. Besides using model organisms, one study in humans found that the *OSR1* rs12329305 polymorphism, located

in exon 2, is associated with prenatal and neonatal death due to congenital malformations of the heart and kidney (Zemunik, 2014). This suggests that the functions of *OSR1* and the regulatory network it is involved in for heart development might be evolutionarily conserved.

1.3   Epigenetic Regulation of Heart Development

Epigenetic regulatory mechanisms play essential roles in embryonic development and disease progression. Through DNA and histone modifications, chromatin remodeling and non-coding RNAs, epigenetic mechanisms coordinate transcription via a multi-level regulatory system, and work in concert with cardiac transcription factors in setting the molecular basis for the tissue-specific gene expression programs. This section reviews the role of key epigenetic events DNA methylation, chromatin remodeling and histone modifications in heart development and their implications in congenital heart diseases.

1.3.1   DNA Methylation in Heart Development and Disease

DNA methylation distinguishes itself from other epigenetic mechanisms by modifying DNA directly. It is implicated in biological processes such as genomic imprinting, X-chromosome inactivation, repression of transposable elements and regulation of splicing events (Martinez et al., 2015). DNA methylation most often occurs at the fifth carbon of cytosine within CpG dinucleotides, which are distributed throughout the genome. DNA methylation is maintained by the DNA methyltransferase family that includes DNMT1, which maintains methylation patterns during DNA replication, DNMT3A and DNMT3B, which are responsible for *de novo* DNA methylation and DNMT3L, which stimulates the catalytic activity of DNMT3A and DNMT3B (Gowher et al., 2005; Okano et al., 1999; Vilkaitis et al., 2005). A characteristic signature of CpG

methylation is the CpG islands, which are DNA regions of hundreds of base pairs in length that contain densely clustered CpG sites (Martinez et al., 2015; Saxonov et al., 2006). Although correlation between DNA methylation and gene expression is becoming unclear with increasingly disparate evidence, promoter methylation is generally found to inhibit gene expression by impeding the binding of transcription factors or by interacting with methyl-CpG-binding proteins, which further recruit repressive histone modifiers such as histone deacetylases and histone methylase complexes (Bird and Wolffe, 1999; Fujita et al., 2003; Huck-Hui and Bird, 1999; Maurano et al., 2015; Watt and Molloy, 1988).

DNA methylation is essential to mammalian development processes including primordial germ cell specification, embryonic stem cell differentiation as well as postnatal organ maturation (Smith and Meissner, 2013). *In vitro* and *in vivo* systems have been employed to study the significance of DNA methylation on the cellular functions and physiological phenotypes of the developing heart. In murine P19 cells, a well-characterized model for cardiomyocyte differentiation, DNA methyltransferase inhibitor 5-azacytidine induces cardiomyocyte differentiation accompanied by upregulation of cardiac markers *Isl1*, *Bmp2*, *Gata4*, and *αMHC* (Abbey and Seshagiri, 2013). Due to advances in genomic approaches, many recent studies have aimed to investigate the dynamic DNA methylation patterns on the genome-wide scale (Chamberlain et al., 2014; Gilsbach et al., 2014; Serra-Juhé et al., 2015; Sim et al., 2015). DNA methylation profiling of mouse embryonic hearts at ACGT sites revealed that the global DNA methylation level remains stable between E11.5 and E14.5 and although a small set of genes with essential cardiac functions exhibits both differential methylation and

differential gene expression, the correlation between them is not clear. Interestingly, *Has2*, a critical factor for EndoMT and cardiac valve and septum formation, exhibits hypermethylation at an enhancer, concurrent with diminished gene expression at E14.5, which is consistent with its function in EndoMT around E11.5 for cardiac cushion development (Camenisch et al., 2001; Chamberlain et al., 2014). On the other hand, DNA methylation is required for maintaining normal heart size by controlling postnatal cardiomyocyte cell cycle arrest. Methyl binding domain enrichment sequencing (MBD-seq) has uncovered a hypermethylation of the majority of differentially methylated regions (DMRs) between P1 and P14 which are associated with transcriptional inactivation of key cardiac development pathways including Hedgehog, Fgf, Notch and the canonical Wnt pathway, suggesting a role of DNA methylation in postnatal cardiomyocyte maturation and proliferation arrest (Sim et al., 2015). Furthermore, whole-genome bisulfite sequencing (WGBS) of purified cardiomyocytes has identified an enrichment of enhancer signatures at hypomethylated regions in adult cardiomyocytes, represented by cardiac transcription factor binding motifs and active histone marks, and a resemblance of failing cardiomyocytes to neonatal methylation patterns (Gilsbach et al., 2014). In humans, promoter hypermethylation, reduced transcript and protein levels of *VANGL2*, a critical gene for planar cell polarity in the myocardium of right ventricular OFT are associated with increased Tetralogy of Fallot incidence (Yuan et al., 2014). Additional correlation has been found in the fetal heart tissue between congenital heart diseases and hypermethylation of multiple CpGs in the *GATA4* gene body with, notably, increased *GATA4* expression. These studies have established DNA methylation as a highly dynamic process that regulates heart development and disease. However, the role

17

of DNA methylation in the cardiac progenitor populations and cell fate determination remains largely unknown.

1.3.2 Chromatin Remodeling and Histone Modifications in Cardiac Progenitor Lineage Commitment

In eukaryotes, DNA is wrapped around histone octamers, consisting of two H2A, H2B, H3, and H4 core histone proteins. The resulting nucleosomes constitute the basic units of chromosomes, which allows the entire genome to be packaged tightly into the nucleus (Martinez et al., 2015; Vallaster et al., 2012). In addition to epigenetic regulation on the DNA level, the chromatin is also susceptible to modulations by epigenetic mechanisms. During cardiac development, chromatin regulation is accomplished mainly via ATP-dependent chromatin-remodeling complexes and histone modifiers. Chromatin-remodeling complexes alter the chromatin architecture between an open, permissive state known as euchromatin, allowing for transcription factor binding and active gene transcription, and a condensed, repressive state known as heterochromatin. Histone modifiers, on the other hand, modulate nucleosomes via covalent post-translational modification to histone proteins including methylation, phosphorylation, acetylation, ubiquitylation, and sumoylation. These modifications, or "histone marks", independently or combinatorially comprise signatures for transcriptionally active or repressive regions in the genome (Chang and Bruneau, 2012; Vallaster et al., 2012). Histone modifiers and chromatin remodelers often work in concert in regulating chromatin structure and function (Swygert and Peterson, 2014).

The functional importance of chromatin modulators in cardiac development is evidenced by the myriad of cardiovascular malformations or prenatal death observed in

mutants of members of chromatin remodeling complexes BAF, CHD, INO80, ISWI and of histone methyltransferases, demethylases, acetyltransferases, deacetylases, polycomb repressive complexes and poly (ADP-ribose) polymerases (PARP) (Chang and Bruneau, 2012; Martinez et al., 2015; Ohtani and Dimmeler, 2011; Vallaster et al., 2012). These modulators coordinate cardiac lineage commitment by forming complexes with cardiac transcription factors and controlling the activity of gene regulatory elements such as promoters, enhancers, and insulators (Zhou et al., 2011). In particular, the BAF complex has been implicated in mesoderm differentiation and cardiomyocyte proliferation (Hang et al., 2010; Takeuchi and Bruneau, 2009). BAF60C, a cardiac-specific subunit of the BAF complex encoded by *Smarcd3*, recruits BAF complex to cardiac enhancers and potentiates the activation of target genes by promoting BAF complex interactions with TBX5, NKX2.5, GATA4 and the binding of transcription factors to gene regulatory regions (Lickert et al., 2004; Takeuchi and Bruneau, 2009). In addition, BRG1, the ATPase subunit of the BAF complex, physically interacts with two other classes of chromatin-modifying enzymes, histone deacetylase (HDAC) and PARP to regulate promoter activity of myosin heavy chain isoforms during myocardium differentiation (Hang et al., 2010). Globally, chromatin patterns represented by active and repressive histone marks as well as RNA polymerase II binding, can predict sets of functionally related genes and identify stage or cell type-specific enhancers during the differentiation of embryonic stem cells to cardiomyocytes (Wamstad et al., 2012).

Many techniques exist for examining chromatin landscape on the genome-wide scale such as DNase-seq, MNase-seq and ChIP-seq (Landt et al., 2012; Song and Crawford, 2010; Zaret, 2005). One of the recent innovations is the Assay for Transposase

Accessible Chromatin with high-throughput sequencing (ATAC-seq), which uses hyperactive Tn5 transposase to simultaneously target accessible regions on the chromatin and add barcodes for sequencing (Buenrostro et al., 2015, 2013). Due to its speed and high sensitivity, this method has gained increasing popularity and has become a standard tool for examining the combined output of chromatin regulation.

1.4   Preliminary Results

*Osr*1 mutation causes atrioventricular septal defects, atrium dilation and venous valve hypoplasticity in mice (Wang et al., 2005; Zhang et al., 2015; Zhou et al., 2015) and is associated with prenatal and neonatal death due to congenital malformations of the heart and kidney in humans (Zemunik, 2014). However, despite its expression in the developing OFT (Wang et al., 2005), the role of *Osr1* in OFT morphogenesis is not well understood. Our preliminary studies aimed to elucidate the contribution of the Osr1 cell lineage in OFT development and characterize OFT defects in *Osr1* mutants. We found that *Osr1* is expressed in the SHF progenitors at E9.5 and E10.5, and the distal OFT mesenchyme at E11.5. We determined that Osr1$^+$ cells from E8.0 to E10.5 contribute to the pulmonary trunk upon OFT remodeling completion. Importantly, *Osr1* deficiency resulted in abnormal conotruncal transition, OFT elongation as well as conotruncal heart defects including DORV and OA. These phenotypes were recapitulated by SHF-dependent deletion of *Osr1*, suggesting that *Osr1* expression in the SHF is critical for OFT formation. (Liu, J., Cheng, H., Liu, L. Xie, L., unpublished).

1.4.1 *Osr1* is Expressed in the OFT and Osr1$^+$ Cells Contribute to the Pulmonary Trunk

Previous studies have provided an overview of the *Osr1* expression pattern during mouse embryogenesis (So and Danielian, 1999; Wang et al., 2005; Xie et al., 2012; Zhou et al., 2015). A focal examination of the developing heart found that the majority of cells in the SHF express *Osr1* (Figure 3A-F). Osr1$^+$ cells were observed in the dorsal mesocardium and caudal splanchnic mesoderm at E9.5 (Figure 3A-C) and E10.5 (Figure 3D-F). At E11.5, *Osr1* expression expanded to the OFT mesenchyme, however, Osr1$^+$ cells were detected only in the distal OFT, but not the proximal OFT cushion (Figure 3G-I).

In order to delineate the contribution of the Osr1$^+$ cell lineage to OFT development, we performed genetic inducible fate mapping to locate the destination of Osr1$^+$ cells from various time points upon completion of OFT remodeling. Osr1$^+$ cells were marked using a tamoxifen (TM)-induced Cre-lox system by intercrossing mice expressing an *eGFPCreERt2* transgene from the *Osr1* locus (*Osr1$^{GCE/+}$*) (Mugford et al., 2008) and *Cre*-dependent *lacZ* reporter mice (*R26R$^{fl/+}$*) (Soriano, 1999). Dams were administered TM (75 mg/kg) at E6.5, E7.5, E8.5, E9.5 or E10.5 via oral gavage and β-galactosidase expression was evaluated in *Osr1$^{GCE/+}$;R26R$^{fl/+}$* embryos at E14.5 (Figure 4). TM administration at E6.5 did not induce β-galactosidase expression (data not shown). Interestingly, TM administration at E7.5 and E8.5 resulted in β-galactosidase expression in the pulmonary trunk, but not the ascending aorta (Figure 4A, B). However, the pulmonary trunk was not stained in embryos with TM administration at E9.5 (Figure 4C) and E10.5 (data not shown). Considering that TM activates *Cre* expression 12 h after

administration and that the action lasts for 24 h (Hayashi and McMahon, 2002), these results suggest that the *Osr1* promoter is activated between E8.0 and E10.5 and descendants of Osr1$^+$ cells from the corresponding time period contribute to the pulmonary trunk.

1.4.2   *Osr1* is Required in the SHF for OFT Formation

To elucidate the processes in which *Osr1* is involved during OFT development, we examined OFT elongation and remodeling in *wildtype*, *Osr1$^{LacZ/+}$* and *Osr1$^{LacZ/LacZ}$* embryos. In *wildtype* or *Osr1$^{LacZ/+}$* control embryos, OFT displayed a normal turn at the junction of the conal and truncal OFT lumen (Figure 5A, B), however, this turn was less distinct in *Osr1$^{LacZ/LacZ}$* embryos (Figure 5C, D). In addition, the combined length of proximal and distal OFT was significantly reduced in *Osr1$^{LacZ/LacZ}$* embryos when compared to controls (Figure 5E-H). These results indicate that *Osr1* is required for OFT elongation and remodeling.

Given the OFT anomalies seen in *Osr1*-deficient embryos, we proceeded to test if these embryos harbor any defects in OFT-derived structures. As previously reported (Wang et al., 2005; Zhang et al., 2015; Zhou et al., 2015), *Osr1$^{LacZ/LacZ}$* embryos displayed AVSD (18/21, 85.71%) (Figure 6B, C) at E13.5. Notably, conotruncal heart defects as a result of OFT misalignment were also observed in *Osr1$^{LacZ/LacZ}$* embryos, including DORV (14/21, 66.67%) (Figure 6E, H) and OA (3/21, 14.29%) (Figure 6F, I), which were recapitulated in *Osr1$^{GCE/LacZ}$* embryos (data not shown). Only one case of DORV was seen in the *Osr1$^{LacZ/+}$* embryos examined (1/16, 6.25%) and all *wildtype* embryos were normal (0/16, 0%) (Figure 6A, D, G).

Since *Osr1* is required for maintaining the normal state of SHF, we asked if *Osr1* deficiency in SHF alone can cause conotruncal heart defects. Conditional knockout of *Osr1* in SHF was performed by intercrossing *Mef2c$^{AHF-Cre/+}$;Osr1$^{fl/+}$* mice with *Osr1$^{fl/fl}$* mice (Lan et al., 2011; Verzi et al., 2005). *Mef2c$^{AHF-Cre/+}$;Osr1$^{fl/fl}$* mice recapitulated the OFT phenotypes observed in *Osr1$^{LacZ/LacZ}$* mice. Whereas *Osr1$^{fl/+}$* and *Osr1$^{fl/fl}$* control embryos displayed normal OFT alignment (0/12, 0%) (Figure 7A, B), *Mef2c$^{AHF-Cre/+}$;Osr1$^{fl/fl}$* embryos were found with OA (3/13, 23.08%) (Figure 7C, D) and DORV (6/13, 46.15%) (Figure 7E, F). This suggests that *Osr1* expression in the SHF is critical for OFT formation.

1.5   Research Direction

Osr1 is required for the formation of the chambers, septa and valves of the heart, as well as the proliferation and cell cycle progression of SHF progenitor cells (Wang et al., 2005; Xie et al., 2012; Zhou et al., 2015). Our preliminary results further characterized the contribution of the Osr1 cell lineage in OFT development and revealed various OFT anomalies in *Osr1* mutants. While histological and cellular evidence support a regulatory role of *Osr1* in OFT development, the molecular mechanisms underlying such regulation remain unknown. In addition, the SHF is a heterogeneous population and consists of subregions anterior SHF (aSHF) and posterior SHF (pSHF). Although being adjacent to each other and of similar cell types, their cell fates significantly differ, in that the aSHF contributes to the developing OFT and right ventricle, whereas the pSHF contributes mainly to the atria and inflow tract (Galli et al., 2008; van Vliet et al., 2017). The molecular profiles of aSHF and pSHF that may cause the disparity in their cell fates are not well studied.

In the present study, we applied systems biology approaches to investigate the transcriptional regulation of OFT development by *Osr1*. We observed aberrant distribution of the Osr1 lineage in *Osr1* null mutants, suggesting that *Osr1* regulates cell migration in a cell autonomous manner. We identified the downstream targets of *Osr1* in Osr1$^+$ SHF populations and confirmed a subset of the targets in the migration path from SHF to OFT. We also investigated the molecular determinants of the aSHF and pSHF cell fates. We found tissue-specific transcription factor binding motifs in accessible genomic regions that might contribute to the tissue-specific transcription profiles. Differential DNA methylation was also observed at key cardiac transcription factors, suggesting that the regional specificity in the SHF might be mediated by DNA methylation and chromatin accessibility.
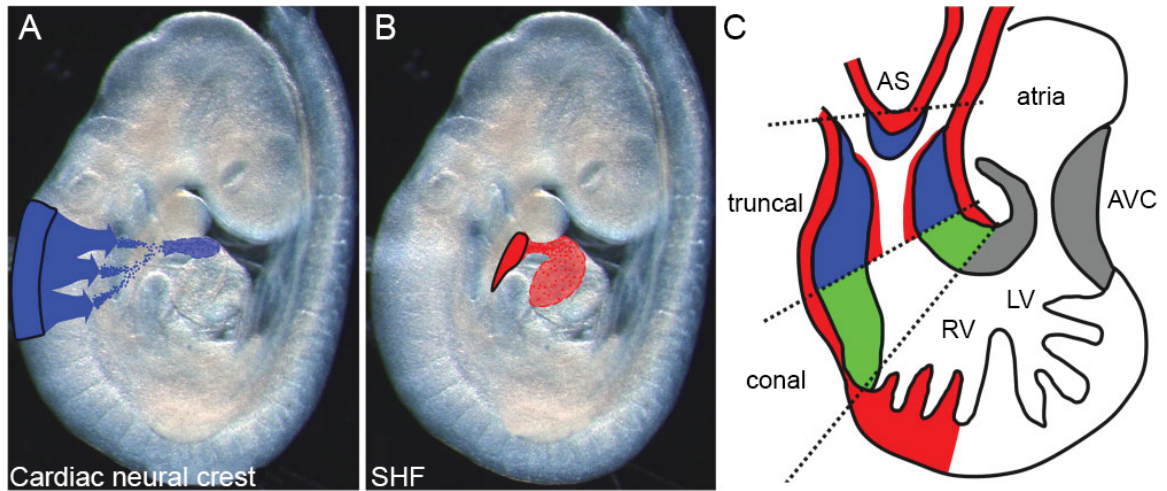
Figure 1. Cell sources contributing to the OFT (adapted from Neeb et al., 2013).

(A, B) Origin (black outline) and migration pathways of CNC (blue in A) to OFT truncal cushions and SHF (red in B) to OFT myocardial cuff and overlying endocardial cells within truncal region in E9.5 mouse embryo. (C) Schematic of OFT colonization by the extra-cardiac CNC (blue), SHF (red) and the location of the EndoMT-derived conal endocardial cushions (green). SHF, second heart field; AS, aortic sac; AVC, atrio-ventricular cushions; LV, left ventricle; RV, right ventricle.
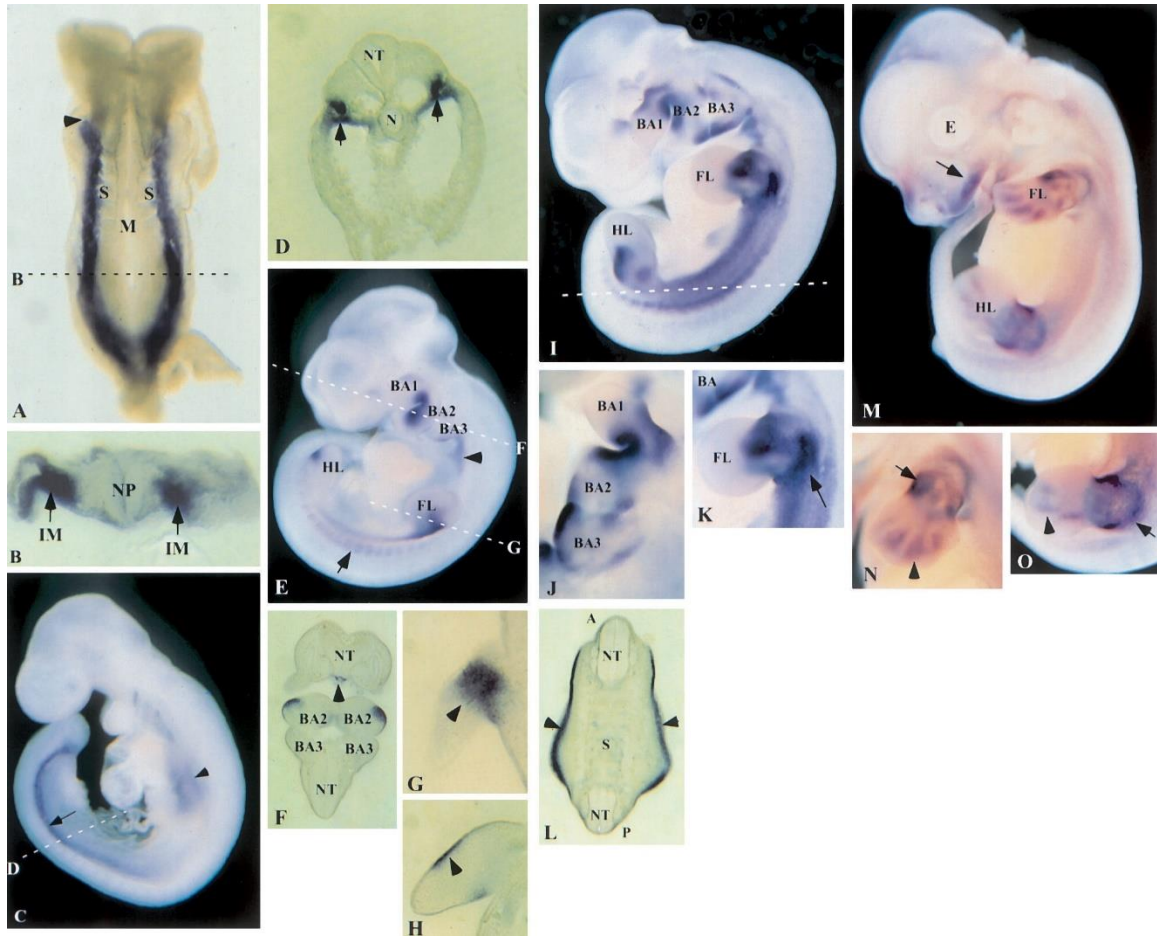
Figure 2. Expression of *Osr1* during mouse embryogenesis (adapted from So and Danielian, 1999).

(A) *Osr1* expression in the mesoderm at E8.5. (B) Section of embryo in (A) with *Osr1* transcripts in the intermediate mesoderm. (C) High expression of *Osr1* in the caudal somites (arrows) and low expression in region posterior to the third branchial arch (arrowhead) at E9.5. (D) Section of embryo in (C) showing *Osr1* transcripts in the intermediate mesoderm (arrows). (E) *Osr1* expression in the branchial arches and the trunk caudal to the branchial arches (arrowhead) and caudal to the forelimb (arrow) at E10.5. (F-H) *Osr1* transcripts in the second branchial arch (BA2) and in the forebrain (arrowhead) (F), and in the mesenchyme underlying the ectoderm of the forelimb (arrowheads) (G, H) on sections of (E). (I-K) *Osr1* expression in all three branchial arches (I, J) and the limb bud (K) (arrow) at E11.5. (L) *Osr1* transcripts in the mesenchyme underlying the ectoderm in the ventral embryonic trunk on the section from (I). (M-O) *Osr1* expression in the mouth region (arrow) (M), interdigital regions (arrowheads) and areas around the proximal limb (arrows) (N, O) at E12.5. A, anterior; BA, branchial arch; E, eye; FL, forelimb; HL, hindlimb; IM, intermediate mesoderm; M, midline; N, notochord; NT, neural tube; P, posterior; S, somites.

26
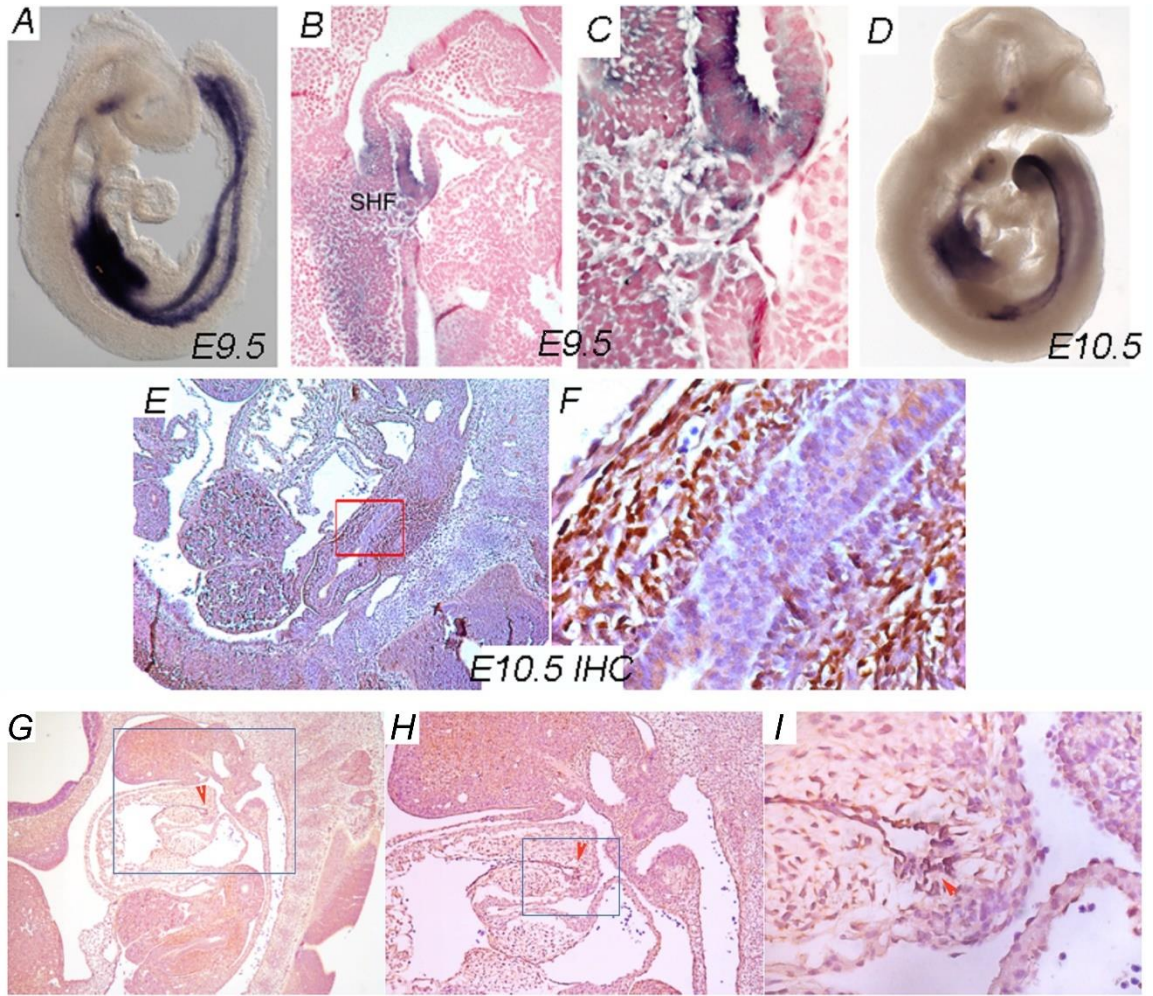
Figure 3. *Osr1* is expressed in the SHF at E9.5, E10.5, and the distal OFT at E11.5.

(A-D) *Osr1* expression was assessed by in situ hybridization on whole-mount embryos (A, D) or sagittal sections (B, C) (adapted from Xie et al., 2012). Osr1^{+} cells are found in the dorsal mesocardium and caudal splanchnic mesoderm at E9.5 (A-C) and E10.5 (D). (E-F) Immunohistochemical staining showed *Osr1* expression in the dorsal mesocardium, but not the endothelium at E10.5 ($n = 3$). (G-I) *Osr1* expression analyzed by immunohistochemical staining using E11.5 sagittal sections. (H, I) Magnifications of the boxed region in (G), (H) respectively. Arrowheads indicate Osr1^{+} cells ($n = 3$). SHF, second heart field. Magnification: (A, D, G) 40×; (B, E, H) 100×; (C, F) 400×; (I) 630×.
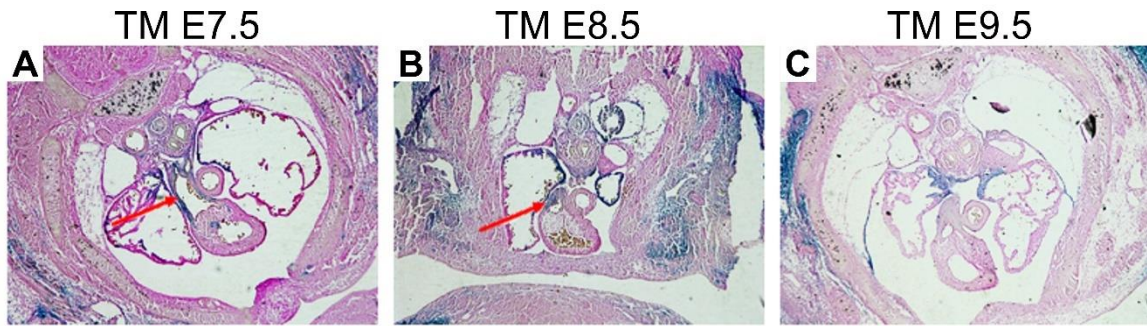
Figure 4. Osr1$^+$ cells contribute to the pulmonary trunk between E8.0 and E10.5.

Osr1 cell lineage assessed by X-gal staining of TM-administered $Osr1^{GCE/+};R26R^{fl/+}$ embryos on transverse sections. (A, B) TM administration at E7.5 and E8.5 marked Osr1$^+$ cells in the pulmonary trunk at E14.5. (C) No Osr1$^+$ cells were identified in the pulmonary trunk with TM administration at E9.5 ($n = 3$). TM, tamoxifen.
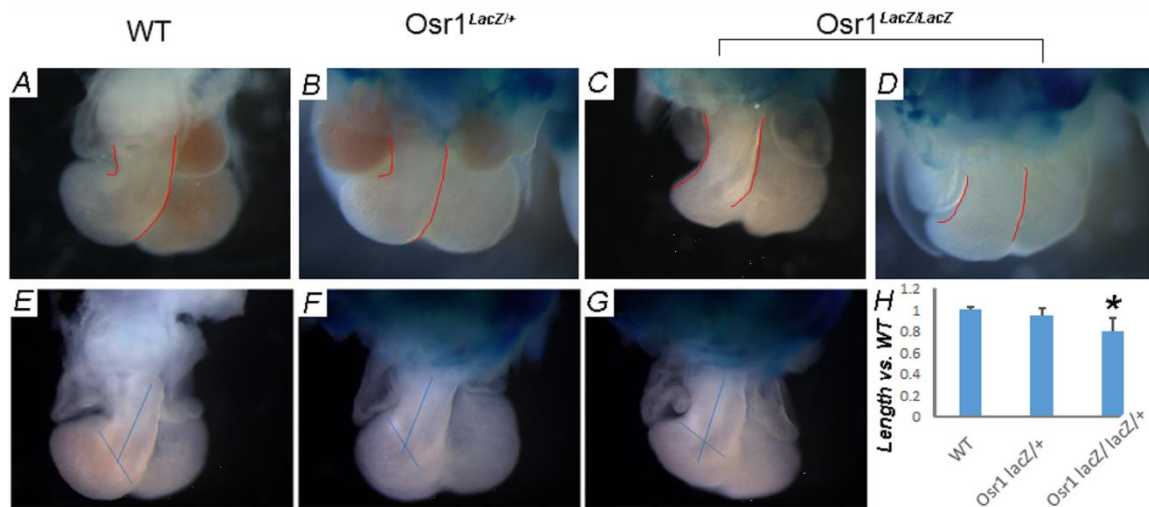
Figure 5. *Osr1*-deficient embryos exhibit conotruncal transition and OFT elongation anomalies at E11.5.

(A-D) Conotruncal transition assessed in whole-mount hearts as outlined by red curves. OFT in *wildtype* embryos displayed a normal turn at the junction of the conal and truncal OFT lumen (A, B) while the turn was less distinct in $Osr1^{LacZ/LacZ}$ embryos ($n = 3$). (C-E) OFT length indicated by the upper end of the longitudinal line and where it intersects with the transverse line. (H) Relative OFT length in E11.5 embryos. Values represent mean $\pm$ SEM ($n = 3$-5).
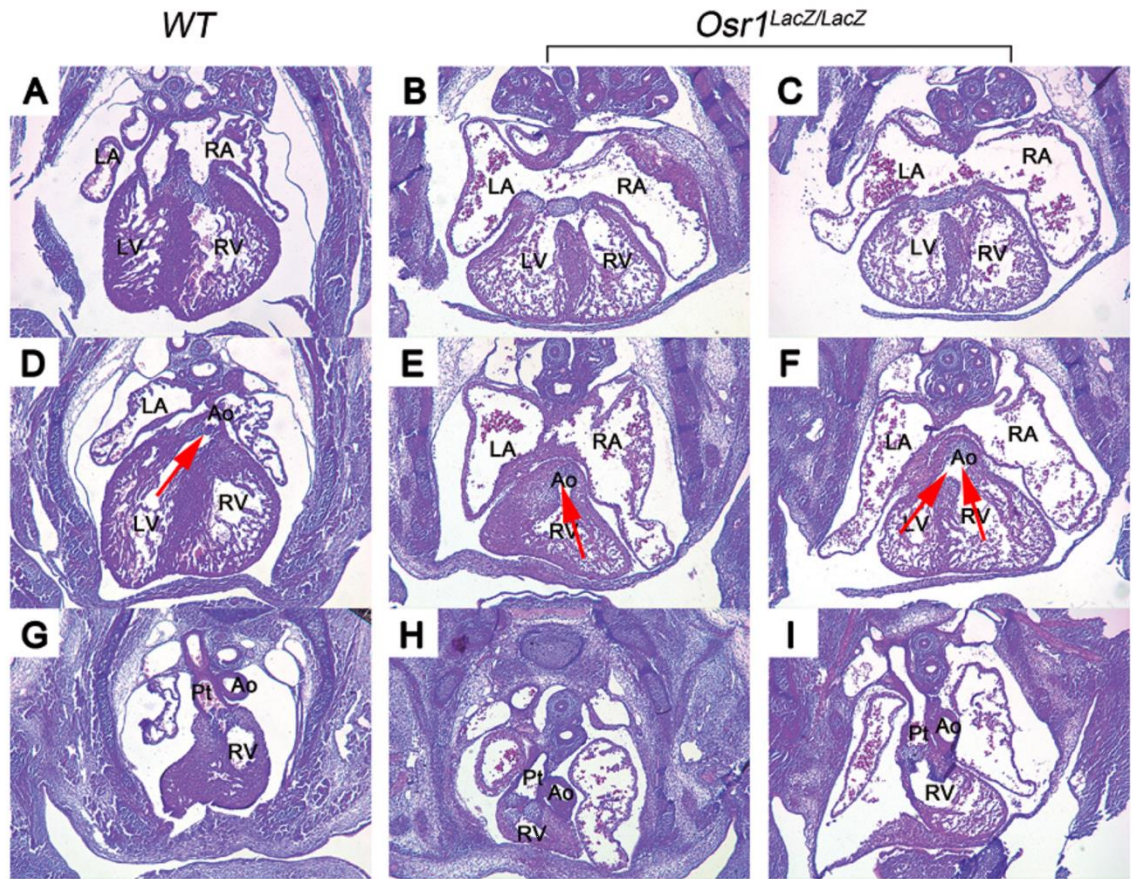
Figure 6. *Osr1*-deficient embryos exhibit heart defects at E13.5.

Types of heart defects assessed by transverse sectioning of *wildtype* and *Osr1$^{LacZ/LacZ}$* embryos. (A-C) *Wildtype* embryos undergo complete septation (A) while *Osr1$^{LacZ/LacZ}$* embryos displayed AVSDs (18/21, 85.71%) (B, C). (D-I) Conotruncal heart defects were observed in *Osr1$^{LacZ/LacZ}$* embryos including DORV (14/21, 66.67%) (E, H) and OA (3/21, 14.29%) (F, I), whereas *wildtype* embryos displayed normal OFT alignment (0/16, 0%) (D, G). LA, left atrium; RA, right atrium; LV, left ventricle; RV, right ventricle; Ao, aorta; Pt, pulmonary trunk. Red arrows indicate the direction of blood flow (*n* = 16-21).
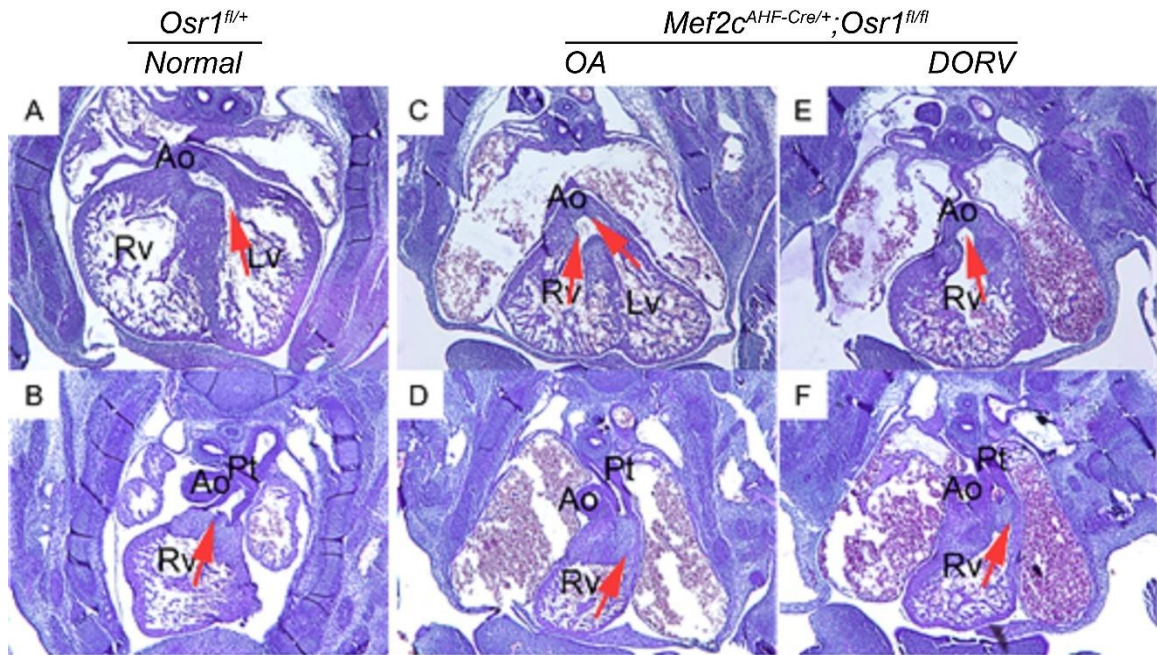
Figure 7. *Osr1* deficiency in SHF causes conotruncal heart defects at E13.5.

(A, B) *Osr1*^{fl/+} embryos displayed normal OFT alignment (0/12, 0%). (C-F) Conotruncal heart defects due to OFT misalignment were observed in *Osr1*^{fl/fl};*Mef2c*^{AHF-Cre/+} embryos including OA (3/13, 23.08%) (C, D) and DORV (6/13, 46.15%) (E, F). LV, left ventricle; RV, right ventricle; Ao, aorta; Pt, pulmonary trunk. Red arrows indicate the direction of blood flow (*n* = 12-13).

CHAPTER II

METHODS

2.1   Experimental Procedures

2.1.1   Animal Models

Mice were maintained in a mixed C57BL/6 and 129/SvEv background. The

$Osr1^{GCE}$ transgenic allele was generated by inserting an *eGFPCreERt2* (*GCE*) cassette to

the endogenous *Osr1* locus, which replaced the *Osr1* start codon with the start codon of

GCE (Mugford et al., 2008). Adult mice and embryos were genotyped by PCR using

primers 5'-GGG CAC AAG CTG GAG TAC AA-3' and 5'-CTC AGG TAG TGG TTG

TCG GG-3' and a 194-bp product indicates a mutant allele. The $Osr1^{tm1RJ}$ mutant allele

was generated by inserting a modified bacterial *lacZ* gene to the exon 2 of *Osr1*, resulting

in a nuclearly localized β-galactosidase fusion protein containing the N-terminal 16

amino acids of OSR1 and loss of *Osr1* function (Wang et al., 2005). The mutant allele

was detected by PCR using primers 5'-CTG GAC TGG AAT TCT GGA GGA AG-3'

and 5'-GTG CTG CAA GGC GAT TAA GTT G-3', provided by Dr. Rulang Jiang from

Cincinnati Children's Hospital Medical Center and a product of 360 bp indicates a mutant

allele.

Mouse experiments were completed according to a protocol reviewed and

approved by the Institutional Animal Care and Use Committee of the University of North

Dakota in compliance with the US Public Health Service Policy on Humane Care and

Use of Laboratory Animals.

2.1.2 Timed Mating

Superovulation techniques were adopted from the Jackson Laboratory and used to obtain a greater number of embryos from each pregnancy. Female mice aged 5 to 8 weeks were injected interperitoneally (IP) with 5 international units (IU) of pregnant mare serum (PMS) (Sigma-Aldrich) between 1:00 and 4:00 pm. They received another IP injection of 5 IU human chorionic gonadotropin (HCG) (Sigma-Aldrich) 42 to 50 hours after PMS injection. Each female was then mated with an appropriate male overnight and the midnight after HCG injection was considered embryonic day (E) 0.

2.1.3 Embryonic Heart Dissection

E9.5 and E10.5 embryos were dissected in cold PBS under a dissecting microscope. Thoracic region was obtained by removing the head and tail from the embryo and neural tube was removed by cutting through the foregut. FHF was separated from the SHF, which was further bisected into the anterior SHF (aSHF) and posterior SHF (pSHF). For E11.5 embryos, tissue in the region overlapping the former pSHF and aSHF was further bisected into R1, R2 and R3, R4, respectively. Proximal OFT and distal OFT were also dissected. Tails were kept for genotyping if necessary.

2.1.4 Fluorescence-Activated Cell Sorting

GFP signal was identified using a fluorescence dissecting microscope. GFP$^+$ and control SHF tissue from each E9.5 or E10.5 embryo was dissected and individually placed in 1.5 ml microcentrifuge tubes containing 50 μl sort buffer (PBS with 2% FBS and 25 mM HEPES) on ice. Sort buffer was then removed carefully and 50 μl 0.25% trypsin-EDTA was added to each tube. Tissues were digested into single cells by

33

incubating at 37°C on Thermomixer R (Eppendorf) for 10 minutes, along with pipetting

up and down every 2 minutes to facilitate tissue dissociation. Cells were then pelleted at

1,000 g for 3 minutes at 4°C and washed with 100 μl sort buffer. Centrifugation was

repeated and cells were resuspended in 500 μl sort buffer.

Cells were sorted using FACSAria IIu (BD Biosciences). Parameters used

depended on each run but generally the voltage for FSC, SSC and FITC was set to 126-

132, 226, and 445-451, respectively. Population of interest was first selected using a

SSC-A vs. FSC-A gate (P1) and singlets were selected using a SSC-A vs. FSC-W gate

(P2). The cutoff for calling a cell GFP$^+$ or GFP$^-$ was defined by selecting the maximum

FITC-A value generated by cells in the GFP$^-$ sample. Cells that fell in the intersection of

P1 and P2 and with FITC-A greater than the cutoff were sorted into 200 μl lysis buffer

from the RNA extraction kit. Approximately 1,000 to 4,000 cells were collected from

each E9.5 embryo and 7,000 to 28,000 cells were collected from each E10.5 embryo.

2.1.5 Low-Input RNA Sequencing

RNA from sorted E9.5 or E10.5 GFP$^+$ cells, or E11.5 tissues was extracted using

Absolutely RNA Nanoprep Kit (Agilent Technologies) and suspended in 5 μl Elution

Buffer. RNA quantification was performed on Bioanalyzer (Agilent Technologies) and a

relationship of approximately 3,500 cells corresponding to 1 ng RNA was established.

All RNA from each sample was used as input for reverse transcription using the

SMART-Seq v4 Ultra Low Input RNA Kit (Takara Bio). Briefly, first-strand cDNA

synthesis was performed according to manufacturer's instructions and cDNA was further

amplified using 12, 9, or 8 PCR cycles for E9.5, E10.5 or E11.5 samples, respectively, to

ensure similar yields. cDNA was quantified using Qubit (Thermo Fisher) and

34

Bioanalyzer and 1 ng was used as input for library preparation using Nextera XT DNA

Library Prep Kit (Illumina) and Nextera XT Index Kit (Illumina). Libraries were

quantified, normalized to 8 nM, pooled and further diluted to be sequenced on the

NextSeq (Illumina) using 75 bp paired-end sequencing.

2.1.6   Assay for Transposase Accessible Chromatin Sequencing

FHF, aSHF and pSHF tissues from E9.5 and E10.5 *wildtype* embryos were

collected and digested into single cell suspensions as described previously. Since the

transposition reaction is sensitive to input cell number, cells were counted on the cell

sorter and approximately 50,000 cells were used for each sample. Cells were lysed, open

chromatin regions were obtained and DNA libraries were prepared as described in the

standard protocol (Buenrostro et al., 2015). Briefly, genomic DNA fragments from open

chromatin regions were harvested using the Tn5 transposome from Nextera DNA Library

Preparation Kit (Illumina) and purified with MinElute Reaction Cleanup Kit (Qiagen).

Sequencing indices were added to the DNA fragments using 11 cycles of PCR, as

determined by qPCR side reaction. Libraries were then purified, quantified, normalized

and pooled for 75 bp paired-end sequencing.

2.1.7   Whole-Genome Bisulfite Sequencing

FHF, aSHF and pSHF tissues from E9.5 and E10.5 *wildtype* embryos were

collected and pooled in 500 µl lysis buffer (100 mM Tris-HCl, pH 8.5, 5 mM EDTA,

0.2% SDS, 200 mM NaCl and 0.5 mg/ml Proteinase K). Tissues were incubated at 56°C

overnight, followed by RNA removal by adding 2 µl RNAse A (10 mg/ml) and

incubating at 37°C for 1 hour. DNA was then extracted using phenol-chloroform

extraction and ethanol precipitation method. To prepare sequencing libraries, purified

genomic DNA was sonicated using Q700 Sonicator (Qsonica) to generate 400-500 bp

fragments. Index adaptors were ligated to the fragments using NEBNext Ultra II DNA

Library Prep Kit (NEB) and adaptor-ligated DNA was cleaned up without size selection.

Bisulfite conversion was performed using MethylCode Bisulfite Conversion Kit (Thermo

Fisher). An 8-cycle PCR was performed to add sequencing indices to the fragments using

KAPA HiFi HotStart Uracil+ ReadyMix (2X) (Kapa Biosystems) and NEBNext

Multiplex Oligos for Illumina (NEB). Libraries were then purified, quantified using

KAPA Library Quantification Kit (Kapa Biosystems), normalized and pooled for 75 bp

paired-end sequencing.

2.1.8   Chromatin Immunoprecipitation

SHF tissues from E9.5 and E10.5 *wildtype* embryos were collected and pooled in

PBS containing Complete Mini EDTA-free Protease Inhibitor Cocktail (Sigma-Aldrich)

on ice. Tissues were crosslinked in 1% formaldehyde in PBS on the rotator for 10

minutes. Crosslink was quenched by adding glycine to a final concentration of 0.125 M

and incubating for 5 minutes. Tissues were pelleted, washed once with PBS and stored at

-80°C until sufficient material was acquired for one chromatin immunoprecipitation

(ChIP). Approximately 100 or 60 SHF tissues were used for one E9.5 or E10.5 ChIP,

respectively. Tissues were pooled into Sonication Buffer (0.5% SDS, 20 mM Tris, pH

8.0, 2 mM EDTA, 0.5 mM EGTA, with freshly added 0.5 mM PMSF and Protease

Inhibitor), homogenized using Tissue Grinder (Axygen) and incubated for 30 minutes on

ice for cell lysis. Chromatin was sheared for 12 minutes into 200-1,000 bp fragments

using the S220 sonicator (Covaris) and the High Cell program, then diluted 5-fold in IP

Buffer (0.5% Triton X-100, 2 mM EDTA, 20 mM Tris, pH 8.0, 150 mM NaCl, 10%

glycerol, with freshly added 0.5 mM PMSF and Protease Inhibitor). After 1 hour of pre-clear at 4°C using Dynabeads Protein G (Life Technologies), chromatin was incubated with OSR1 antibody (sc-376529X, Santa Cruz) with rotation at 4°C overnight. Chromatin-antibody complexes were captured using Dynabeads Protein G and washed with Low Salt Buffer (0.1% SDS, 1% Triton X-100, 2 mM EDTA, 20 mM Tris, pH 8.0, 150 mM NaCl), High Salt Buffer (0.1% SDS, 1% Triton X-100, 2 mM EDTA, 20 mM Tris, pH 8.0, 500 mM NaCl), LiCl Buffer (1 mM EDTA, 10 mM Tris, pH 8.0, 0.25 M LiCl, 1% NP-40, 1% sodium deoxycholate) and TE Buffer (10 mM Tris, pH 8.0, 1 mM EDTA). Chromatin-antibody complexes were then eluted with Elution Buffer (1% SDS, 0.1 M NaHCO3), and reverse-crosslinked overnight at 65°C using NaCl. RNA and proteins were digested by incubating with RNAse A (Thermo Scientific) at 37°C and Proteinase K (Invitrogen) at 65°C, respectively. DNA was then purified using phenol-chloroform followed by ethanol precipitation.

2.1.9 RNA Extraction

Tissues used for independent validation of gene expression were stored in RNAlater Stabilization Solution (Thermo Fisher) upon collection, permeabilized at 4°C overnight and then transferred to -80°C for long-term storage. Tissues were homogenized on ice using PowerGen 125 (Fisher Scientific) and total RNA was extracted using RNeasy Mini Kit (Qiagen). Approximately 100 ng RNA was used for reverse transcription using ReadyScript cDNA Synthesis Mix (Sigma-Aldrich).

2.1.10 Quantitative PCR

Quantitative PCR (qPCR) was performed using PowerUp SYBR Green Master Mix (Applied Biosystems) on the CFX96 real-time system (Bio-Rad). Cycling program

included 2 minutes at 50°C, 2 minutes at 95°C, followed by 40 cycles of 15 seconds of denaturation at 95°C, 15 seconds of annealing at 55-60°C and 1 minute of extension at 72°C. Melt curve analysis was performed immediately after amplification to confirm primer specificity. 3 or more biological replicates were used for each condition and 2 technical replicates were performed for each sample.

Quantification data was analyzed using methods derived from the comparative C_T method (Schmittgen and Livak, 2008). For gene expression analysis, genes of interest were normalized to Gapdh and data was expressed as fold change against Gapdh ($\pm$ SEM). For ChIP assay analysis, enrichment of a region of interest was determined by interpolating from a standard curve generated with serial dilutions of the input control and data was shown in percentage of input (% input). Student's t-test was performed to determine statistical significance and $p < 0.05$ was considered significant.

2.1.11 Luciferase Reporter Assay

Regulatory regions were cloned upstream of a firefly *luc2* gene in the pGL4.23 reporter vector (Promega). pcDNA3 *Osr1* was a gift from Paul Danielian (Addgene plasmid # 26485; http://www.addgene.org/26485/; RRID: Addgene_26485). 2×10^4 HEK293 cells were plated per well in a 96-well plate containing 100 µl culture media (DMEM with 5% FBS and $1\times$ Antibiotic-Antimycotic). After 24 h, reporter vectors were transfected into the cells, with or without *Osr1* vector, using FuGENE HD Transfection Reagent (Promega). Cells were lysed and assayed 24 h after transfection using the Dual-Luciferase Reporter Assay System (Promega). Student's t-test was performed to determine statistical significance and $p < 0.05$ was considered significant.

2.1.12 Tissue Dehydration and Sectioning

Embryos were fixed in 10% buffered formalin phosphate at 4°C overnight. Tissues were washed in PBS for 15 minutes on an orbital shaker, then dehydrated in 50%, 70%, 80%, 95% (×2), and 100% (×2) Flex 100 alcohol (Thermo Scientific) sequentially. Clearing was performed using two rounds of xylene and infiltration was performed using three rounds of paraffin. Tissues were embedded in sagittal orientation and sectioned serially at 5 μm.

2.1.13 Immunohistochemical Staining

Tissue sections were deparaffinized using two rounds of xylene and rehydrated in 100% (×2), 90%, and 70% (×2) Flex 100 alcohol. Antigen retrieval was performed by incubating with 1× Citrate-Based Antigen Unmasking Solution, pH 6 (Vector Laboratories) for 20 minutes at above 95°C. After the slides have cooled down to room temperature, endogenous peroxidase activity was quenched by incubating in 3% H_2O_2 for 5 minutes. Immunolabeling was performed using the VECTASTAIN ABC Kit (Vector Laboratories) according to manufacturer's instructions with modifications for primary antibody incubation. Sections were incubated with SHH (ab86462, Abcam) or PTCH2 (MAB8096, R&D Systems) antibodies at 1:50 dilution overnight at 4°C, and with PDGFRB (3169, Cell Signaling Technology) antibody at 1:100 dilution for 2 hours at room temperature. Sections labeled with PTCH2, SHH or PDGFRB antibody were incubated with ImmPACT DAB peroxidase substrate (Vector Laboratories) for 5, 10, 10 minutes respectively, counterstained with hematoxylin for 10 seconds and dehydrated in 70%, 90%, 100% (×2) Flex 100 alcohol and xylene (×2).

2.1.14 RNA interference

Drosophila lines were obtained from the Bloomington Drosophila Stock Center at Indiana University. *Dot-Gal4* and *UAS-GFP* homozygous lines were balanced, then crossed with *Odd* or *Pvr* RNAi lines. Embryos were placed in a drop of halocarbon oil suspended from a coverslip and evaluated at the end of stage 16 by confocal microscopy (Reed et al., 2009).

2.1.15 Imaging

Endogenous $Osr1^{GFP}$ expression in E10.5 or E12.5 whole-mount embryos was detected using the FV3000 confocal laser scanning microscope (Olympus) with parameters: excitation wavelength = 488 nm, emission wavelength = 543 nm, laser intensity = 35%, high voltage = 700 volts, gain = 1.25×, offset = 3%, scanning speed = 4.0 µs/pixel, averaging = 2×. Z-stack images were captured at 10-20 µm intervals. Immunohistochemical staining was imaged using the BX63 upright microscope (Olympus).

2.2   Bioinformatic Analysis

2.2.1   Sequencing Quality Control and Alignment

Quality control was performed on reads from all sequencing runs using FastQC (v0.11.5) (http://www.bioinformatics.babraham.ac.uk/projects/fastqc/). Reads were mapped to the mouse reference genome GRCm38.91 (mm10) using HISAT2 (v2.1.0) (Kim et al., 2015; Pertea et al., 2016). Reads that were mapped to multiple locations were removed and only read pairs that were aligned uniquely and concordantly were retained for further analysis.

2.2.2 RNA-Seq Analysis

Transcript quantification and differential gene analysis were performed using the Cufflinks suite (v2.2.1) (Trapnell et al., 2012). Genes with false discovery rate (FDR) less than 0.05 were considered differentially expressed. Gene ontology (GO) and KEGG pathway analyses were performed using the R package clusterProfiler (v3.10.1) (Yu et al., 2012).

2.2.3 ATAC-Seq Analysis

Aligned reads were used for peak calling by MACS (v2.1.0) (Zhang et al., 2008) using FDR = 0.05 as cutoff. Peaks from biological replicates were merged using BEDTools (v2.28.0) (Quinlan and Hall, 2010) and assigned to the nearest gene using the R package ChIPseeker (v1.18.0) (Yu et al., 2015). Motif analysis of differential peaks was performed using the HOMER suite function findMotifsGenome.pl using default settings (v.4.10.4) (Heinz et al., 2010). Raw read counts were normalized to $1\times$ genome coverage for visualization.

2.2.4 Whole-Genome Bisulfite Sequencing Analysis

Bisulfite sequencing reads were aligned and CpG methylation was analyzed using Bismark (v0.16.3) (Krueger and Andrews, 2011). Regional methylation was defined as the average methylation level of 50-bp sliding windows. Differential methylation analysis was performed using an in-house program, which models the methylation percentage of each CpG site with a normal distribution and implements a t-test with regularized standard deviation. Differentially methylated regions (DMRs) located within 5 kb upstream to 1 kb downstream of transcription start sites were considered for integrative DNA methylation/gene expression analysis.

CHAPTER III

OSR1 REGULATES SECOND HEART FIELD PROGENITOR CELL MIGRATION DURING OUTFLOW TRACT FORMATION VIA *PDGFRB*

3.1   *Osr1* is Implicated in SHF Cell Migration

Given that conditional knockout of *Osr1* in the SHF results in OFT defects

(Figure 7), we hypothesized that the Osr1$^+$ population in SHF is critical for OFT

development. We evaluated the distribution of *Osr1$^{GCE/+}$* and *Osr1$^{GCE/LacZ}$* cells at E10.5

and E12.5 using whole-mount confocal microscopy and found an ectopic distribution of

the Osr1$^+$ population at both stages (Figure 8). At E10.5, whereas *Osr1* expression was

located mainly in the posterior SHF (pSHF) at caudal splanchnic mesoderm in *Osr1$^{GCE/+}$*

control embryos, it was shifted rostrally towards the anterior SHF (aSHF) in *Osr1$^{GCE/LacZ}$*

mutants (Figures 3D-F and 8A). Preliminary genetic inducible fate mapping studies have

shown that descendants of Osr1$^+$ cells contribute to the pulmonary trunk in

Osr1$^{GCE/+}$;R26R$^{fl/+}$ embryos (Figure 4). Expression analysis confirmed *Osr1* expression

in the pulmonary trunk in E12.5 *Osr1$^{GCE/+}$* control embryos (Figure 8B, upper panel).

Strikingly, in *Osr1$^{GCE/LacZ}$* mutants *Osr1* expression was also found in the aorta, in

addition to the pulmonary trunk (Figure 8B, lower panel).

3.2 Transcriptional Profiling of Osr1$^+$ SHF Population

In order to identify *Osr1* target genes that are involved in SHF progenitor migration, we sought to analyze the transcriptome of *Osr1$^{GCE/+}$* (Het) and *Osr1$^{GCE/LacZ}$* (KO) cells. Since the SHF is a heterogeneous progenitor population composed of multiple cell lineages, we purified the Osr1 cell lineage from E9.5 and E10.5 SHF using fluorescence-activated cell sorting (FACS) (Figure 9A). *Osr1$^{GCE/+}$* and *Osr1$^{GCE/LacZ}$* cells were isolated, with *Osr1$^{+/+}$* or *Osr1$^{LacZ/+}$* cells as negative controls (Figure 9B, C). Cells from select embryos were reanalyzed after sorting. The respective proportion of Osr1-GFP$^+$ cells in E9.5 and E10.5 SHF before sorting was 18.47±1.02% and 29.50±1.22%, and was 95.67±2.33% and 91.95±1.95% after sorting (mean ± SEM, $n = 2$-3; Figure 9D), confirming that FACS achieved high purity. Analysis of cells collected per embryo revealed that the number of Osr1-GFP$^+$ cells in *Osr1$^{GCE/+}$* SHF increased from 3199.82±587.10 at E9.5 to 15475.80±3122.04 at E10.5, and from 2486.00±605.00 at E9.5 to 13556.62±2565.89 at E10.5 in *Osr1$^{GCE/LacZ}$* SHF (mean ± SEM, $n = 4$-7; Figure 9E), demonstrating no genotype-specific difference.

To investigate the transcriptome of *Osr1$^{GCE/+}$* and *Osr1$^{GCE/LacZ}$* cells, total RNA was extracted from the cells and mRNA was subjected to RNA sequencing (RNA-seq). Data quality and reproducibility were accessed by performing principal component analysis (PCA) using 2474 most variable genes among all samples (Figure 10A). Stage-specific difference was clearly distinguished on PC1 (Figure 10A). Interestingly, *Osr1$^{GCE/+}$* and *Osr1$^{GCE/LacZ}$* cells demonstrated more differential transcriptional profiles at E10.5, compared to E9.5 (Figure 10B). To understand the cause of this phenomenon, a regression model was used to identify the genes that were differentially expressed only as

a result of stage difference, but not due to genotype difference. 4240 differentially expressed genes (DEGs) were found between E9.5 and E10.5 (FDR < 0.05). Gene ontology (GO) analysis of the "biological process" category formed several clusters of ontology terms (Figure 11). The largest cluster, as well as a smaller cluster highlighted enrichment for nucleotide synthesis and metabolism. In addition, two small clusters showed enrichment for mesenchyme and muscle tissue development.

To identify the candidate targets that are transcriptionally regulated by *Osr1*, we compared the transcriptome of *Osr1$^{GCE/+}$* and *Osr1$^{GCE/LacZ}$* cells at E9.5 and E10.5. At E9.5, 109 genes were upregulated and 98 genes were downregulated, and 390 and 429 genes were up- or downregulated at E10.5 (FDR < 0.05, fold change > 1.2 or < 0.83; Figure 12, Table S3 and S4, Appendix). GO analysis of DEGs from E9.5 and E10.5 identified similar overrepresented terms in the "biological process" category, such as "epithelial tube morphogenesis", "mesenchyme development", and "mesenchymal cell differentiation" (Figure 13A, B). KEGG pathways such as "focal adhesion", "cell adhesion molecules", and "ECM-receptor interaction" were also enriched at both E9.5 and E10.5 (Figure 13C, D). Among the DEGs overlapped between E9.5 and E10.5, many are involved in tight junctions, cell adhesions, tissue connectivity and movement including *Cdh1*, *Cdh3*, *Cldn4*, *Cldn6*, *Cldn7*, *Col1a2*, *Col3a1*, *Col9a1*, *Itga6*, *Itga8*, *Myl7*, and *Mylk3* (Figure 14).

3.3   *Osr1* Mediates OFT Formation via *Pdgfrb*

We hypothesized that the ectopic distribution of Osr1$^+$ cells might be caused by a dysregulation of cell migration in the *Osr1* mutants at early stages. We intersected the DEGs between *Osr1$^{GCE/+}$* and *Osr1$^{GCE/LacZ}$* cells with 1414 genes under the "cell

migration" GO term and found that 41 out of 207 DEGs and 62 out of 819 DEGs were involved in cell migration processes at E9.5 and E10.5, respectively (Figure 15). We further hypothesized that cell signaling receptors are important mediators that transduce external migration cues to the SHF. We validated the expression of key receptors with known functions in migration (Abe et al., 2007; Duchek et al., 2001; High et al., 2009; Riahi et al., 2015; Ruest and Clouthier, 2009; Veevers-Lowe et al., 2011) by performing qPCR using sorted $Osr1^{GCE/+}$ and $Osr1^{GCE/LacZ}$ cells and found that all but $Notch1$ were significantly downregulated in $Osr1^{GCE/LacZ}$ cells (E9.5: $Ackr3$: fold change = 0.78, p = 0.0234; $Ednra$: fold change = 0.44, p = 0.0397; $Pdgfrb$: fold change = 0.65, p = 0.0264; E10.5: $Ackr3$: fold change = 0.82, p = 0.0052; $Ednra$: fold change = 0.61, p = 0.0120; $Pdgfrb$ = 0.67, p = 0.0333; $Notch1$: fold change = 1.60, p = 0.0133) (Figure 16).

We next sought to test whether $Osr1$ activates these genes via physical interaction. OSR1-bound genomic regions were captured by performing ChIP on pooled *wildtype* SHF tissues and multiple pairs of primers were designed to examine OSR1 binding at the promoter of our genes of interest by qPCR (Table S2, Appendix). As expected, OSR1 bound to the promoter of $Pdgfrb$, $Ackr3$ and $Ednra$ ($Pdgfrb$-R3: 0.15±0.03% input; $Ackr3$-R1: 0.11±0.01% input; $Ednra$-R1: 0.11±0.03% input, $Ednra$-R3: 0.15±0.11% input) (Figure 17A). To further test for $Osr1$ induction, we cloned the promoter region of $Pdgfrb$ containing the confirmed OSR1 binding region upstream of a firefly $luc2$ gene in the pGL4.23 reporter vector and transfected into HEK293 cells with an $Osr1$ expression vector (Table S2). $Osr1$ significantly transactivated the expression of the $luc2$ reporter gene in cells transfected with the $Pdgfrb$-pGL4 vector, compared to

those transfected with pGL4, which contains a minimal promoter (fold change = 2.41, p = 0.0005) (Figure 17B).

To further investigate the dynamic signaling patterns in the migration path to OFT, we dissected the E11.5 $Osr1^{GCE/+}$ or $Osr1^{GCE/LacZ}$ embryos sequentially. Since SHF cell identity is lost at E11.5, we dissected what was originally pSHF into R1 and R2 regions, what was originally aSHF into R3 and R4 regions, bisected the OFT into distal OFT (dOFT) and proximal OFT (pOFT), and subjected the tissues to RNA-seq (Figure 18A). A linear regression model was used to identify the genes that exhibited an expression gradient from R1 to pOFT in $Osr1^{GCE/+}$ control embryos that was disrupted in $Osr1^{GCE/LacZ}$ mutants. After removal of low-expressing genes which could constitute background noise, 634 genes were found with an $Osr1$-dependent expression gradient, which included 257 genes with increasing expression from R1 to pOFT and 377 genes with decreasing expression ($p < 0.05$) (Table S5). Interestingly, $Osr1$ expression exhibited a dramatic decrease from R1 to pOFT, which was reduced to background level in mutants (Figure 18B). The averaged expression increase from R1 to pOFT was relatively mild, with little variation between $Osr1^{GCE/+}$ and $Osr1^{GCE/LacZ}$ embryos (Figure 18C). To confirm this, we tested for Dhh, the ligand of Hh pathway and $Pdgfd$, the ligand of PDGF pathway by qPCR, which showed increasing, albeit $Osr1$-independent expression from R1, R2 to OFT (Figure 19). In contrast, the averaged expression decrease was more pronounced, and the gradient was almost completely obliterated in $Osr1^{GCE/LacZ}$ mutants (Figure 18D), which is demonstrated by $Pdgfrb$ expression (Figure 20).

To functionally test the requirement of *Osr1* for *Pdgfrb* in the developing OFT, we examined the PDGFRB protein levels at E11.5. Sagittal sections of *Osr1$^{GCE/+}$* and *Osr1$^{GCE/LacZ}$* embryos were immunostained with antibodies against PDGFRB. In *Osr1$^{GCE/+}$* control embryos, PDGFRB was highly expressed in dOFT (Figure 21b) and exhibited an expression decrease from dOFT to pOFT, consistent with mRNA levels (Figure 20). In contrast, in *Osr1$^{GCE/LacZ}$* mutants the expression decrease was lost (Figure 21b') and expression was significantly reduced (Figure 21c and c'), indicating that *Osr1* deficiency disrupted the PDGFRB gradient in OFT and *Osr1* is required for PDGFRB normal expression. Interestingly, PDGFRB expression was also observed in the atrioventricular (AV) cushions, with similar levels in control and mutant embryos (Figure 21d and 21d').

To investigate whether the roles of our target genes in heart development are evolutionarily conserved, we further performed functional studies in *Drosophila* in collaboration with the laboratory of Dr. Linglin Xie at Texas A&M University. During *Drosophila* cardiogenesis, *Odd* is expressed in pericardial cells starting at stage 12/2 (Ward and Skeath, 2000). The transgene *Dorothy-Gal4* (*Dot-Gal4*) marks the hematopoietic system and pericardial cells in the larvae (Kimbrell et al., 2002). When evaluated at the end of stage 16, GFP$^+$ pericardial cells formed two rows residing along the dorsal midline in control larvae (Figure 22A), as previously reported (Kimbrell et al., 2002). In contrast, knockdown of *Odd* in pericardial cells via RNA interference (RNAi) resulted in a disorganization of pericardial cell alignment, as evidenced by the two rows becoming discontinuous and scattered (Figure 22B). Strikingly, larvae with Dot-Gal4$^+$ cell-specific deletion of *PDGF- and VEGF-receptor related* (*Pvr*), homolog of the mouse

Pdgfrb, displayed more anomalies, with pericardial cells mislocated not only in regions surrounding the midline, but also at the anterior and posterior poles of the larvae (Figure 22C).

3.4   Several Hedgehog Signaling Molecules Exhibit *Osr1*-Independent Expression in the Developing OFT

A key regulator of SHF proliferation and migration is Hedgehog (Hh) signaling (Dyer and Kirby, 2009; Dyer et al., 2010). Deficiency in Hh signaling leads to OFT elongation and septation defects, arch artery defects and right ventricle hypoplasia (Dyer and Kirby, 2009; Goddeeris et al., 2007; Smoak et al., 2005). In addition, fate mapping of Hh-receiving SHF cells reveals the lineage migration from the pharyngeal mesoderm into the pulmonary artery between E9.5 and E11.5 (Hoffmann et al., 2009). We asked if Hh signaling is perturbed in *Osr1* mutant cells. The main Hh receptors *Smo* and *Disp1*, as well as the downstream effector *Gli1* remained unchanged in the Osr1 cell lineage in mutant embryos (Figure 23A). We simultaneously interrogated the promoter of these genes for OSR1 binding. *Smo* and *Disp1* promoters demonstrated OSR1 binding, with highest enrichment of 0.18±0.06% and 0.46±0.09% of input control, respectively, whereas *Gli1* showed minimal binding, with highest enrichment of 0.06±0.02% of input control (mean ± SEM; $n = 3$) (Figure 23B). Notably, both *Smo* and *Disp1* promoters exhibited an increasing OSR1 binding intensity from distal to proximal promoter, suggesting that the most active OSR1-DNA interactions within the promoter occur near the TSS.

Shh is a major ligand of the Hh pathway that is required for the survival of SHF and CNC (Goddeeris et al., 2007; Smoak et al., 2005). We asked if *Osr1* plays a role in

the expression of *Shh* and its receptor *Ptch2*. Immunostaining showed that SHH and PTCH2 were stably expressed in OFT and AV cushions, however, no significant difference in expression could not be detected between mutant and control embryos (Figure 24).
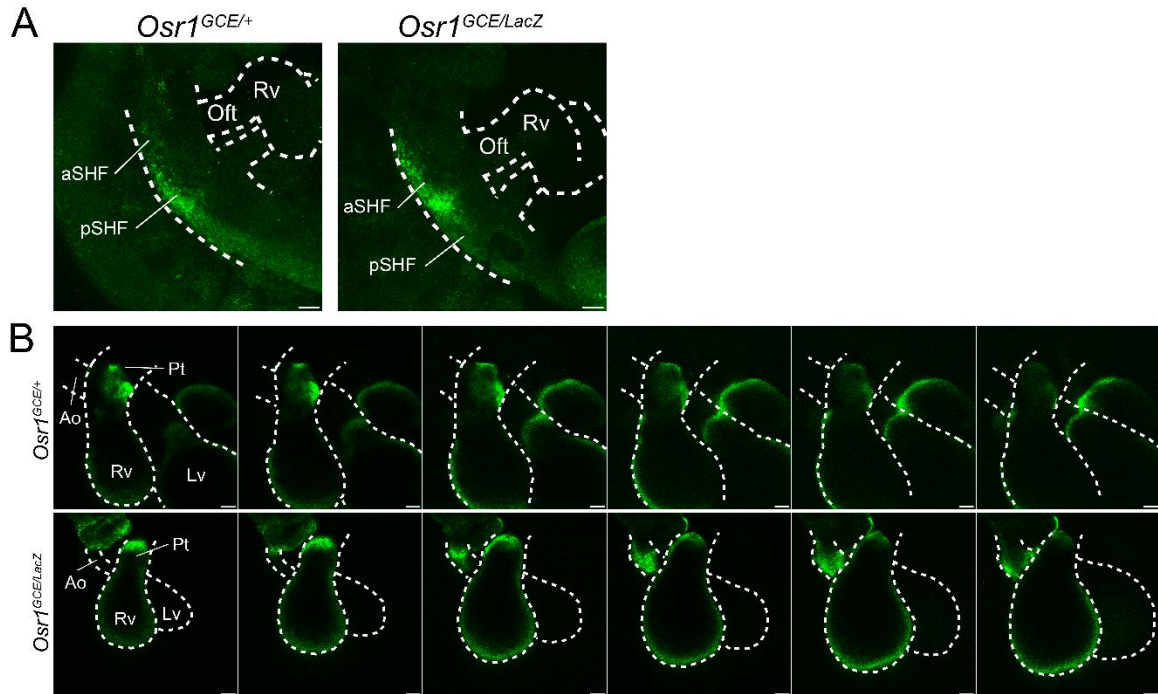
Figure 8. Osr1$^+$ population is ectopically distributed at E10.5 and E12.5.

(A) Whole-mount confocal microscopy of E10.5 hearts. (B) Whole-mount confocal microscopy of E12.5 hearts. aSHF, anterior second heart field; pSHF, posterior second heart field; Oft, outflow tract; Rv, right ventricle; Lv, left ventricle; Ao, aorta; Pt, pulmonary trunk. Scale bars, 100 µm.
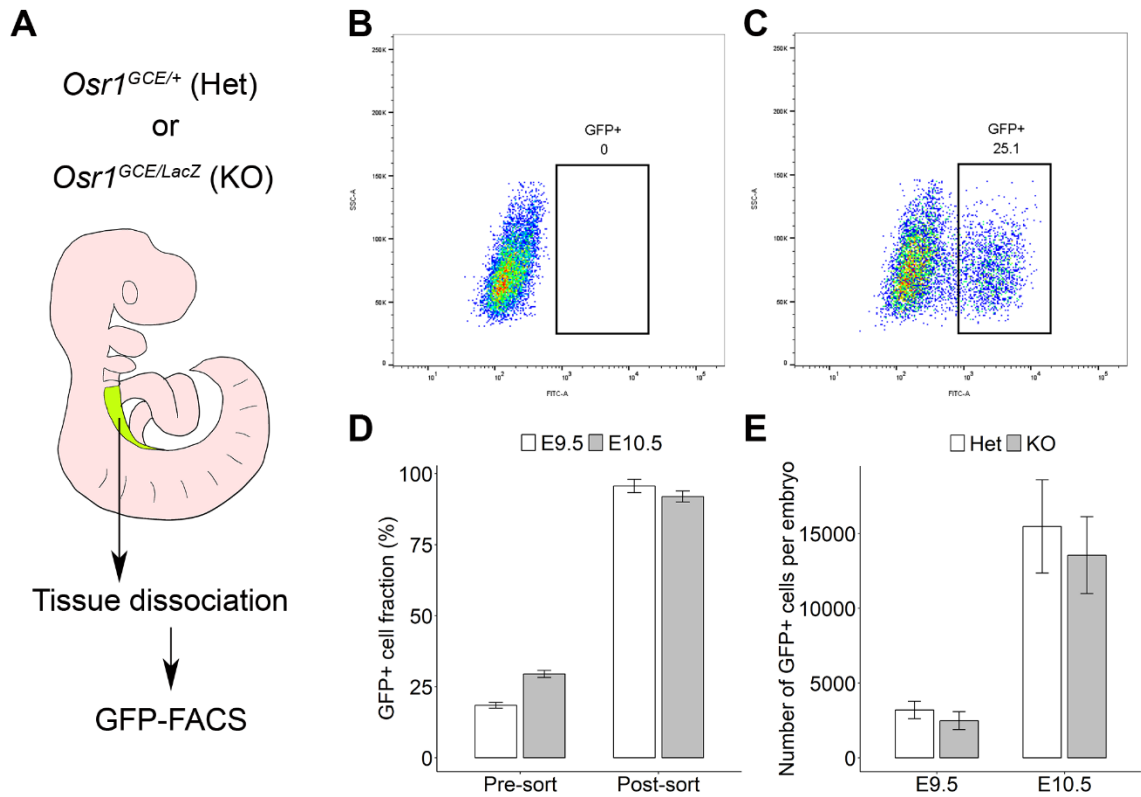
Figure 9. Isolation of Osr1-GFP$^+$ population in the SHF.

(A) Schematic diagram of the FACS isolation procedure of Osr1-GFP$^+$ cells from SHF. (B, C) Example dot plots of events from an Osr1-GFP$^-$ embryo and an Osr1-GFP$^+$ embryo. Rectangle in (C) marks Osr1-GFP$^+$ cells collected. (D) Percentage of Osr1-GFP$^+$ cells before and after FACS isolation (mean ± SEM, n = 2-3). (E) Average number of cells collected per embryo (mean ± SEM, n = 4-7). Het, heterozygous; KO, knockout.
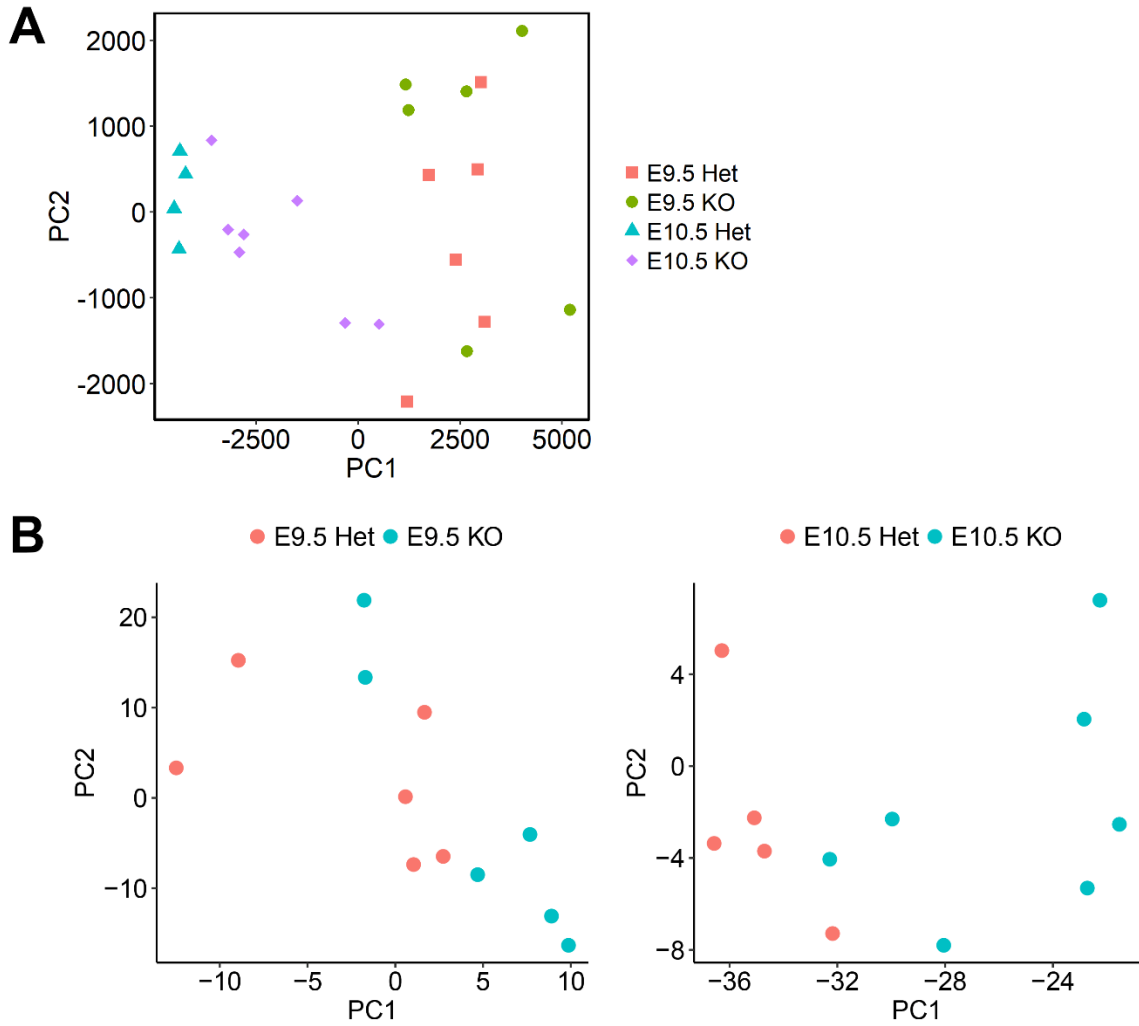
Figure 10. Principal component analysis of E9.5 and E10.5 RNA-seq profiles.

(A) Principal components of all E9.5 and E10.5 samples. (B) Principal components of E9.5 samples (left) and E10.5 samples (right).
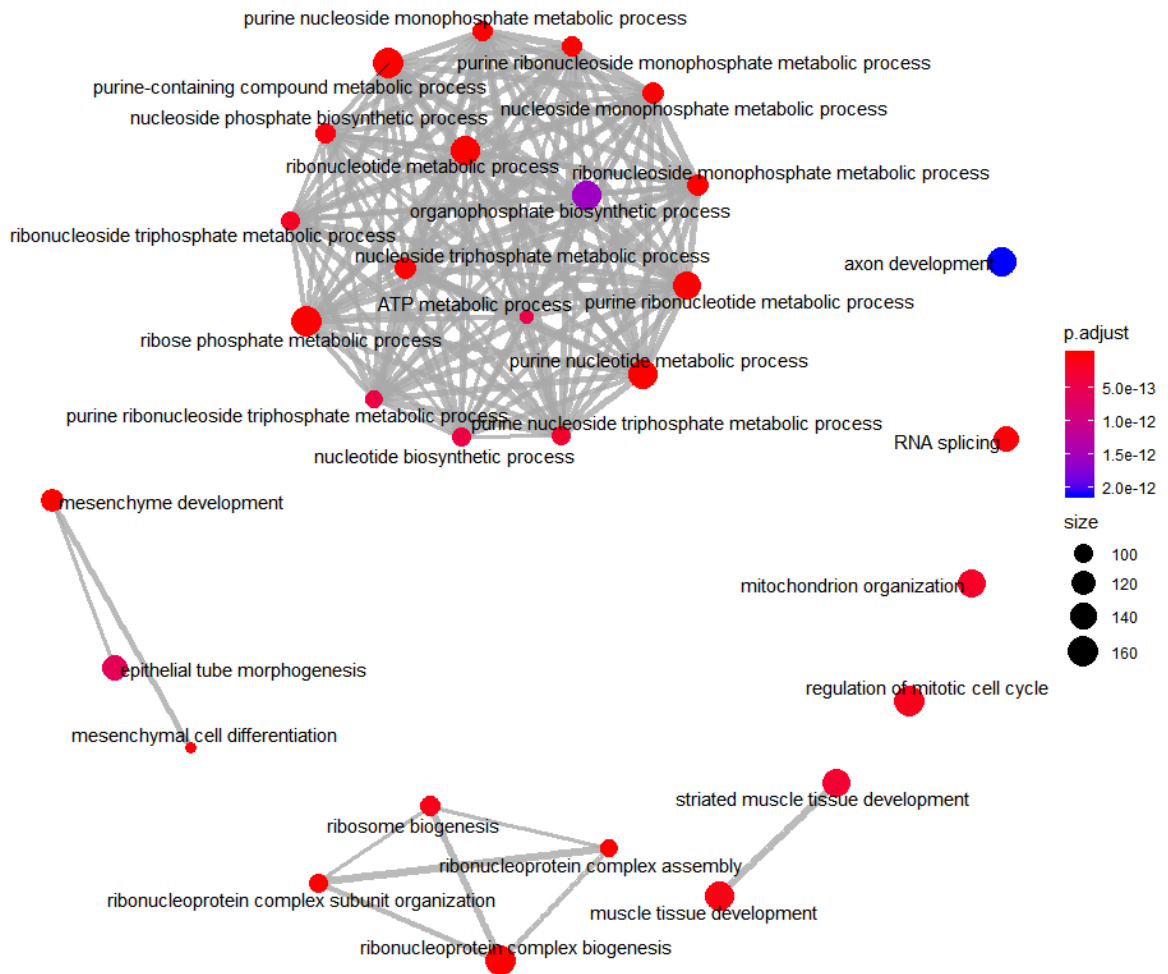
Figure 11. Osr1^{+} population undergoes active proliferation and differentiation between E9.5 and E10.5.

Enrichment map of GO "biological process" terms representing stage-specific DEGs between E9.5 and E10.5. Het, heterozygous; KO, knockout; DEG, differentially expressed gene.
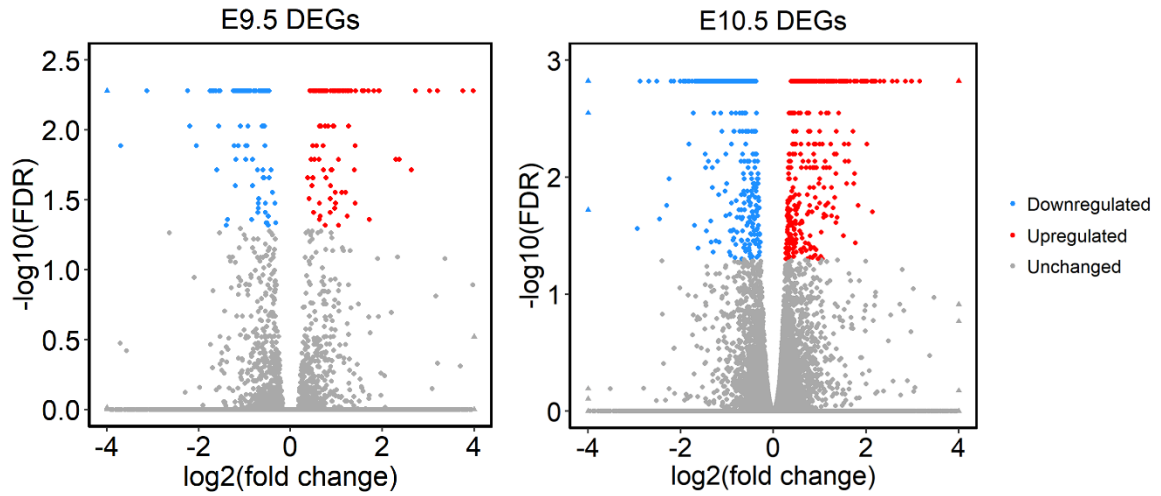
Figure 12. Differentially expressed genes between *Osr1*^{GCE/LacZ} and *Osr1*^{GCE/+} cells at E9.5 and E10.5.

Volcano plots of DEGs defined as genes with FDR < 0.05 and log2(fold change) > 0.26 (upregulated, red) or < -0.26 (downregulated, blue). DEG, differentially expressed gene; FDR, false discovery rate.
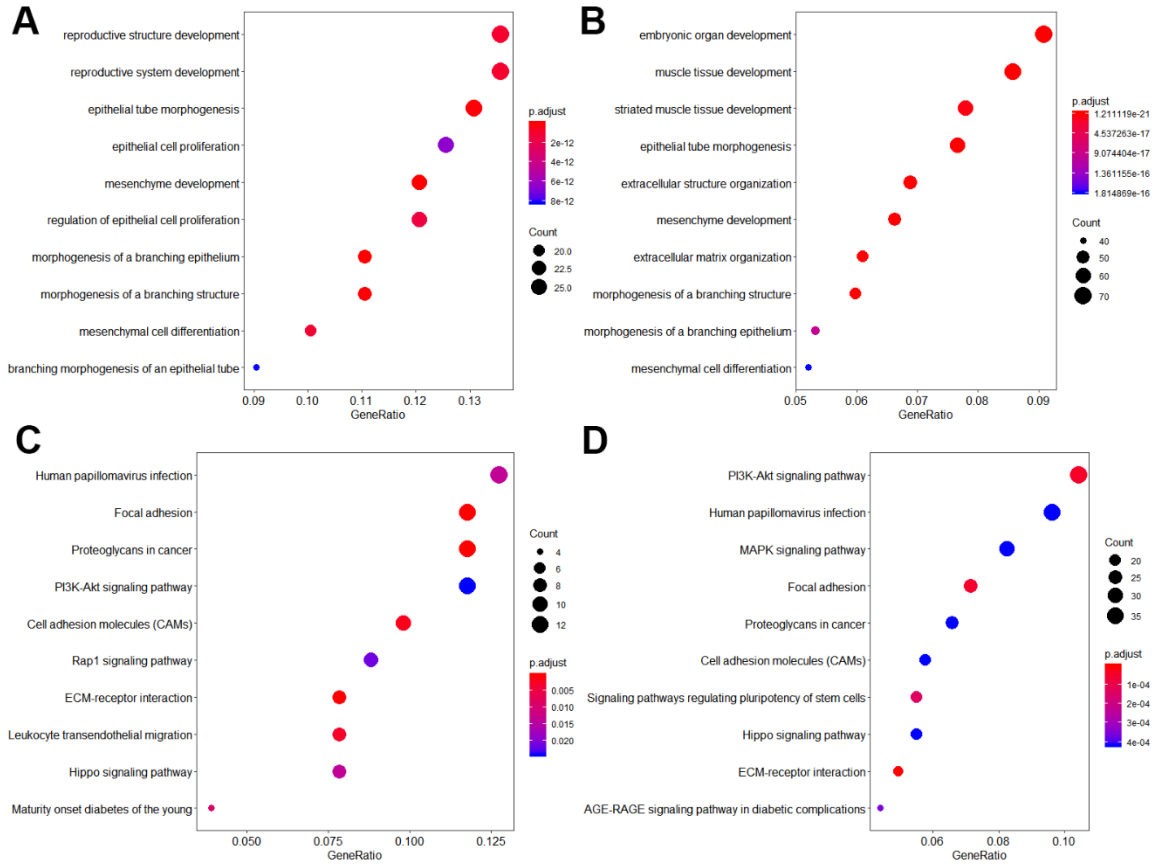
Figure 13. GO and KEGG pathway analysis at E9.5 and E10.5.

(A, B) Overrepresented GO biological processes at E9.5 (A) and E10.5 (B). (C, D) Overrepresented KEGG pathways at E9.5 (C) and E10.5 (D). GeneRatio, ratio between the number of genes in the pathway of interest and the number of total DEGs.
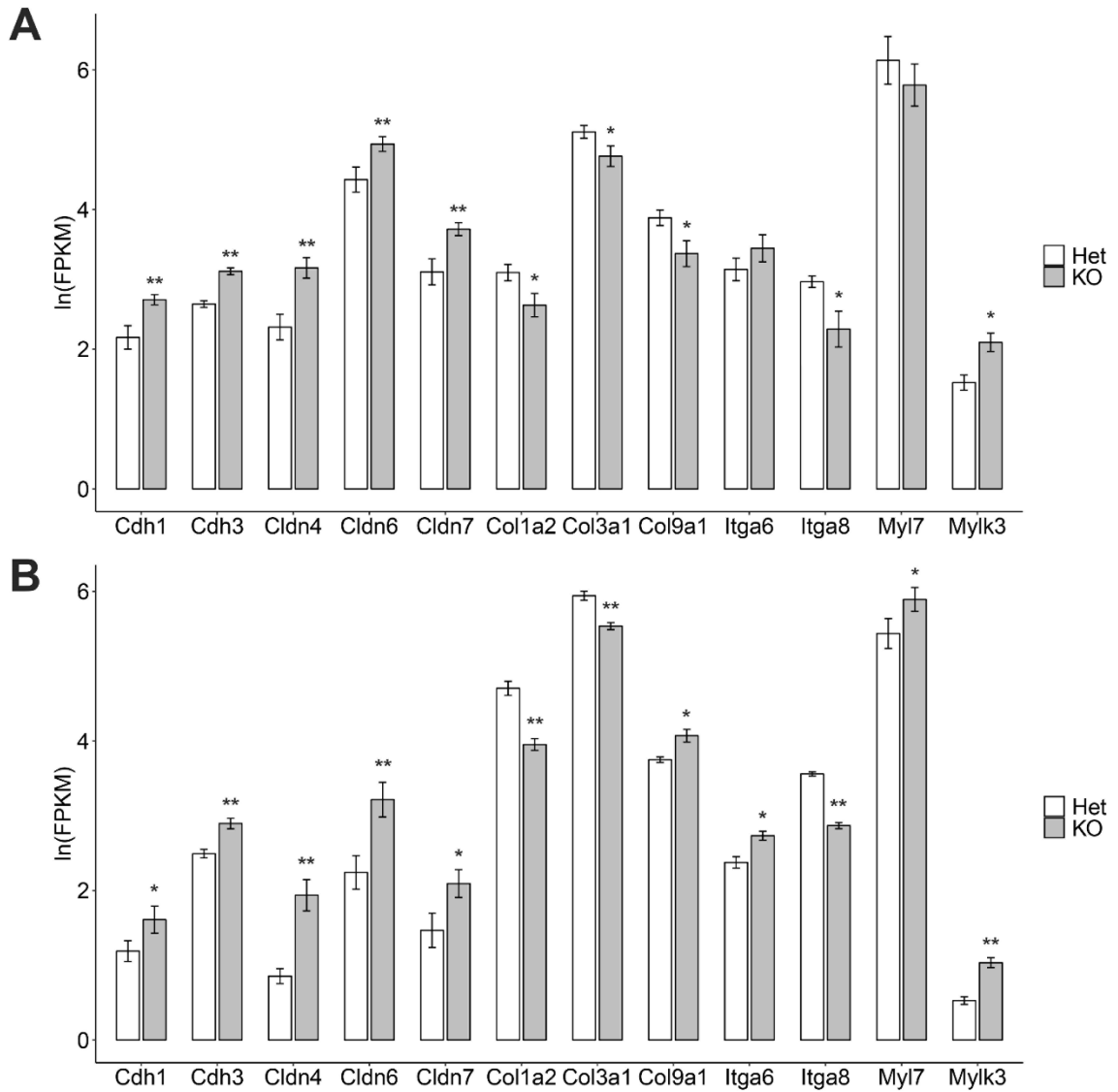
Figure 14. *Osr1* is required for genes involved in tight junctions, cell adhesions, tissue connectivity and movement.

(A) Gene expression in E9.5 sorted cells. (B) Gene expression in E10.5 sorted cells. *: FDR < 0.05, **: FDR < 0.01.
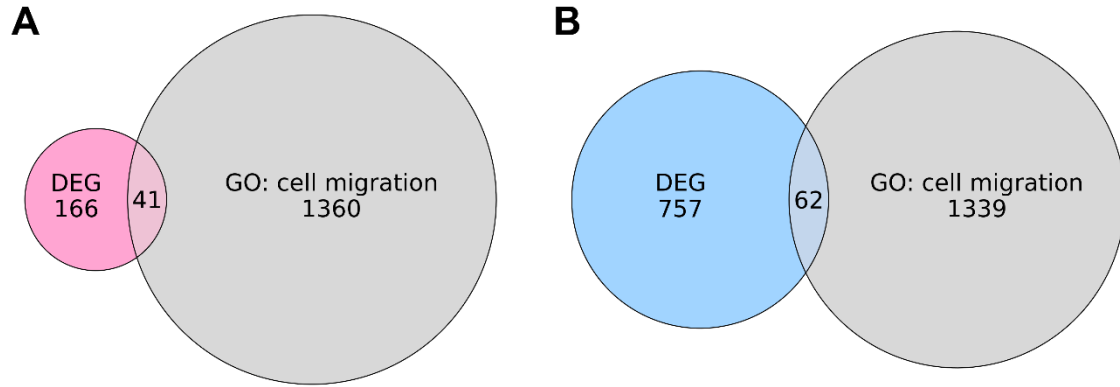
Figure 15. *Osr1*-dependent genes are involved in cell migration.

(A) The overlap between E9.5 DEGs and genes under the "cell migration" GO term. (B) The overlap between E10.5 DEGs and genes under the "cell migration" GO term.
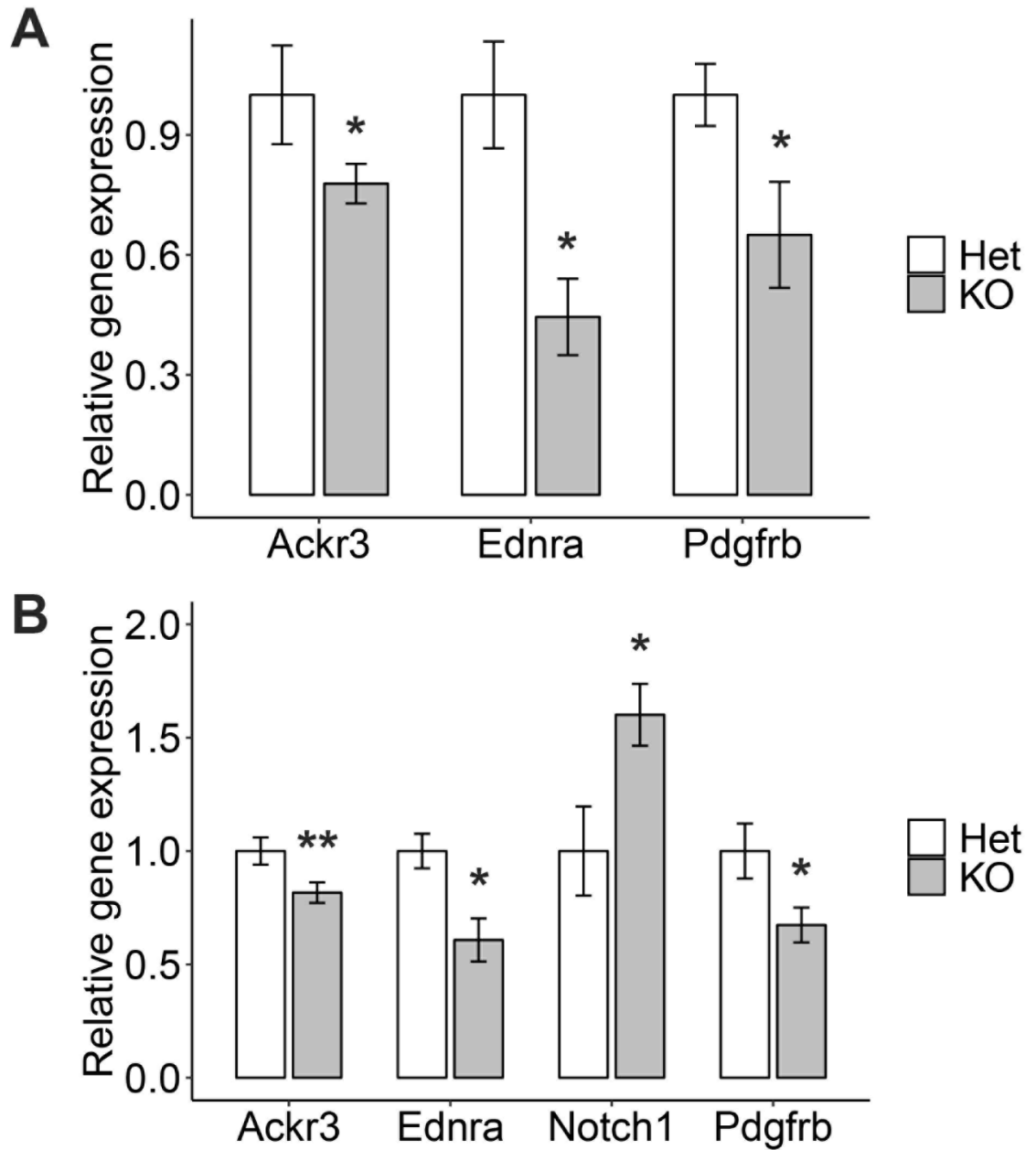
Figure 16. *Osr1* is required for cell migration receptor expression.

(A) Relative expression of signaling receptor genes involved in cell migration at E9.5 evaluated by qPCR. (B) Relative expression of signaling receptor genes involved in cell migration at E10.5 evaluated by qPCR. Values represent mean ± SEM (n = 5-7). *: $p < 0.05$, **: $p < 0.01$.
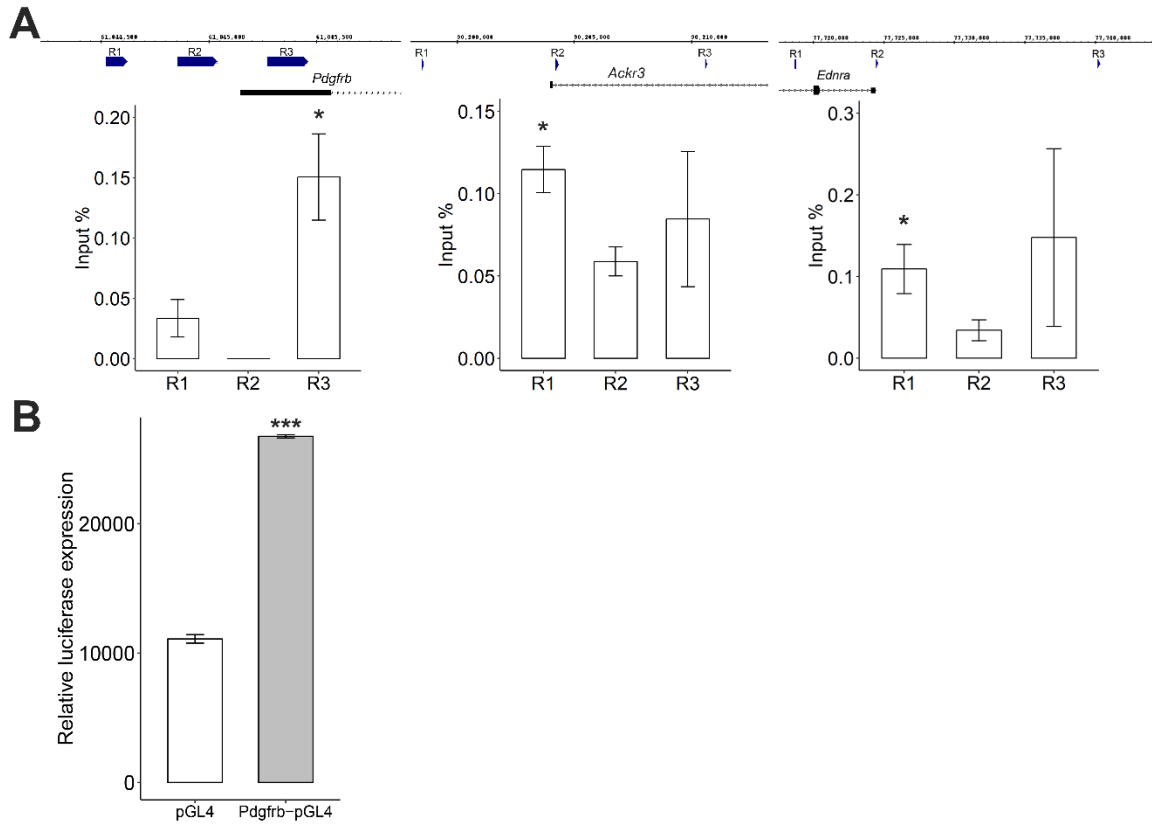
Figure 17. OSR1 interacts with the promoter of cell migration markers in SHF.

(A) OSR1 binding examined at multiple promoter regions of *Pdgfrb*, *Ackr3*, and *Ednra*.
(B) Effect of *Osr1* on *Pdgfrb* promoter assessed by promoter-driven *luc2* reporter
activity. Values represent mean ± SEM ($n = 3$). *: $p < 0.05$, ***: $p < 0.001$.
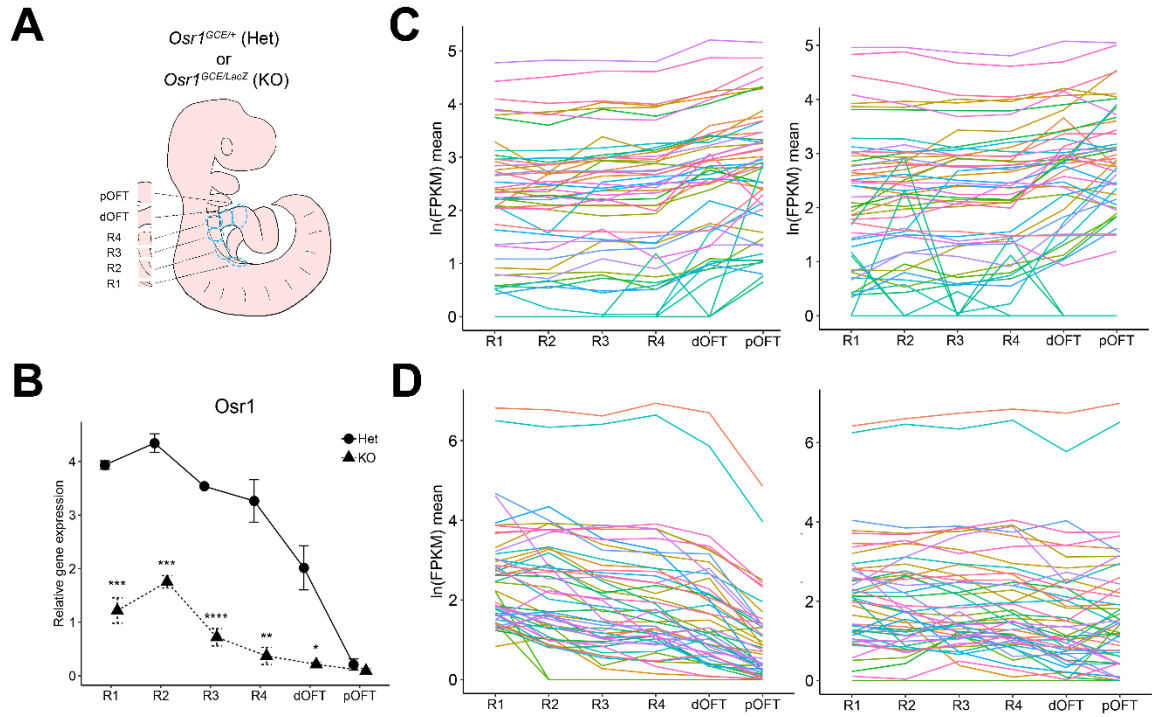
Figure 18. *Osr1* maintains gene expression gradients between SHF and OFT.

(A) Schematic depiction of dissection strategy for tissue RNA-seq. (B) Expression of *Osr1* from R1 to pOFT. (C) Expression distributions of top 50 genes with increasing gradients from R1 to pOFT. (D) Expression distributions of top 50 genes with decreasing gradients from R1 to pOFT. *: $p < 0.05$, **: $p < 0.01$, ***: $p < 0.001$, ****: $p < 0.0001$.
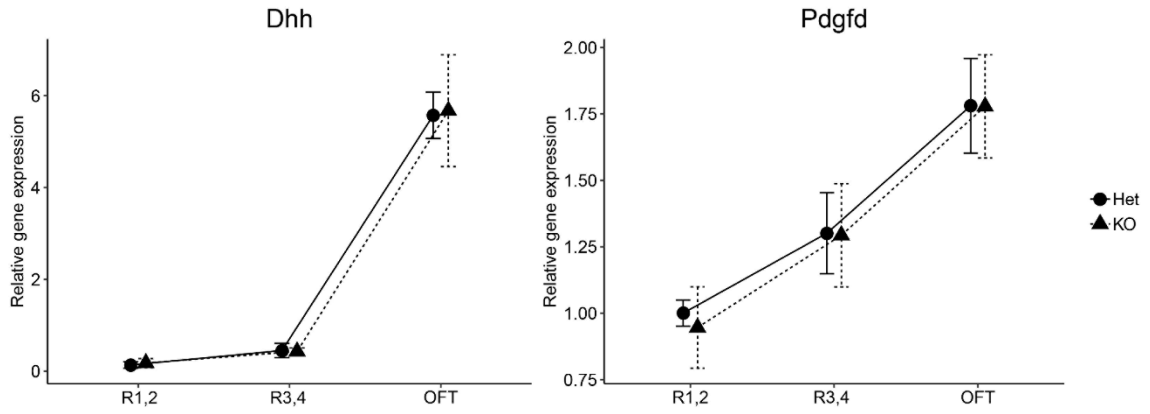
Figure 19. *Dhh* and *Pdgfd* show increasing gradient from R1, R2 to OFT.

Relative expression of Hh and PDGF ligands at E11.5 evaluated by qPCR. Values represent mean ± SEM (*n* = 3).
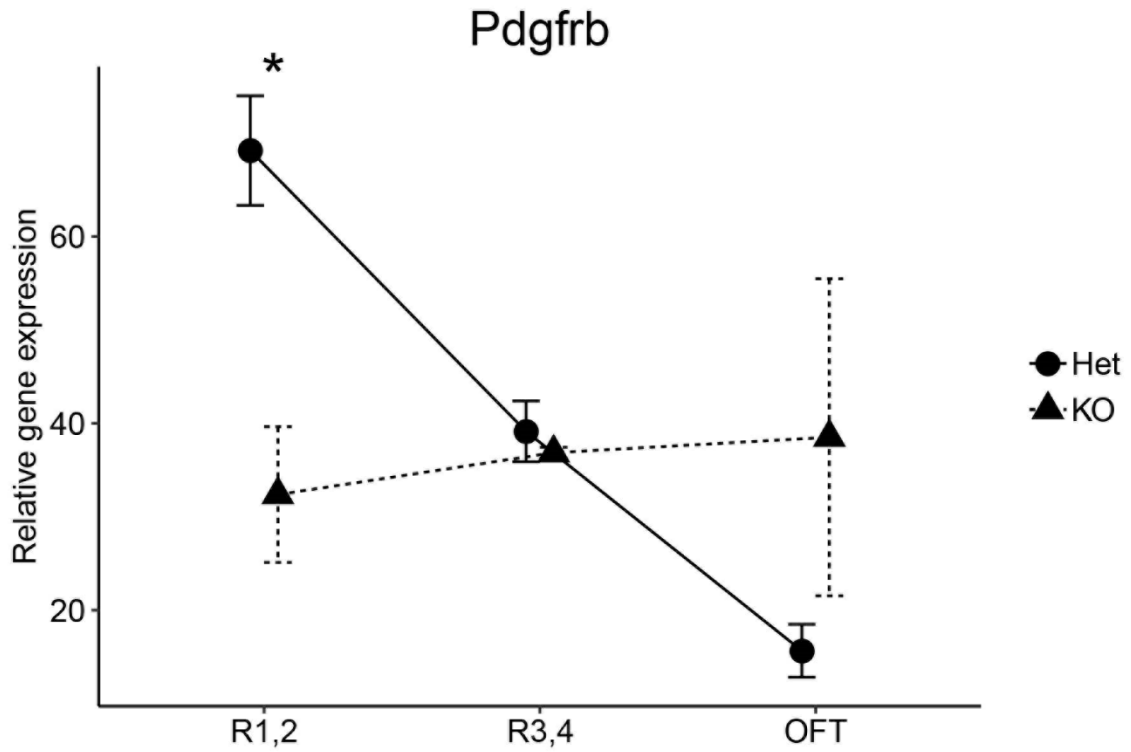
Figure 20. *Pdgfrb* expression gradient is maintained by *Osr1* from pSHF to OFT.

Relative expression at E11.5 evaluated by qPCR. Values represent mean ± SEM ($n = 3$).
*: $p < 0.05$.
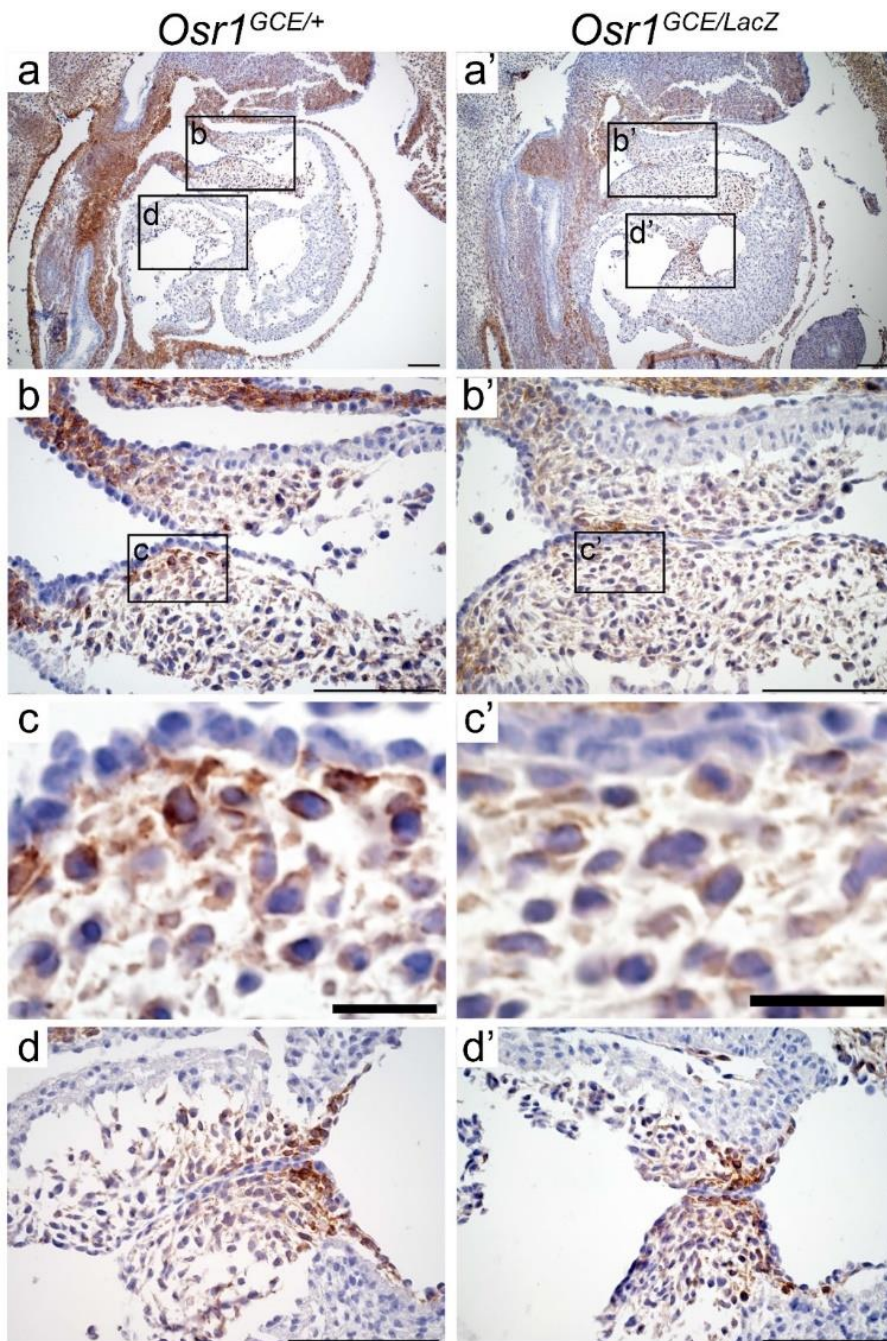
Figure 21. *Osr1* maintains PDGFRB gradient in OFT.

PDGFRB staining in E11.5 heart sections. (a and a') Expression of PDGFRB in the whole heart region. (b and b') Expression of PDGFRB in the OFT cushion. (c and c') PDGFRB expression in OFT cushion at higher magnification. (d and d') Expression of PDGFRB in the AV cushion. Scale bars, 100 µm except 20 µm in (c) and (c'). *n* = 3-5.
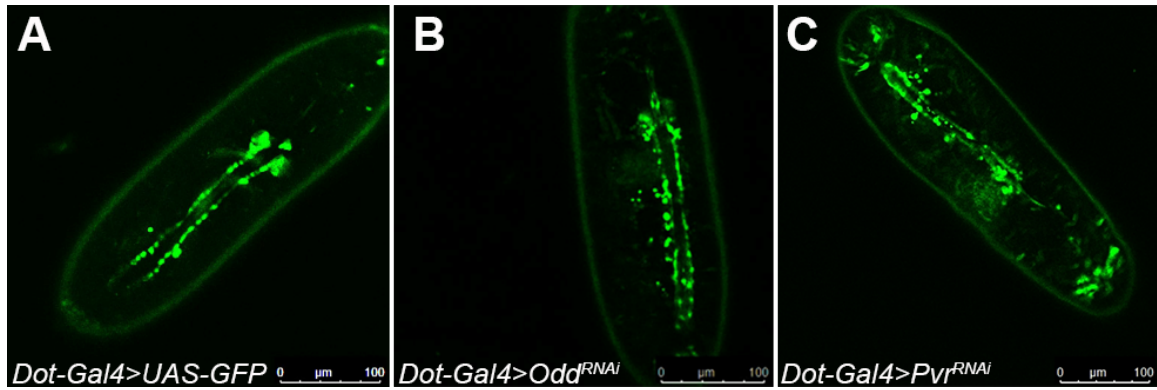
Figure 22. *Odd* and *Pvr* are required for *Drosophila* pericardial cell organization.

(A) Pericardial cells in control larvae. (B) Pericardial cells in larvae with pericardial cell-specific *Odd* RNAi. (C) Pericardial cells in larvae with pericardial cell-specific *Pvr* RNAi. Scale bars, 100 µm.
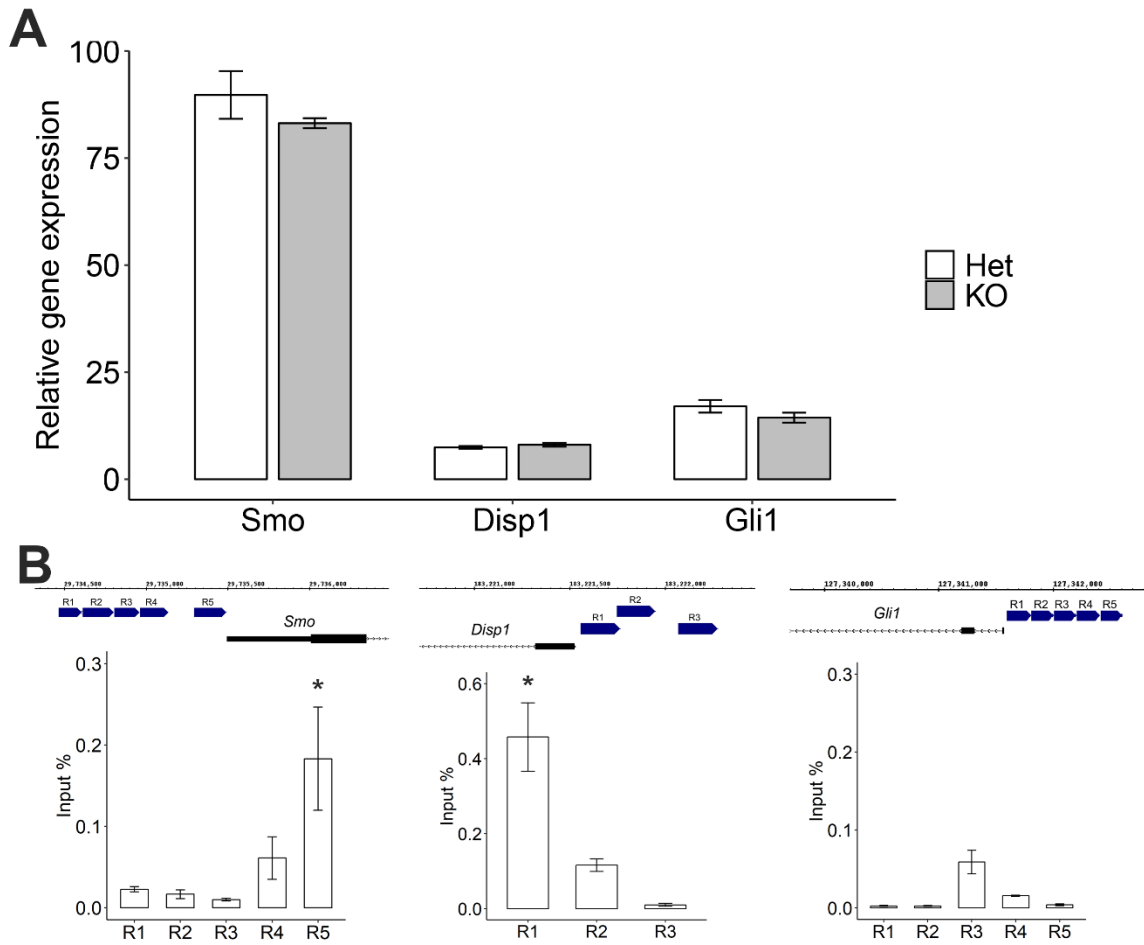
Figure 23. OSR1 interacts with the promoter of *Smo*, *Disp1* and *Gli1* in SHF.

(A) Relative expression of Hh signaling genes at E9.5. (B) OSR1 binding examined at multiple promoter regions of *Smo*, *Disp1*, and *Gli1*. Values represent mean ± SEM (*n* = 3).
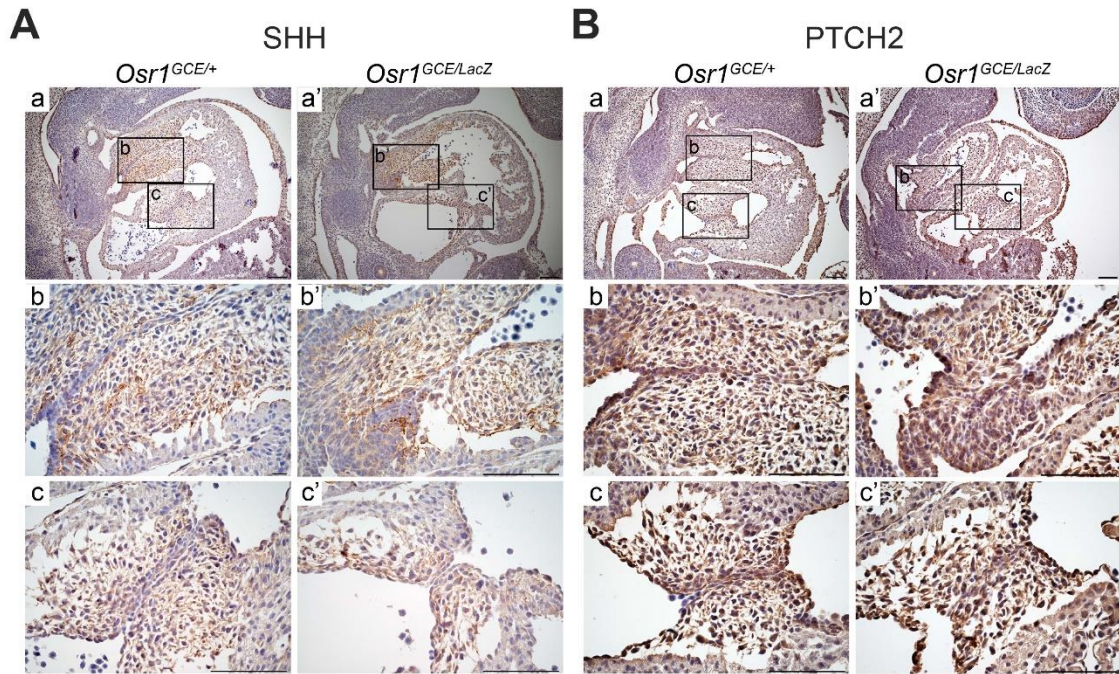
Figure 24. SHH and PTCH2 levels are unchanged in *Osr1* mutants.

SHH and PTCH2 staining in E11.5 heart sagittal sections. (Aa, Ba and Aa', Ba')
Expression of target proteins in the whole heart region. (Ab, Bb and Ab', Bb')
Expression of target proteins in the OFT cushion. (Ac, Bc and Ac', Bc') Expression of
target proteins in the AV cushion. Scale bars, 100 µm. n = 3-5.

CHAPTER IV

EPIGENETIC MECHANISMS ORCHESTRATING HEART FIELD SPECIFICATION

The SHF is a heterogeneous population and consists of subregions that have distinct cell fates. Whereas aSHF contributes to the developing OFT and right ventricle, pSHF contributes mainly to the atria and inflow tract (Galli et al., 2008; van Vliet et al., 2017). Our previous RNA-seq data (unpublished) has identified key cardiac transcription factors that display differential expression patterns in aSHF and pSHF, which may contribute to the disparity in their cell fates. Here we aimed to elucidate the molecular mechanisms that shape the transcriptional profiles of aSHF, pSHF and FHF.

4.1 Transcription Factor Binding Sites in Accessible Genomic Regions Demonstrate Tissue-Specificity

We hypothesized that the cell identities of FHF and SHF might be orchestrated by epigenetic mechanisms, which modulate transcriptional activities by altering chromatin configurations and accessibility of gene regulatory elements. We first sought to obtain an overview of the global chromatin landscape of aSHF, pSHF and FHF using Assay for Transposase Accessible Chromatin sequencing (ATAC-seq), a next generation sequencing technique which identifies open genomic regions using the Tn5 transposome (Buenrostro et al., 2015, 2013). Two biological replicates were used for each group and only the open genomic regions detected by both replicates were considered for analysis. Interestingly, large proportions of open regions were located within promoters, defined

67

by 1 kb upstream of the transcription start site (TSS) to 1 kb downstream, although the percentages decreased from E9.5 to E10.5 significantly (Figure 25). We next compared the tissue-specific open regions at the two stages and found that the vast majority of regions were shared between aSHF and pSHF at both E9.5 and E10.5 (Figure 26). When comparing chromatin accessibility between stages, we found that aSHF, pSHF and FHF all had a significantly greater number of peaks at E10.5, which overlapped with the vast majority of peaks at E9.5 in the respective tissues (Figure 27).

Open chromatin configuration generally indicates active transcription activities. We performed transcription factor binding motif analysis to determine possible tissue-specific transcription factor regulation (Table 1). We found that MEF2C and GATA4 motifs were enriched in the FHF when compared to SHF (Table 1). Interestingly, we observed an enrichment of PDX1, HOX, LHX and ISL1 motifs in SHF-specific peaks, when compared to FHF (Table 1). However, when comparing accessible regions between E9.5 and E10.5 of the same tissue, no stage-specific motif enrichment was found (data not shown).

4.2   DNA Methylation is Correlated with Tissue-Specific Gene Expression

We hypothesized that the region-specific expression of cardiac transcription factors is coordinated by DNA methylation and examined the global DNA methylation states in aSHF and pSHF by performing whole-genome bisulfite sequencing (WGBS). Both aSHF and pSHF demonstrated high average genome-wide CpG methylation at both E9.5 and E10.5 (Figure 29A). However, when focusing on the CpG sites located in accessible genomic regions, average CpG methylation decreased significantly and exhibited tissue-specific and stage-specific difference (Figure 29B). Using an in-house

program, we identified differentially methylated regions (DMRs) of 50 base pairs, and associated gene expression with DMRs located within promoter regions. Heatmap and hierarchical clustering using variable DMRs across all samples showed distinct DNA methylation profiles between SHF and FHF, as well as between aSHF and pSHF (Figure 29). As expected, the difference between regions (SHF vs FHF) was larger than the difference between stages (E9.5 vs E10.5). Since promoter DNA methylation has been shown to inhibit gene expression (Bird and Wolffe, 1999; Fujita et al., 2003; Huck-Hui and Bird, 1999; Maurano et al., 2015; Watt and Molloy, 1988), we performed KEGG pathway analysis on genes showing inversely correlated expression and DNA methylation patterns between aSHF and pSHF, aSHF and FHF, and pSHF and FHF (Table 2). DEGs associated with DMRs between aSHF and pSHF were involved in cell adhesion, extracellular matrix, and cell cycle, whereas those between SHF and FHF were involved in major heart development signaling pathways such as Hedgehog pathway and Notch pathway (Table 2).

We investigated the relationship between DNA methylation and gene expression at specific SHF markers and cardiac transcription factors. *Tbx5* showed a highly methylated site within its promoter in aSHF, in accord to a low expression in aSHF (Figure 30A). In contrast, *Fgfr3* showed a highly methylated site within its promoter in pSHF, in accord to a low expression in pSHF (Figure 30B). In addition, we integrated ATAC-seq data and found that cardiac transcription factors *Gata3*, *Hey1* and *Osr1* were differentially expressed in aSHF and pSHF, although chromatin was equally accessible at these loci in aSHF and pSHF (Figure 31). DMRs were found near these genes and methylation level was inversely correlated with their gene expression, suggesting that

69

DNA methylation might play an inhibitory role in region-specific cardiac transcription factor expression in the SHF.
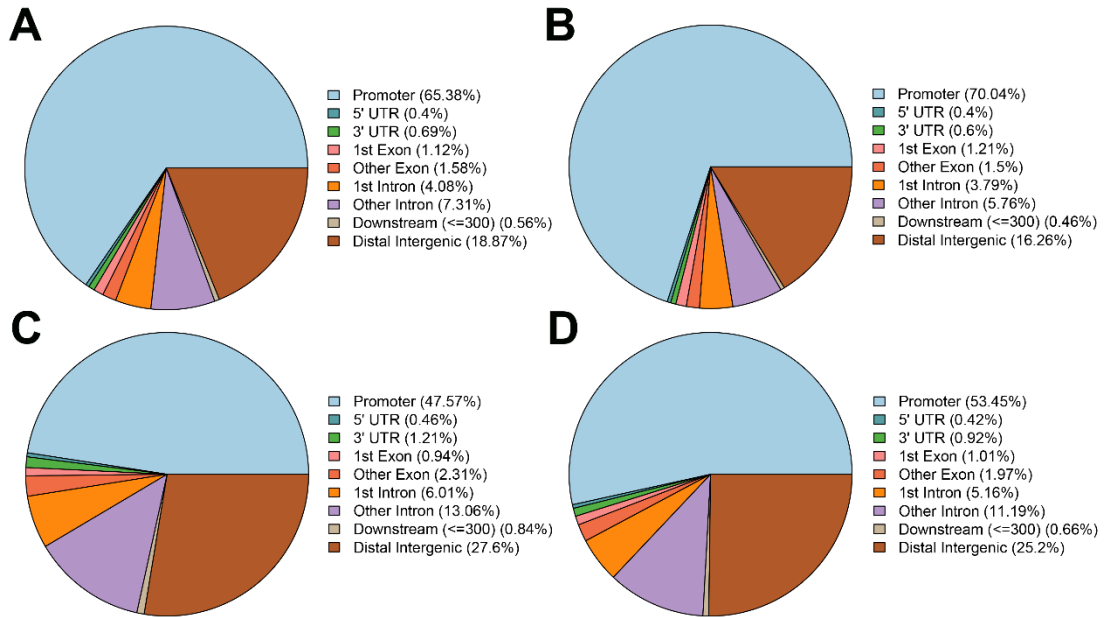
Figure 25. Genomic distribution of open chromatin regions.

(A) Genomic distribution of open chromatin regions in E9.5 aSHF. (B) Genomic distribution of open chromatin regions in E9.5 pSHF. (C) Genomic distribution of open chromatin regions in E10.5 aSHF. (D) Genomic distribution of open chromatin regions in E10.5 pSHF.
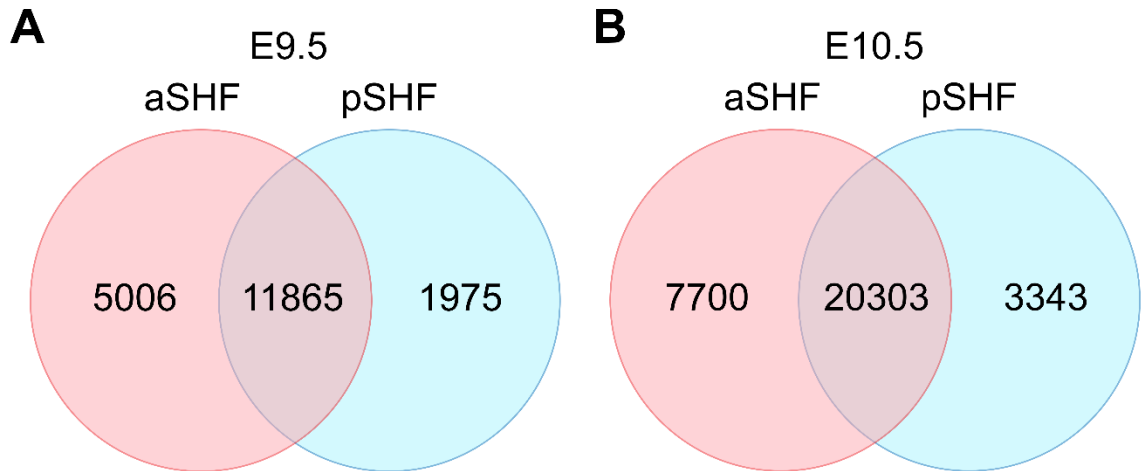
Figure 26. aSHF and pSHF share accessible chromatin regions.

(A) Number of accessible chromatin regions unique to aSHF, pSHF or shared between them at E9.5. (B) Number of accessible chromatin regions unique to aSHF, pSHF or shared between them at E10.5.
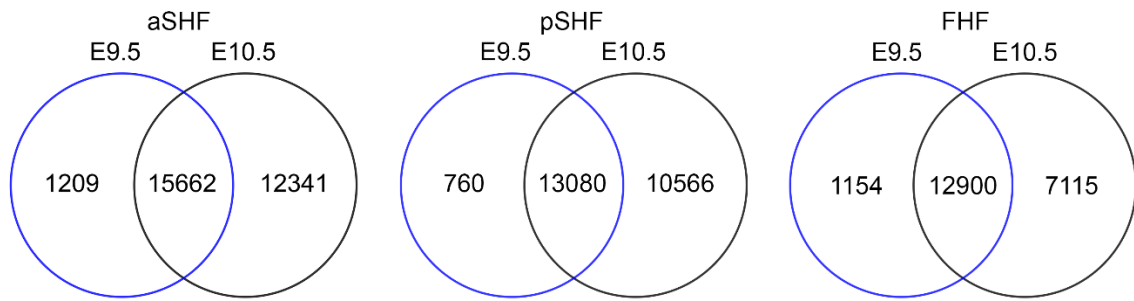
Figure 27. Accessible chromatin regions are shared between stages.

Table 1. Tissue-specific transcription factor binding motifs.

FHF v SHF			SHF v FHF		
TF	*p*-value	Motif	TF	*p*-value	Motif
MEF2C	1e-31	CTATTTTTAG	PDX1	1e-20	CCATCAATCA
GATA4	1e-8	CTGATAAGG	HOX	1e-18	TGATTGATGG
GATA1	1e-7	CCATATAAGG	PBX2	1e-14	GTGATTTATGGC
SIX1	1e-6	TATCAGGCTC	LHX	1e-9	AATTAATTAA
SNRNP70	1e-6	GTCATCAAGCAC	SIX1	1e-7	GGATCACTTAC
ETS	1e-4	CAGGAGACAGCT	ISL1	1e-7	CTAATTGC
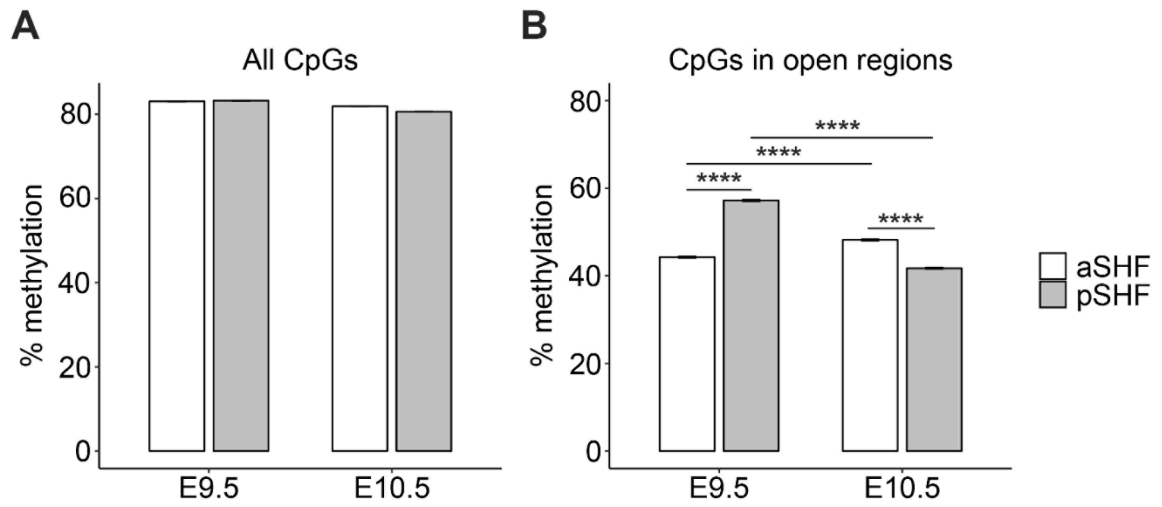
Figure 28. Genome-wide CpG methylation levels.

(A) Average methylation levels of all CpG sites. (B) Average methylation levels of CpG sites in accessible genomic regions. ****: $p < 0.0001$.
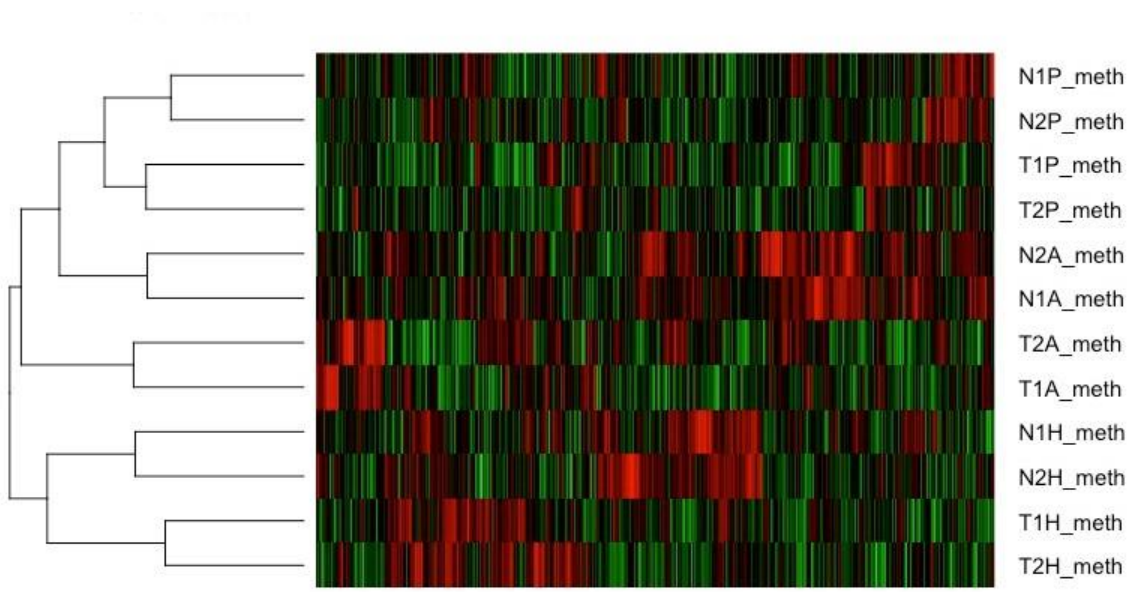
Figure 29. Heatmap of variable DMRs.

Table 2. Heart development-related KEGG pathways of DMRs

aSHF v pSHF		aSHF v FHF		pSHF v FHF	
Pathway	*p*-value	Pathway	*p*-value	Pathway	*p*-value
ECM-receptor interaction	0.000342	Cardiac muscle contraction	0.002411	Adherens junction	0.001280
DNA replication	0.002126	Hedgehog signaling pathway	0.015686	Signaling pathways regulating pluripotency of stem cells	0.007377
Focal adhesion	0.008448	Notch signaling pathway	0.020902	Hedgehog signaling pathway	0.035469
Dilated cardiomyopathy	0.013422	Dilated cardiomyopathy	0.022970	Notch signaling pathway	0.046524
TGF-beta signaling pathway	0.013707			Wnt signaling pathway	0.048551
Cell cycle	0.024199				
Cell adhesion molecules	0.043409				
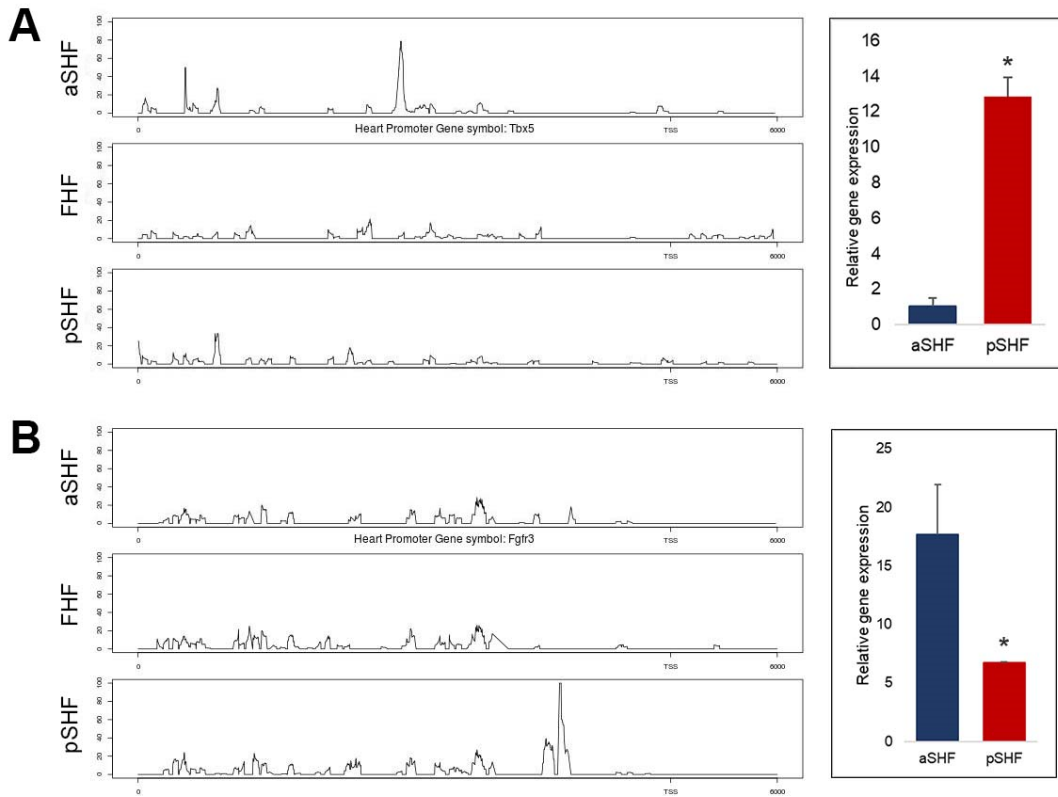
Figure 30. DNA methylation is correlated with regional expression of SHF markers.

(A) Promoter DNA methylation level and gene expression of *Tbx5*. (B) Promoter DNA methylation level and gene expression of *Fgfr3*.
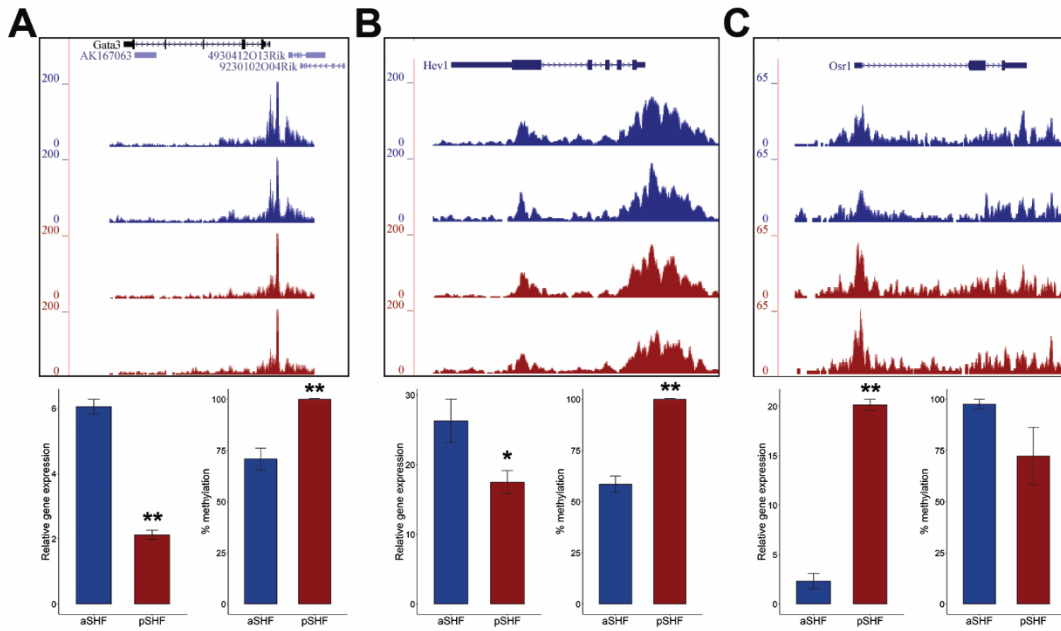
Figure 31. DNA methylation is correlated with regional expression of cardiac transcription factors in the SHF.

(A) Open chromatin sequence coverage, relative gene expression and methylation rate of *Gata3*. (B) Open chromatin sequence coverage, relative gene expression and methylation rate of *Hey1*. (C) Open chromatin sequence coverage, relative gene expression and methylation rate of *Osr1*.

CHAPTER V

DISCUSSION

The cardiac outflow tract (OFT) is a transient conduit that develops into the aorta and pulmonary trunk which connect the embryonic heart chambers to the vascular network. OFT defects constitute approximately 30% of congenital heart defects and are detrimental to the establishment of separate systemic and pulmonary circulations (Benjamin et al., 2018). The extra-cardiac cell population originating from the splanchnic mesoderm, known as the second heart field (SHF), is a multipotent progenitor population that plays critical roles in the arterial and venous poles of the elongating heart tube and contributes to the myocardium and endocardium of the OFT (Buckingham et al., 2005; Hoffmann et al., 2009; Kelly et al., 2001; Lin et al., 2012; Mjaatvedt et al., 2001; Verzi et al., 2005; Waldo et al., 2001).

Our group has devoted large efforts to studying the role of transcription factor *Osr1* in SHF and the mechanisms that lead to various congenital heart diseases as a result of *Osr1* dysfunction. We found that *Osr1* is essential for the proliferation and cell cycle progression, but not the survival of posterior SHF progenitor cells (Zhou et al., 2015). On the molecular level, we found that *Osr1* is a downstream target of *Tbx5*, and that compound *Osr1* and *Tbx5* deficiency increase the incidence of septal defects (Xie et al., 2012; Zhou et al., 2015). In addition, we found that *Osr1* expression is dependent on

Gata4 and *Shh* (Zhou et al., 2017). These evidences place *Osr1* in the cardiac regulatory network that orchestrates progenitor specialization.

SHF-specific *Osr1* deficiency resulted in abnormal conotruncal transition, OFT elongation as well as conotruncal heart defects including DORV and OA (Figure 5-7), which suggest that *Osr1* in the SHF is critical for OFT formation. The current study aimed to determine the cellular and molecular functions of *Osr1* during OFT development. It is the first study to map the fate of the Osr1 cell lineage in OFT formation and the first study to identify *Osr1* transcription targets on a global scale using gene perturbation with a systems approach. Using a tamoxifen-induced Cre-lox system, we localized the Osr1$^+$ descendent cells in the pulmonary trunk upon OFT remodeling completion (Figure 4). However, the cell lineage was found to be ectopically distributed in the aorta instead in *Osr1* knockout embryos (Figure 8), which suggests that the *Osr1* lineage might undergo aberrant migration when the *Osr1* signal is lost, an indication of a cell autonomous mechanism for *Osr1* regulation of OFT development. To identify the possible signals for the Osr1 lineage migration, we performed RNA-seq on *Osr1* heterozygous and knockout cells sorted from the SHF. Differentially expressed genes (DEGs) from E9.5 and E10.5 showed enrichment of elevated GO biological processes such as nucleotide synthesis and metabolism, as well as mesenchyme and muscle tissue development, indicating that the Osr1$^+$ population is undergoing active proliferation and transcription, confirming the multipotent nature of SHF mesenchymal progenitors (Figure 11, Table S4 and S5, Appendix). In addition, many DEGs shared between E9.5 and E10.5 were involved in tight junctions, cell adhesions, tissue connectivity and movement

(Figure 13 and 14), suggesting that *Osr1* may be an essential regulator for cell interaction activities in the SHF.

We further investigated the segmental changes in migration signals by performing RNA-seq on contiguous tissue sections in the migration path from SHF to OFT (Figure 18, Table S5). On the genome-wide scale, the increasing gene expression gradients from R1 to pOFT were relatively mild, whereas the increasing gene expression gradients were more pronounced, and the gradients were almost completely obliterated in *Osr1* mutants (Figure 18). This suggests that *Osr1* is required to maintain the expression gradient of genes from SHF to OFT, especially those that exhibit higher expression in SHF and lower expression in OFT.

The platelet-derived growth factor (PDGF) pathway plays critical roles in embryonic development, cell migration, and angiogenesis. We discovered *Pdgfrb*, cell surface receptor for PDGF, as a novel transcription target of *Osr1*. In the developing heart, *Pdgfrb* is expressed in atrioventricular cushion mesenchymal cells and mutation of *Pdgfrb* gives rise to atrioventricular septal defects, and hypoplasia of the valves or compact myocardium (Van den Akker et al., 2008; Bax et al., 2010; Peng et al., 2017). We found consistent downregulation of *Pdgfrb* in *Osr1* knockout SHF progenitors at both E9.5 and E10.5 (Figure 16), and confirmed that OSR1 acts on *Pdgfrb* promoter via direct binding (Figure 17). In addition to atrioventricular cushion, we also observed PDGFRB expression in the OFT cushion, as well as in the SHF (Figure 21). *Pdgfrb* showed a decreasing expression gradient from SHF to OFT that was *Osr1*-dependent, both transcript and protein level (Figure 20 and 21). Furthermore, we showed that the *Drosophila Pdgfrb* homolog *Pvr* is required for the alignment and organization of *Odd-*

expressing pericardial cells in the *Drosophila* larvae (Figure 22), demonstrating that the *Osr1-Pdgfrb* function is evolutionarily conserved.

One of our long-term interests is interactions between transcription factors and the Hedgehog (Hh) pathway. Hh signaling has been implicated in OFT elongation and septation (Dyer and Kirby, 2009; Goddeeris et al., 2007; Smoak et al., 2005). Between E9.5 and E11.5, the Hh-receiving SHF cells migrate from the pharyngeal mesoderm, enter the OFT, then populate the pulmonary region and finally incorporate into the OFT endocardial cushions and pulmonary artery wall (Hoffmann et al., 2009). Given the high resemblance between the cells fates of the Hh and Osr1 lineages and our previous finding of *Osr1*-dependent expression of *Smo* and *Gli1*, critical components of the Hh pathway in the bulk SHF tissue (Zhou et al., 2015), we initially hypothesized that *Osr1* acts upstream of the Hh pathway in OFT development. *Smo* and *Disp1* promoters demonstrated OSR1 binding in the SHF, however the transcription level of *Smo*, *Disp1* and *Gli1* was not *Osr1*-dependent in the Osr1 cell lineage (Figure 23). Based on our data, we cannot make the conclusion whether Hh signaling is an *Osr1* target and this will remain as a subject for future studies.

Epigenetic regulations such as DNA methylation, chromatin remodeling and histone modifications play essential roles in embryonic development and disease progression. During heart development, the global DNA methylation level remains stable between E11.5 and E14.5 (Camenisch et al., 2001; Chamberlain et al., 2014) whereas in a heart failure model the methylome resembles that of the neonatal heart (Gilsbach et al., 2014). However, the role of DNA methylation in the cardiac progenitor populations and cell fate determination remains largely unknown. On the other hand, chromatin-

remodeling complexes alter the chromatin architecture between an open, permissive state known as euchromatin, allowing for transcription factor binding and active gene transcription, and a condensed, repressive state known as heterochromatin via interacting with gene regulatory regions and transcription factors (Hang et al., 2010; Lickert et al., 2004; Takeuchi and Bruneau, 2009).

Our previous studies have shown distinct transcription profiles of FHF and SHF subregions aSHF and pSHF, including differential expression patterns of key cardiac transcription factors (Zhang et al., 2015; Zhou et al., 2015). In this study, we aimed to determine whether chromatin accessibility and DNA methylation play a role in tissue-specific gene expression in the developing heart. Using Accessible Chromatin with high-throughput sequencing (ATAC-seq) we identified euchromatin regions in aSHF, pSHF and FHF at E9.5 and E10.5 (Figure 25-27). By comparing euchromatin regions between tissues, we found an enrichment of PDX1, HOX, LHX and ISL1 binding motifs in SHF-specific peaks, when compared to FHF. In addition, MEF2C and GATA4 motifs were enriched in the FHF euchromatin regions when compared to both SHF (Table 1). This suggests that transcription factors might activate their target genes in a tissue-specific manner and bind to the gene regulatory regions in a sequence-specific manner. However, when comparing accessible regions between E9.5 and E10.5 of the same tissue, no stage-specific motif enrichment was found, consistent with the fact that the majority of euchromatin regions had similar states at E9.5 and E10.5 (Figure 27). This could be due to closeness of the two stages and that little difference in gene expression exists between the two stages in *wildtype* embryos.

In addition, we hypothesized that the region-specific expression of cardiac transcription factors is coordinated by DNA methylation and examined the global DNA methylation states in aSHF, pSHF and FHF by whole-genome bisulfite sequencing (WGBS). On the genome level, both aSHF and pSHF demonstrated high average CpG methylation levels at both E9.5 and E10.5 (Figure 29A), which were significantly decreased and exhibited tissue- and stage-specific differences when focusing on the CpG sites located in accessible genomic regions (Figure 29B). This suggests that CpG sites located in heterochromatin regions were likely also hypermethylated. Since promoter DNA methylation has been shown to inhibit gene expression (Bird and Wolffe, 1999; Fujita et al., 2003; Huck-Hui and Bird, 1999; Maurano et al., 2015; Watt and Molloy, 1988), we identified DMR-driven DEGs that showed inverse correlations between DNA methylation and gene expression such as *Tbx5*, *Fgfr3*, *Gata3*, *Hey1* and *Osr1* (Figure 30 and 31). DEGs associated with DMRs between aSHF and pSHF were involved in cell adhesion, extracellular matrix, and cell cycle, whereas those between SHF and FHF were involved in major heart development signaling pathways such as Hedgehog pathway and Notch pathway (Table 2), suggesting that DNA methylation controls genes required for heart progenitor functions. Therefore this study proposed a multi-tier regulatory mechanism for progenitor heart field specification.

APPENDICES

Appendix A

List of Abbreviations

aSHF   Anterior second heart field

ATAC-seq   Assay for transposase accessible chromatin with high-throughput

            sequencing

AVC   Atrioventricular canal

Bmp   Bone morphogenic protein

CHD   Congenital heart disease

ChIP   Chromatin immunoprecipitation

CNC   Cardiac neural crest

DEG   Differentially expressed gene

DMR   Differentially methylated region

DORV   Double outlet right ventricle

daSHF   Distal anterior second heart field

dOFT   Distal outflow tract

dpSHF   Distal posterior second heart field

EndoMT   Endothelial-mesenchymal transition

FACS   Fluorescence-activated cell sorting

FDR   False discovery rate

Fgf   Fibroblast growth factor

FHF   First heart field

GCE   eGFPCreERt2 transgene

GFP   Green fluorescent protein

GO	Gene ontology
HCG	Human chorionic gonadotropin
HDAC	Histone deacetylase
Het	Heterozygous
Hh	Hedgehog
KO	Knockout
MBD-seq	Methyl binding domain enrichment sequencing
OA	Overriding aorta
OFT	Outflow tract
PARP	Poly (ADP-ribose) polymerase
PCA	Principal component analysis
PDGF	Platelet-derived growth factor
PMS	Pregnant mare serum
paSHF	Proximal anterior second heart field
pOFT	Proximal outflow tract
ppSHF	Proximal posterior second heart field
pSHF	Posterior second heart field
PTA	Persistent truncus arteriosus
qPCR	Quantitative polymerase chain reaction
RNA-seq	RNA sequencing
SEM	Standard error of the mean
SHF	Second heart field
TGA	Transposition of the great arteries

TM   Tamoxifen

TSS   Transcription start site

WGBS   Whole-genome bisulfite sequencing

Wnt   Wingless/integrated

Appendix B

Primer Sequences

Table S1. Primers used for RT-qPCR

Gene	Forward primer (5' to 3')	Reverse primer (5' to 3')
Ackr3	TCCTACGTGGTGGTCTTCCT	TCCAGCTGACAGGTAAACGG
Ednra	TTGACCTCCCCATCAACGTG	AGCACAGAGGTTCAAGACGG
Pdgfrb	ATGGGTGGAGATTCGCAGGAG	TCGGATCTCATAGCGTGGCTTC
Notch1	AGAACGGAGCCAACAAGGAC	CGGCAATCGGTCCATGTGAT
Dhh	TCGTACCCAACTACAACCCC	GTACTCCGGGCCACATGTTC
Pdgfd	TGAGAGCAATCACCTCACAGAC	CAGAAGCAGGTTCCTTGGGT

Table S2. Primers used for ChIP-qPCR and luciferase assay constructs

Amplicon	Forward primer (5' to 3')	Reverse primer (5' to 3')	Genomic region
Smo-R1	CGATCTATATCTGGCTGACTG	CCCTAAGCAAGTCTCCCTC	chr6: 29734468-29734611
Smo-R2	GCTGTGACTTAAAGAAGCTGC	GGATGAATACCTGTGGCC	chr6: 29734614-29734806
Smo-R3	GATGGACTAGTTTCCTGCGG	AGTAGCTGCTGTTACCTGTG	chr6: 29734809-29734963
Smo-R4	AGTGACTCCGAGGTTATTTCC	TTTCACTCCATTCCTGCCC	chr6: 29734967-29735143
Smo-R5	ACTCTTGCCTGCTTTAGGC	GGGATGCGTGCAAGTTGTG	chr6: 29735144-29735279
Disp1-R1	CCTCCTGCTACTCAAAGCCG	ACATAGTCCTTCGCGGTGTC	chr1: 183221559-183221767
Disp1-R2	GACACCGCGAAGGACTATGT	GAGTCCCCAGCCTTGACTTC	chr1: 183221748-183221950
Disp1-R3	TTGGAGCACAGGCTGTAACC	GCCTGAACAAGACAGGCTCT	chr1: 183222069-183222276
Gli1-R1	GCTGGAAACTGGGCTGGG	TAGCGTGCGGGTGGCAACAG	chr10: 127341597-127341817
Gli1-R2	CGGCTCTTCCCGCTCACTTC	ACTGTCCACCAAGAGCAGC	chr10: 127341818-127342015
Gli1-R3	AAATCCCGGCGCGGATCC	TGAGGCTGGCCTACAGAC	chr10: 127342016-127342214
Gli1-R4	CTCTTTGGATGGAACGTGG	GAGAACGGAGTTTCTCCAGAG	chr10: 127342215-127342422
Gli1-R5	CATCTCCAAATTCTGGACGCAG	TTCTTTGAGCTCACGCAGC	chr10: 127342423-127342616
Pdgfrb-R1	AACAGTAGCAGTGTCAGCCC	GCCACCTGAGTTGGAGAGAC	chr18: 61044524-61044625
Pdgfrb-R2	TGGGGCAGGCCACTCTAATA	GGACGCGTGTGTCTGTTTTC	chr18: 61044857-61045042
Pdgfrb-R3	AAACAGTCCAGAGCCAGAGC	CTGGCCTGATTGCGGAAAAC	chr18: 61045272-61045466
Notch1-R1	ACCAAAAGTTTGAGCTGGCG	CTCCAGGATGGAGCTGGTTC	chr2: 26504095-26504245
Notch1-R2	GATTGAGGCCAGGCACTCTT	CGTGGAACGTCTAGACTCGG	chr2: 26504402-26504588
Notch1-R3	GGCCTCAGTTTTCCCCCTAC	ACCAACACCAGTCACAAGGG	chr2: 26506343-26506516
Ednra-R1	TACAGATTCCCACGTTGTGG	GGGCCTTAGTGTCTCATAAC	chr8: 77718682-77718818
Ednra-R2	TGGGACCTAACTGCAAGAGC	CCTTGAGTCTGGTCTGTTGCT	chr8: 77724451-77724630
Ednra-R3	GCCATATGCTCTTGTGGTTGC	GCAGTCTTTGTGTTCGCACC	chr8: 77740187-77740381
Pdgfrb-luc	TGACGGTACCAGTCCCGGCTA CCCTATCTG	ACTGAAGCTTCCACCTCGCTG TCTTCTGTT	chr18: 61045201-61045524

Appendix C

Supplemental Data

Table S3. Differentially expressed genes at E9.5.

Gene symbol	Fold change	p-value	FDR
Cdh1	1.703805	5.00E-05	0.005253
Car4	1.649445	5.00E-05	0.005253
Meox1	2.046289	5.00E-05	0.005253
Shh	1.921605	5.00E-05	0.005253
Slc2a3	1.678763	5.00E-05	0.005253
Mapk13	1.533709	5.00E-05	0.005253
Cldn7	1.732333	5.00E-05	0.005253
Sfrp5	1.67785	5.00E-05	0.005253
Grb7	2.050421	5.00E-05	0.005253
Hkdc1	3.039913	5.00E-05	0.005253
Pttg1	1.582199	5.00E-05	0.005253
Ccdc88c	1.830759	5.00E-05	0.005253
Barx1	2.18651	5.00E-05	0.005253
Ocln	2.404522	5.00E-05	0.005253
Plk2	1.428175	5.00E-05	0.005253
Emb	1.465079	5.00E-05	0.005253
Dab2	1.6855	5.00E-05	0.005253
Angpt1	1.52626	5.00E-05	0.005253
Clic6	3.834105	5.00E-05	0.005253
Krt18	1.425397	5.00E-05	0.005253
Cldn6	1.599026	5.00E-05	0.005253
Tle4	1.668783	5.00E-05	0.005253
Rbp4	15.84307	5.00E-05	0.005253
Rdh10	1.5688	5.00E-05	0.005253
Nr4a2	2.961176	5.00E-05	0.005253
Jag1	1.533391	5.00E-05	0.005253
Tnc	2.223835	5.00E-05	0.005253
Ociad2	1.930268	5.00E-05	0.005253
Fgf15	3.535392	5.00E-05	0.005253
Adgrg1	2.230535	5.00E-05	0.005253
Cgnl1	1.462654	5.00E-05	0.005253
Foxa1	2.108782	5.00E-05	0.005253
Frmpd1	2.296203	5.00E-05	0.005253
Cfap61	13.52025	5.00E-05	0.005253

Table S3 cont.

Lgi2	2.052995	5.00E-05	0.005253
Cdh6	2.411499	5.00E-05	0.005253
Mreg	1.906943	5.00E-05	0.005253
Stk32a	1.917903	5.00E-05	0.005253
Hey1	1.959779	5.00E-05	0.005253
Cmtm8	2.3767	5.00E-05	0.005253
Plekha6	2.492667	5.00E-05	0.005253
Onecut1	3.799817	5.00E-05	0.005253
Nkx2-6	1.958463	5.00E-05	0.005253
Epcam	1.535156	5.00E-05	0.005253
Cldn4	2.40209	5.00E-05	0.005253
Bex4	1.651913	5.00E-05	0.005253
Krt8	1.526599	5.00E-05	0.005253
Bex1	1.475438	5.00E-05	0.005253
Gdf6	3.246083	5.00E-05	0.005253
Hbb-y	6.632074	5.00E-05	0.005253
Hbb-bh1	8.184079	5.00E-05	0.005253
Cdh3	1.631476	5.00E-05	0.005253
mt-Rnr1	1.571323	5.00E-05	0.005253
mt-Nd2	1.341641	5.00E-05	0.005253
mt-Nd4	1.42055	5.00E-05	0.005253
mt-Nd5	1.353327	5.00E-05	0.005253
mt-Cytb	1.411223	5.00E-05	0.005253
Ddx3y	2.675095	5.00E-05	0.005253
Rasgrp3	1.573469	5.00E-05	0.005253
Gdf2	9.227501	5.00E-05	0.005253
Spint2	1.560764	5.00E-05	0.005253
Apela	1.644855	5.00E-05	0.005253
Rasgef1b	2.955639	5.00E-05	0.005253
Ihh	2.400858	1.00E-04	0.009399
Vtn	1.69127	1.00E-04	0.009399
Cpm	1.551113	1.00E-04	0.009399
Trib2	1.583389	1.00E-04	0.009399
Fos	1.928826	1.00E-04	0.009399
Cpn1	1.902374	1.00E-04	0.009399
Spint1	1.761059	1.00E-04	0.009399
Hyou1	1.477686	0.00015	0.013022
Crabp1	1.633883	0.00015	0.013022
F11r	1.398531	0.00015	0.013022

Table S3 cont.

Nkx2-3	2.65323	0.00015	0.013022
Stard13	5.16934	2.00E-04	0.016341
Errfi1	1.431145	2.00E-04	0.016341
Kcnk1	1.538037	2.00E-04	0.016341
Enpp1	2.06878	2.00E-04	0.016341
Id1	1.365611	2.00E-04	0.016341
St8sia3	4.920244	2.00E-04	0.016341
Thg1l	1.84246	0.00025	0.019292
Upp1	1.651173	0.00025	0.019292
Sema3a	2.61692	0.00025	0.019292
Col12a1	6.19232	0.00025	0.019292
Atp2c2	1.871508	0.00025	0.019292
Col18a1	1.298172	3.00E-04	0.022061
Gldc	1.39952	3.00E-04	0.022061
Itga6	1.409164	3.00E-04	0.022061
Foxa2	1.713101	3.00E-04	0.022061
mt-Nd1	1.294554	3.00E-04	0.022061
Krt20	1.83163	0.00035	0.025146
Hs3st3b1	1.378579	0.00035	0.025146
Ecm1	1.967611	4.00E-04	0.028092
Cdcp1	2.301365	4.00E-04	0.028092
Gpr20	2.169045	4.00E-04	0.028092
Iqgap1	1.322203	0.00045	0.03108
Sox2	1.818039	0.00045	0.03108
Mrm1	1.974591	5.00E-04	0.033425
Tagln2	1.545948	5.00E-04	0.033425
Kdm5d	2.658109	5.00E-04	0.033425
Sorbs2	1.949346	0.00055	0.036379
Mylk3	1.824241	6.00E-04	0.038863
Gm26917	1.420753	6.00E-04	0.038863
Igfbpl1	2.358795	0.00065	0.041457
Fam84b	1.571608	0.00065	0.041457
Cd200	3.301061	7.00E-04	0.043754
Lad1	1.543601	7.00E-04	0.043754
Rfx6	2.070286	8.00E-04	0.048313
Pcbd1	1.693261	8.00E-04	0.048313
Ppp1r17	0.211096	5.00E-05	0.005253
Eno2	0.341288	5.00E-05	0.005253
Pgf	0.644779	5.00E-05	0.005253

94

Table S3 cont.

Etv2	0.439962	5.00E-05	0.005253
Wnt2	0.620429	5.00E-05	0.005253
Aldh1a2	0.495432	5.00E-05	0.005253
Wnt11	0.429241	5.00E-05	0.005253
Pmp22	0.622703	5.00E-05	0.005253
Tbx5	0.448388	5.00E-05	0.005253
Pdlim4	0.53255	5.00E-05	0.005253
Myl7	0.696975	5.00E-05	0.005253
Smoc1	0.521711	5.00E-05	0.005253
Thbs4	0.301828	5.00E-05	0.005253
Fbxo32	0.312386	5.00E-05	0.005253
Adamts20	0.439017	5.00E-05	0.005253
Adamts1	0.69017	5.00E-05	0.005253
Fmnl3	0.582779	5.00E-05	0.005253
Cxcl13	0.523753	5.00E-05	0.005253
Smoc2	0.447063	5.00E-05	0.005253
Ankrd1	0.337943	5.00E-05	0.005253
Add3	0.684912	5.00E-05	0.005253
Maged2	0.684546	5.00E-05	0.005253
Msc	0.324372	5.00E-05	0.005253
Col3a1	0.722902	5.00E-05	0.005253
Col9a1	0.623082	5.00E-05	0.005253
Itga8	0.546044	5.00E-05	0.005253
Sfrp2	0.642948	5.00E-05	0.005253
Rspo1	0.45614	5.00E-05	0.005253
Sparcl1	0.678797	5.00E-05	0.005253
Col1a2	0.632176	5.00E-05	0.005253
Casp3	0.473931	5.00E-05	0.005253
Nkd1	0.657497	5.00E-05	0.005253
Anxa2	0.515073	5.00E-05	0.005253
Tbx18	0.529987	5.00E-05	0.005253
Ephb1	0.585667	5.00E-05	0.005253
Nkx6-1	0.296505	5.00E-05	0.005253
Colec12	0.661804	5.00E-05	0.005253
Prickle1	0.621712	5.00E-05	0.005253
Wnt4	0.34511	5.00E-05	0.005253
Pcdh18	0.663572	5.00E-05	0.005253
Foxf2	0.630903	5.00E-05	0.005253
Rhod	0.42116	5.00E-05	0.005253

Table S3 cont.

Pnliprp1	0.574774	5.00E-05	0.005253
Dpy19l1	0.719814	5.00E-05	0.005253
Fut10	0.584385	5.00E-05	0.005253
Arl4a	0.591165	5.00E-05	0.005253
Osr1	0.113642	5.00E-05	0.005253
Vsnl1	0.314005	5.00E-05	0.005253
Cd248	0.710103	5.00E-05	0.005253
Eno1b	0.465512	5.00E-05	0.005253
Kdr	0.510808	5.00E-05	0.005253
S1pr3	0.440261	5.00E-05	0.005253
Actc1	0.661489	5.00E-05	0.005253
Bves	0.507514	5.00E-05	0.005253
Foxd1	0.487813	5.00E-05	0.005253
Gm13394	0.023393	5.00E-05	0.005253
Calcoco1	0.676859	1.00E-04	0.009399
Bnc1	0.468945	1.00E-04	0.009399
Vcam1	0.338125	1.00E-04	0.009399
Epha8	0.217746	1.00E-04	0.009399
Ednra	0.664885	1.00E-04	0.009399
Stra6	0.649494	1.00E-04	0.009399
Sv2a	0.524496	1.00E-04	0.009399
Cav1	0.076835	0.00015	0.013022
Bicc1	0.677743	0.00015	0.013022
Hspa12a	0.510399	0.00015	0.013022
Cd55	0.425972	0.00015	0.013022
Mgp	0.240665	0.00015	0.013022
Csrp3	0.519655	0.00015	0.013022
Sh3gl3	0.453863	0.00015	0.013022
Rasl12	0.508643	2.00E-04	0.016341
Nrk	0.563694	2.00E-04	0.016341
Foxd2	0.437881	2.00E-04	0.016341
Kitl	0.607706	0.00025	0.019292
Plxdc2	0.658573	0.00025	0.019292
Egflam	0.327982	0.00025	0.019292
Gas1	0.7445	0.00025	0.019292
Gsto1	0.723786	3.00E-04	0.022061
Efnb1	0.669544	3.00E-04	0.022061
Rbm24	0.66271	3.00E-04	0.022061
Cnn1	0.56408	0.00035	0.025146

Table S3 cont.

Crhbp	0.434004	0.00035	0.025146
Plat	0.759434	4.00E-04	0.028092
Msx1	0.617847	0.00045	0.03108
Gata5	0.789041	5.00E-04	0.033425
Npr3	0.682716	5.00E-04	0.033425
Upk3b	0.615392	5.00E-04	0.033425
Fam49a	0.6145	0.00055	0.036379
Cald1	0.611968	6.00E-04	0.038863
Rspo2	0.685874	6.00E-04	0.038863
P4ha2	0.712541	0.00065	0.041457
Colgalt2	0.55664	7.00E-04	0.043754
Kcnk3	0.385571	7.00E-04	0.043754
Nid1	0.702013	0.00075	0.046186
Aplp1	0.694521	0.00075	0.046186
Nrep	0.80234	0.00075	0.046186
Hmgcs2	0.37885	8.00E-04	0.048313
Prnp	0.715202	8.00E-04	0.048313

Table S4. Differentially expressed genes at E10.5.

Gene symbol	Fold change	p-value	FDR
Ccnd2	1.429838	5.00E-05	0.001507
Lhx2	7.948375	5.00E-05	0.001507
Cdh1	1.855069	5.00E-05	0.001507
Ckb	1.616104	5.00E-05	0.001507
Col18a1	2.110069	5.00E-05	0.001507
Tubb6	1.537614	5.00E-05	0.001507
Nkx2-1	5.944313	5.00E-05	0.001507
Sipa1l2	1.35746	5.00E-05	0.001507
Ap1m2	2.84179	5.00E-05	0.001507
Mapk13	2.362919	5.00E-05	0.001507
Crabp2	1.427417	5.00E-05	0.001507
Mef2c	1.479255	5.00E-05	0.001507
Etv2	2.313264	5.00E-05	0.001507
Crip2	1.850407	5.00E-05	0.001507
Atp7b	1.849662	5.00E-05	0.001507
Tbx1	1.808229	5.00E-05	0.001507
Gata3	2.758837	5.00E-05	0.001507
Rxrg	2.262692	5.00E-05	0.001507
Cd34	3.7081	5.00E-05	0.001507
Scube1	1.790509	5.00E-05	0.001507
Etv4	3.803796	5.00E-05	0.001507
Gpx3	1.303931	5.00E-05	0.001507
Unc45b	1.849598	5.00E-05	0.001507
Hoxb1	1.644014	5.00E-05	0.001507
Rspo3	1.744035	5.00E-05	0.001507
Moxd1	1.463597	5.00E-05	0.001507
Ppa1	1.304221	5.00E-05	0.001507
Unc5b	1.498571	5.00E-05	0.001507
Myl7	1.574773	5.00E-05	0.001507
Pgam2	2.263115	5.00E-05	0.001507
Tspan13	1.66846	5.00E-05	0.001507
Slc9a3r1	1.674072	5.00E-05	0.001507
Grin2c	4.068001	5.00E-05	0.001507
Lsm12	2.375103	5.00E-05	0.001507
Ccdc88c	2.020483	5.00E-05	0.001507
Barx1	2.939315	5.00E-05	0.001507
Pitx1	4.524348	5.00E-05	0.001507
Emb	1.89437	5.00E-05	0.001507
Fgf10	1.519875	5.00E-05	0.001507

Table S4 cont.

Bmp4	1.549639	5.00E-05	0.001507
Fgf9	1.758261	5.00E-05	0.001507
Ctnnd2	1.849571	5.00E-05	0.001507
Wnt7b	7.215903	5.00E-05	0.001507
Col2a1	1.497996	5.00E-05	0.001507
Sdf2l1	1.463664	5.00E-05	0.001507
Krt18	1.865278	5.00E-05	0.001507
Rps6ka2	2.051544	5.00E-05	0.001507
Cldn6	2.94429	5.00E-05	0.001507
Pim1	1.660432	5.00E-05	0.001507
Ppp2r2b	2.7945	5.00E-05	0.001507
Dpysl3	1.475108	5.00E-05	0.001507
Psat1	1.709028	5.00E-05	0.001507
Tle4	1.382557	5.00E-05	0.001507
Ankrd1	2.792602	5.00E-05	0.001507
Tjp2	1.433696	5.00E-05	0.001507
Gldc	2.389419	5.00E-05	0.001507
Dkk1	2.96553	5.00E-05	0.001507
Gal	1.91308	5.00E-05	0.001507
Cpn1	3.866183	5.00E-05	0.001507
Cd151	1.909885	5.00E-05	0.001507
Dock9	1.839715	5.00E-05	0.001507
Hprt	1.367026	5.00E-05	0.001507
Slco3a1	2.958672	5.00E-05	0.001507
Col9a1	1.427319	5.00E-05	0.001507
Dbi	1.334171	5.00E-05	0.001507
Tnnt2	1.560358	5.00E-05	0.001507
Tnni1	1.636156	5.00E-05	0.001507
Nek2	1.599277	5.00E-05	0.001507
Notch1	3.396879	5.00E-05	0.001507
Hsd17b12	1.332856	5.00E-05	0.001507
Gatm	2.488282	5.00E-05	0.001507
Atp9a	1.847874	5.00E-05	0.001507
Sall4	2.465585	5.00E-05	0.001507
Procr	2.945434	5.00E-05	0.001507
Pdlim5	1.824844	5.00E-05	0.001507
Sema3a	3.018747	5.00E-05	0.001507
Errfi1	1.535026	5.00E-05	0.001507
Ociad2	2.069855	5.00E-05	0.001507
Uchl1	1.675626	5.00E-05	0.001507

Table S4 cont.

Nup210	2.333928	5.00E-05	0.001507
Adm	2.902407	5.00E-05	0.001507
Stk26	1.89429	5.00E-05	0.001507
Stard8	3.500109	5.00E-05	0.001507
Dusp9	1.541159	5.00E-05	0.001507
Prps1	1.442366	5.00E-05	0.001507
Dusp4	1.849978	5.00E-05	0.001507
Gsr	1.604406	5.00E-05	0.001507
Msmo1	1.395683	5.00E-05	0.001507
Galnt7	1.407659	5.00E-05	0.001507
Casp3	1.852264	5.00E-05	0.001507
Pdlim3	1.561034	5.00E-05	0.001507
Irx3	2.677766	5.00E-05	0.001507
Irx5	2.257538	5.00E-05	0.001507
Adgrg1	2.560135	5.00E-05	0.001507
Cryab	2.349706	5.00E-05	0.001507
Plet1	2.919659	5.00E-05	0.001507
Cadm1	1.419541	5.00E-05	0.001507
Hyou1	1.620938	5.00E-05	0.001507
Parp16	1.841658	5.00E-05	0.001507
Igdcc3	1.399023	5.00E-05	0.001507
Lmo2	3.835647	5.00E-05	0.001507
Afap1l1	1.710149	5.00E-05	0.001507
Cdc14b	1.404197	5.00E-05	0.001507
Atp1a1	1.49507	5.00E-05	0.001507
Mif	1.403301	5.00E-05	0.001507
Foxa1	2.262723	5.00E-05	0.001507
Supt16	1.327445	5.00E-05	0.001507
Krt20	4.015779	5.00E-05	0.001507
3632451O06Rik	1.429918	5.00E-05	0.001507
Foxa2	2.470735	5.00E-05	0.001507
Scd1	1.583713	5.00E-05	0.001507
Mycn	1.681646	5.00E-05	0.001507
Hand1	3.154278	5.00E-05	0.001507
Prdm1	2.327676	5.00E-05	0.001507
Stk32a	3.360742	5.00E-05	0.001507
Hey1	1.702218	5.00E-05	0.001507
Ppp1r14c	4.942154	5.00E-05	0.001507
Cmtm8	2.936607	5.00E-05	0.001507
Cldn5	7.897303	5.00E-05	0.001507

Table S4 cont.

Stx3	1.614008	5.00E-05	0.001507
Plekha6	2.213777	5.00E-05	0.001507
Rhod	2.485042	5.00E-05	0.001507
Rnpep	1.356057	5.00E-05	0.001507
Abhd14b	3.024297	5.00E-05	0.001507
Kcns3	5.222136	5.00E-05	0.001507
Aplnr	4.328299	5.00E-05	0.001507
Rasip1	2.746796	5.00E-05	0.001507
Gpr20	8.955848	5.00E-05	0.001507
Epcam	2.280231	5.00E-05	0.001507
Rbp1	1.36224	5.00E-05	0.001507
Sox18	3.923932	5.00E-05	0.001507
Kctd11	1.690519	5.00E-05	0.001507
1110032F04Rik	1.980056	5.00E-05	0.001507
Cldn4	4.396697	5.00E-05	0.001507
Dact2	2.671167	5.00E-05	0.001507
Krt8	2.429097	5.00E-05	0.001507
Bex1	1.693259	5.00E-05	0.001507
Gdf6	2.317212	5.00E-05	0.001507
Ttn	3.351414	5.00E-05	0.001507
Hbb-bh1	Inf	5.00E-05	0.001507
Rras2	1.364493	5.00E-05	0.001507
Tpm3-rs7	1.35393	5.00E-05	0.001507
Col13a1	1.739477	5.00E-05	0.001507
Myl3	2.767858	5.00E-05	0.001507
Ptp4a3	1.596533	5.00E-05	0.001507
Eno3	1.320772	5.00E-05	0.001507
Irx1	2.494118	5.00E-05	0.001507
Cdh3	1.544388	5.00E-05	0.001507
Myl4	1.98156	5.00E-05	0.001507
Kdr	1.612536	5.00E-05	0.001507
Sox7	6.383156	5.00E-05	0.001507
Ldha	1.520272	5.00E-05	0.001507
Cldn9	2.719818	5.00E-05	0.001507
Actc1	1.427165	5.00E-05	0.001507
Ddx3y	1.849815	5.00E-05	0.001507
Gm10260	1.809905	5.00E-05	0.001507
3000002C10Rik	2.896659	5.00E-05	0.001507
Ccnd1	1.357603	5.00E-05	0.001507
Hs3st3b1	1.906368	5.00E-05	0.001507

Table S4 cont.

Rasgrp3	2.935569	5.00E-05	0.001507
Fndc1	4.621144	5.00E-05	0.001507
H2-D1	2.277104	5.00E-05	0.001507
Spint2	1.82065	5.00E-05	0.001507
Kcng1	2.319815	5.00E-05	0.001507
Sox2	2.990258	5.00E-05	0.001507
Slc45a4	1.89173	5.00E-05	0.001507
Apela	2.869263	5.00E-05	0.001507
Gm13394	40.76559	5.00E-05	0.001507
Gm3571	1.360837	5.00E-05	0.001507
Bend4	1.541612	5.00E-05	0.001507
BC023719	2.144914	5.00E-05	0.001507
Gm26917	1.538269	5.00E-05	0.001507
Prkch	1.502488	1.00E-04	0.002828
Mal2	2.282429	1.00E-04	0.002828
Sytl2	2.217048	1.00E-04	0.002828
Mylk3	2.65312	1.00E-04	0.002828
Cpe	1.301901	1.00E-04	0.002828
Akap12	1.376084	1.00E-04	0.002828
Lgi2	1.655187	1.00E-04	0.002828
Megf9	1.458158	1.00E-04	0.002828
Bex2	1.31863	1.00E-04	0.002828
Tubb2b	1.671626	1.00E-04	0.002828
Gm9833	1.707383	1.00E-04	0.002828
Map1b	1.28591	1.00E-04	0.002828
Nebl	2.040355	1.00E-04	0.002828
Tuba1a	1.266002	1.00E-04	0.002828
Hmga1b	1.348495	1.00E-04	0.002828
Snrpn	1.371724	1.00E-04	0.002828
Meox1	1.997627	0.00015	0.004063
Nkx2-5	1.730849	0.00015	0.004063
Nme6	1.353379	0.00015	0.004063
Rcan2	2.562301	0.00015	0.004063
Garem1	1.403767	0.00015	0.004063
Pqlc3	3.292789	0.00015	0.004063
Kdm5d	1.689111	0.00015	0.004063
Tgfb1	3.082562	2.00E-04	0.005219
Ripk4	2.088591	2.00E-04	0.005219
Slc25a13	1.335345	2.00E-04	0.005219
Vtn	2.896378	2.00E-04	0.005219

Table S4 cont.

Tnfaip2	4.042646	2.00E-04	0.005219
Amph	1.50954	2.00E-04	0.005219
Mapk12	1.834125	2.00E-04	0.005219
Pcgf5	1.839778	2.00E-04	0.005219
Arhgef16	1.883708	2.00E-04	0.005219
Mmp17	1.998233	2.00E-04	0.005219
Chrdl1	1.365077	2.00E-04	0.005219
St14	2.36156	2.00E-04	0.005219
Dhcr24	1.353225	2.00E-04	0.005219
Elmo1	1.690863	2.00E-04	0.005219
Isl1	1.39949	2.00E-04	0.005219
Psmd14	1.265343	0.00025	0.00633
Mtch2	1.343293	0.00025	0.00633
Ak4	1.379315	0.00025	0.00633
Krtcap3	2.495156	0.00025	0.00633
Bcat1	1.28024	0.00025	0.00633
Gsta4	1.344881	0.00025	0.00633
Agpat1	1.498937	0.00025	0.00633
Rap1gap2	1.825571	0.00025	0.00633
Gm6969	2.564415	0.00025	0.00633
Tmprss2	2.916787	3.00E-04	0.007321
Kitl	1.85856	3.00E-04	0.007321
Wdr82	1.295819	3.00E-04	0.007321
Pdgfa	2.173907	3.00E-04	0.007321
Fn1	1.267914	3.00E-04	0.007321
Rassf9	3.087587	3.00E-04	0.007321
Hs3st3a1	1.692463	3.00E-04	0.007321
Rasgef1b	1.55875	3.00E-04	0.007321
Cox5a	1.305553	0.00035	0.008289
Shh	2.124775	0.00035	0.008289
Klf5	1.852389	0.00035	0.008289
Sptb	1.520379	0.00035	0.008289
Sqle	1.247572	0.00035	0.008289
Vwa2	1.811455	0.00035	0.008289
Cd9	1.91019	0.00035	0.008289
Mfge8	1.274386	0.00035	0.008289
Ap1s2	1.730065	0.00035	0.008289
Ptgir	2.213286	0.00035	0.008289
Hist1h2ak	2.317501	0.00035	0.008289
2700038G22Rik	1.628689	0.00035	0.008289

Table S4 cont.

Ddx39	1.257024	4.00E-04	0.009335
Grb7	3.381117	4.00E-04	0.009335
Espn	2.546049	4.00E-04	0.009335
Ldlr	1.260483	0.00045	0.010332
Spon1	1.270641	0.00045	0.010332
Uqcrq	1.388481	0.00045	0.010332
Lrrc3b	1.997501	0.00045	0.010332
Clic6	3.330157	5.00E-04	0.011318
Ces1d	2.993327	5.00E-04	0.011318
Cgn	1.972349	5.00E-04	0.011318
Nup85	1.341249	0.00055	0.012234
Tnfrsf12a	2.13193	0.00055	0.012234
Pcsk6	1.829765	0.00055	0.012234
Dok4	1.727731	0.00055	0.012234
Hebp1	2.387896	0.00055	0.012234
Mthfd1l	1.314647	6.00E-04	0.013208
Jade1	1.391294	0.00065	0.014139
Il17rd	1.465895	0.00065	0.014139
Uxs1	1.660236	0.00065	0.014139
Gltp	1.323943	7.00E-04	0.014947
Hmgcr	1.289941	7.00E-04	0.014947
Sap130	1.338402	7.00E-04	0.014947
Lrp8	2.501876	7.00E-04	0.014947
Gm14328	1.874473	7.00E-04	0.014947
Uchl5	1.274811	0.00075	0.01583
Ppm1g	1.245107	0.00075	0.01583
Bag2	1.263523	0.00075	0.01583
Gm8203	1.256153	0.00075	0.01583
Igfbp3	1.475097	8.00E-04	0.016693
Shisa3	1.997271	8.00E-04	0.016693
Capn6	1.239404	8.00E-04	0.016693
Saa1	2.26081	8.00E-04	0.016693
Hhex	3.555445	0.00085	0.017508
Itga6	1.370908	0.00085	0.017508
Tspan18	1.723845	0.00085	0.017508
Spint1	2.18501	0.00085	0.017508
Hist1h2ae	1.446244	0.00085	0.017508
Slc43a3	1.433909	9.00E-04	0.018361
Tnc	1.240485	9.00E-04	0.018361
Tmem59l	2.439237	9.00E-04	0.018361

Table S4 cont.

Kifc1	1.915076	9.00E-04	0.018361
Podxl	1.293565	0.00095	0.019077
Idh1	1.231512	0.00095	0.019077
Ndufaf1	1.404242	0.00095	0.019077
Slc16a1	1.246213	0.00095	0.019077
Trim71	1.38033	0.00095	0.019077
Hspa4l	1.701861	0.001	0.019864
Dpysl5	1.787854	0.001	0.019864
Nkx2-6	4.396605	0.001	0.019864
Nmral1	1.256508	0.001	0.019864
Pls3	1.246691	0.00105	0.020665
Dusp6	1.238976	0.00105	0.020665
Spry4	1.66553	0.00105	0.020665
Tfap2c	2.127781	0.00105	0.020665
Cotl1	1.418608	0.00105	0.020665
Cdc34	1.265618	0.0011	0.021418
Pcbp4	1.230937	0.0011	0.021418
Crnde	2.394443	0.0011	0.021418
Gjb2	2.19217	0.0011	0.021418
Etv5	2.116925	0.00115	0.022057
Rrm2	1.242101	0.00115	0.022057
Scarb1	1.306247	0.00115	0.022057
Kcnip1	2.596647	0.00115	0.022057
Slc37a3	1.276431	0.0012	0.022845
Melk	1.256587	0.0012	0.022845
Pimreg	1.258239	0.00125	0.023621
Gm10263	1.532173	0.00125	0.023621
Gm6166	1.394945	0.00125	0.023621
Rerg	1.537328	0.0013	0.024386
Rexo2	1.319534	0.0013	0.024386
C1qtnf2	2.553967	0.0013	0.024386
Nhp2	1.300536	0.00135	0.025067
Fkbp3	1.283151	0.00135	0.025067
Id4	1.398441	0.00135	0.025067
Dera	1.282315	0.00135	0.025067
H2afz	1.307804	0.00135	0.025067
Hlx	1.487709	0.00135	0.025067
Myef2	1.319574	0.0014	0.025771
Ccnjl	1.28573	0.0014	0.025771
Eif5a	1.257403	0.0014	0.025771

Table S4 cont.

Id1	1.241931	0.00145	0.026615
Cgnl1	1.363517	0.0015	0.027415
Rcc1	1.235677	0.00155	0.028168
Thbs1	1.369063	0.00155	0.028168
Raly	1.480744	0.0016	0.028832
Hint1	1.235885	0.00165	0.029608
Saa2	2.041784	0.00165	0.029608
Opn3	1.520663	0.0017	0.030377
Gmnn	1.267364	0.00175	0.030926
Ccdc124	1.269339	0.00175	0.030926
Bmp5	1.392459	0.00175	0.030926
Nrd1	1.298641	0.00175	0.030926
Pnliprp2	2.861973	0.0018	0.031722
Plvap	1.730807	0.0018	0.031722
Mthfd2	1.277685	0.00185	0.032558
Uqcr11	1.31464	0.0019	0.033255
Cmtm7	1.315213	0.0019	0.033255
Cmtm4	1.542275	0.0019	0.033255
F11r	1.403518	0.00195	0.033991
Gm14681	1.277059	0.00195	0.033991
Enkd1	1.346486	0.002	0.034487
Cad	1.22551	0.002	0.034487
Mrpl40	1.295925	0.002	0.034487
Snrnp25	1.294706	0.002	0.034487
Rplp0	1.293029	0.002	0.034487
Gtf2f2	1.302183	0.00205	0.035113
Lypd1	3.419084	0.00215	0.036533
Havcr1	1.610718	0.00215	0.036533
Gm2199	1.402281	0.00215	0.036533
Hat1	1.220788	0.0022	0.037136
Mlh1	1.274961	0.0022	0.037136
Actn2	1.691766	0.0022	0.037136
Lifr	1.334641	0.0022	0.037136
Adamts4	1.758233	0.00235	0.039306
Polr3g	1.376879	0.00235	0.039306
Ccne1	1.224531	0.0024	0.039934
Exoc6	1.571679	0.0024	0.039934
Nkain1	1.836704	0.0024	0.039934
Ube2c	1.214091	0.00245	0.04045
Mthfd1	1.213015	0.00245	0.04045

Table S4 cont.

Kif13a	1.275408	0.00245	0.04045
Hmgcs1	1.207396	0.00245	0.04045
Arg1	1.28027	0.0025	0.041064
Ly75	1.338327	0.0025	0.041064
Spata5l1	1.742891	0.0025	0.041064
Hapln3	1.50679	0.00255	0.041778
Ggta1	1.897682	0.00255	0.041778
Magi2	1.628282	0.0026	0.042435
1810009A15Rik	1.251491	0.0026	0.042435
Ptpn11	1.246139	0.00265	0.043141
Emd	1.404619	0.0027	0.043677
Man1c1	1.529931	0.0027	0.043677
Plk1	1.203898	0.00275	0.044374
Adamts18	1.350167	0.00275	0.044374
Slc38a1	1.213919	0.0028	0.045011
Tubb4b	1.244606	0.0028	0.045011
Ptx3	1.870753	0.0029	0.046444
Tspan12	1.838555	0.00295	0.047126
Gm6781	1.264211	0.00295	0.047126
Efna1	1.359929	0.003	0.047687
Rab38	2.036963	0.003	0.047687
Mfsd2a	1.734451	0.00305	0.048243
0610040J01Rik	1.737647	0.00305	0.048243
Sms-ps	1.258639	0.00305	0.048243
Synpo2l	1.792014	0.0031	0.048913
Bmp7	1.293634	0.00315	0.04958
Scrib	1.27759	0.00315	0.04958
Cldn7	2.083241	0.0032	0.049998
Sgsm1	1.659728	0.0032	0.049998
Bex3	1.206584	0.0032	0.049998
Pdlim1	1.953429	0.0032	0.049998
Tbx4	0.731733	5.00E-05	0.001507
Gcg	0.46994	5.00E-05	0.001507
Egfl6	0.404275	5.00E-05	0.001507
Sez6	0.216867	5.00E-05	0.001507
Col6a1	0.485967	5.00E-05	0.001507
Col1a1	0.568724	5.00E-05	0.001507
Ell2	0.460786	5.00E-05	0.001507
Lamb1	0.710786	5.00E-05	0.001507
Fosb	0.558176	5.00E-05	0.001507

Table S4 cont.

Cavin1	0.414562	5.00E-05	0.001507
Ralb	0.628096	5.00E-05	0.001507
Nid1	0.710185	5.00E-05	0.001507
Fblim1	0.548594	5.00E-05	0.001507
Runx1t1	0.655962	5.00E-05	0.001507
Nfib	0.710132	5.00E-05	0.001507
Aldh1a2	0.557018	5.00E-05	0.001507
Bicc1	0.650535	5.00E-05	0.001507
Abca1	0.453341	5.00E-05	0.001507
Hsd11b1	0.225671	5.00E-05	0.001507
Sulf1	0.595539	5.00E-05	0.001507
Rnd3	0.720315	5.00E-05	0.001507
Rarb	0.663483	5.00E-05	0.001507
Pltp	0.51626	5.00E-05	0.001507
Tbx5	0.685729	5.00E-05	0.001507
6330403K07Rik	0.741772	5.00E-05	0.001507
Natd1	0.706327	5.00E-05	0.001507
Gyg	0.601401	5.00E-05	0.001507
Popdc3	0.346854	5.00E-05	0.001507
Lama2	0.351659	5.00E-05	0.001507
Arid5b	0.620273	5.00E-05	0.001507
Tcp11l2	0.470586	5.00E-05	0.001507
Timp3	0.56232	5.00E-05	0.001507
Ddit4	0.412753	5.00E-05	0.001507
Meis1	0.684474	5.00E-05	0.001507
Col6a2	0.564263	5.00E-05	0.001507
Nrcam	0.461454	5.00E-05	0.001507
Fam84a	0.416853	5.00E-05	0.001507
Klf11	0.61945	5.00E-05	0.001507
Rflnb	0.620505	5.00E-05	0.001507
Foxg1	0.655992	5.00E-05	0.001507
Zfp36l1	0.734413	5.00E-05	0.001507
Smoc1	0.572067	5.00E-05	0.001507
Fos	0.703362	5.00E-05	0.001507
Cep72	0.718357	5.00E-05	0.001507
Iqgap2	0.530561	5.00E-05	0.001507
Crhbp	0.471216	5.00E-05	0.001507
Fam213a	0.736822	5.00E-05	0.001507
Scara5	0.348751	5.00E-05	0.001507
Clu	0.542246	5.00E-05	0.001507

Table S4 cont.

Npr3	0.656034	5.00E-05	0.001507
Sema5a	0.574297	5.00E-05	0.001507
Sdc2	0.669654	5.00E-05	0.001507
Cdh10	0.438127	5.00E-05	0.001507
Myc	0.48327	5.00E-05	0.001507
Tef	0.653155	5.00E-05	0.001507
Enpp2	0.542075	5.00E-05	0.001507
Adamts20	0.471683	5.00E-05	0.001507
Naga	0.636478	5.00E-05	0.001507
Ccdc80	0.628259	5.00E-05	0.001507
Snai2	0.494887	5.00E-05	0.001507
Adamts1	0.742515	5.00E-05	0.001507
Faim2	0.322008	5.00E-05	0.001507
Calcoco1	0.609872	5.00E-05	0.001507
Serping1	0.609144	5.00E-05	0.001507
Thbs2	0.432329	5.00E-05	0.001507
Smoc2	0.44376	5.00E-05	0.001507
Lbh	0.554457	5.00E-05	0.001507
Cyp1b1	0.418547	5.00E-05	0.001507
Dusp1	0.561027	5.00E-05	0.001507
Dsc2	0.463686	5.00E-05	0.001507
Lox	0.310503	5.00E-05	0.001507
Sncaip	0.518739	5.00E-05	0.001507
Pdgfrb	0.746564	5.00E-05	0.001507
Gna14	0.548334	5.00E-05	0.001507
Trim8	0.689699	5.00E-05	0.001507
Gfra1	0.490794	5.00E-05	0.001507
Bnc1	0.467433	5.00E-05	0.001507
Paip1	0.578858	5.00E-05	0.001507
St8sia2	0.610686	5.00E-05	0.001507
Msc	0.741142	5.00E-05	0.001507
Col5a2	0.748376	5.00E-05	0.001507
Col3a1	0.675375	5.00E-05	0.001507
Col19a1	0.539514	5.00E-05	0.001507
Ogfrl1	0.695314	5.00E-05	0.001507
Serpine2	0.757117	5.00E-05	0.001507
Cd55	0.391857	5.00E-05	0.001507
Syt2	0.401884	5.00E-05	0.001507
Ddr2	0.682527	5.00E-05	0.001507
Rgs5	0.364864	5.00E-05	0.001507

Table S4 cont.

Itga8	0.498253	5.00E-05	0.001507
Lamc3	0.376732	5.00E-05	0.001507
Cwc22	0.174544	5.00E-05	0.001507
Creb3l1	0.453841	5.00E-05	0.001507
Car2	0.574973	5.00E-05	0.001507
Nkain4	0.603012	5.00E-05	0.001507
Mbnl1	0.716854	5.00E-05	0.001507
Ngf	0.401004	5.00E-05	0.001507
Hmgcs2	0.456128	5.00E-05	0.001507
Vcam1	0.657436	5.00E-05	0.001507
Sfrp2	0.364548	5.00E-05	0.001507
Adgrl2	0.642729	5.00E-05	0.001507
Cyr61	0.699763	5.00E-05	0.001507
Epha7	0.598779	5.00E-05	0.001507
Brinp1	0.282239	5.00E-05	0.001507
Alad	0.66854	5.00E-05	0.001507
Rspo1	0.625664	5.00E-05	0.001507
Afap1	0.676443	5.00E-05	0.001507
Crmp1	0.317459	5.00E-05	0.001507
Epha5	0.366849	5.00E-05	0.001507
Sparcl1	0.688956	5.00E-05	0.001507
Ccng2	0.690362	5.00E-05	0.001507
Anxa3	0.705981	5.00E-05	0.001507
Col1a2	0.47293	5.00E-05	0.001507
Cald1	0.552599	5.00E-05	0.001507
Akr1b8	0.477827	5.00E-05	0.001507
Ptn	0.691869	5.00E-05	0.001507
Abtb1	0.664454	5.00E-05	0.001507
A2m	0.514652	5.00E-05	0.001507
Emp1	0.506559	5.00E-05	0.001507
Mgp	0.523431	5.00E-05	0.001507
Kcnj8	0.259889	5.00E-05	0.001507
Nr2f2	0.703358	5.00E-05	0.001507
Slc38a5	0.489568	5.00E-05	0.001507
Renbp	0.631758	5.00E-05	0.001507
Plat	0.640039	5.00E-05	0.001507
Sfrp1	0.761487	5.00E-05	0.001507
Ednra	0.557254	5.00E-05	0.001507
Adcy7	0.579597	5.00E-05	0.001507
Cdh11	0.718514	5.00E-05	0.001507

Table S4 cont.

Bmper	0.677861	5.00E-05	0.001507
Ets1	0.585755	5.00E-05	0.001507
Mpzl2	0.309981	5.00E-05	0.001507
Tcf12	0.66961	5.00E-05	0.001507
Anxa2	0.652917	5.00E-05	0.001507
Fam46a	0.452591	5.00E-05	0.001507
Stra6	0.67462	5.00E-05	0.001507
Plod2	0.629112	5.00E-05	0.001507
Tbx18	0.625789	5.00E-05	0.001507
Thsd7a	0.285098	5.00E-05	0.001507
Igdcc4	0.705166	5.00E-05	0.001507
Chst2	0.734287	5.00E-05	0.001507
Adamts15	0.436753	5.00E-05	0.001507
Atp7a	0.668037	5.00E-05	0.001507
Gucy1a1	0.65084	5.00E-05	0.001507
Tmem132c	0.710731	5.00E-05	0.001507
Scara3	0.738088	5.00E-05	0.001507
Pcdh11x	0.343031	5.00E-05	0.001507
Nkx6-1	0.360627	5.00E-05	0.001507
Tpbg	0.734643	5.00E-05	0.001507
Ror1	0.632451	5.00E-05	0.001507
Plk5	0.354528	5.00E-05	0.001507
Aldh1b1	0.678972	5.00E-05	0.001507
Dock4	0.637941	5.00E-05	0.001507
Colec12	0.616411	5.00E-05	0.001507
Meox2	0.496182	5.00E-05	0.001507
Prickle1	0.636353	5.00E-05	0.001507
Btg1	0.739122	5.00E-05	0.001507
Cdh8	0.534657	5.00E-05	0.001507
Cdc42ep3	0.522656	5.00E-05	0.001507
Wnt4	0.431227	5.00E-05	0.001507
Tns2	0.718606	5.00E-05	0.001507
Islr	0.494324	5.00E-05	0.001507
Spon2	0.595641	5.00E-05	0.001507
Cldn11	0.348555	5.00E-05	0.001507
Cdkn1c	0.771259	5.00E-05	0.001507
Pcdh18	0.57538	5.00E-05	0.001507
Slc24a2	0.325051	5.00E-05	0.001507
Mylip	0.529541	5.00E-05	0.001507
Egr1	0.702567	5.00E-05	0.001507

Table S4 cont.

Rgs4	0.155337	5.00E-05	0.001507
Pbx3	0.661641	5.00E-05	0.001507
Gcnt1	0.484292	5.00E-05	0.001507
Pdk2	0.614492	5.00E-05	0.001507
Tgfb2	0.709951	5.00E-05	0.001507
Fn3krp	0.055427	5.00E-05	0.001507
Ncam1	0.632216	5.00E-05	0.001507
Lrrc17	0.644091	5.00E-05	0.001507
Ankrd6	0.593697	5.00E-05	0.001507
St8sia4	0.527222	5.00E-05	0.001507
Tex264	0.675766	5.00E-05	0.001507
Abhd4	0.728816	5.00E-05	0.001507
Nbl1	0.406777	5.00E-05	0.001507
Rasl12	0.557051	5.00E-05	0.001507
Rbm45	0.269493	5.00E-05	0.001507
Egflam	0.40636	5.00E-05	0.001507
Hic1	0.316165	5.00E-05	0.001507
Lrrn4	0.638744	5.00E-05	0.001507
2510009E07Rik	0.559521	5.00E-05	0.001507
Zfp536	0.502048	5.00E-05	0.001507
Ackr3	0.678182	5.00E-05	0.001507
BC024139	0.439879	5.00E-05	0.001507
Fzd1	0.767418	5.00E-05	0.001507
Zfp36	0.6196	5.00E-05	0.001507
Smtnl2	0.722197	5.00E-05	0.001507
Tcf21	0.624924	5.00E-05	0.001507
Slitrk6	0.374947	5.00E-05	0.001507
Arl4a	0.560485	5.00E-05	0.001507
8030462N17Rik	0.32721	5.00E-05	0.001507
Adamts12	0.428465	5.00E-05	0.001507
Stbd1	0.602714	5.00E-05	0.001507
Rgmb	0.56101	5.00E-05	0.001507
Lhfp	0.544581	5.00E-05	0.001507
Osr1	0.136027	5.00E-05	0.001507
Bdnf	0.555569	5.00E-05	0.001507
Myof	0.334621	5.00E-05	0.001507
Insc	0.247914	5.00E-05	0.001507
Prex2	0.638446	5.00E-05	0.001507
Tmem200a	0.492928	5.00E-05	0.001507
Upk1b	0.354299	5.00E-05	0.001507

Table S4 cont.

Neto1	0.280171	5.00E-05	0.001507
Emilin3	0.598716	5.00E-05	0.001507
Pgbd5	0.529527	5.00E-05	0.001507
Irf2bp2	0.656213	5.00E-05	0.001507
Rspo2	0.676928	5.00E-05	0.001507
Epha3	0.382457	5.00E-05	0.001507
Junb	0.678784	5.00E-05	0.001507
Nrk	0.571532	5.00E-05	0.001507
Cntn2	0.542968	5.00E-05	0.001507
Hunk	0.766158	5.00E-05	0.001507
Ppfia2	0.265245	5.00E-05	0.001507
Pde5a	0.675411	5.00E-05	0.001507
Iigp1	0.29674	5.00E-05	0.001507
Tmem158	0.383102	5.00E-05	0.001507
Kbtbd13	0.575272	5.00E-05	0.001507
Zcchc24	0.691237	5.00E-05	0.001507
Tcim	0.502651	5.00E-05	0.001507
Lepr	0.371831	5.00E-05	0.001507
Sh2d3c	0.668291	5.00E-05	0.001507
Pde1a	0.247486	5.00E-05	0.001507
Gm12715	0.702754	5.00E-05	0.001507
Tmem26	0.580488	5.00E-05	0.001507
Nrg2	0.514857	5.00E-05	0.001507
Rxfp3	0.368787	5.00E-05	0.001507
Sphk1	0.408914	5.00E-05	0.001507
Klhl24	0.62926	5.00E-05	0.001507
Col23a1	0.572876	5.00E-05	0.001507
mt-Rnr1	0.724536	5.00E-05	0.001507
mt-Rnr2	0.676591	5.00E-05	0.001507
mt-Co1	0.617126	5.00E-05	0.001507
S1pr3	0.479649	5.00E-05	0.001507
Myadm	0.742748	5.00E-05	0.001507
Scn2b	0.394733	5.00E-05	0.001507
Bves	0.490662	5.00E-05	0.001507
Prr16	0.296121	5.00E-05	0.001507
Wdfy1	0.330889	5.00E-05	0.001507
Lmbrd1	0.661742	5.00E-05	0.001507
6030408B16Rik	0.506653	5.00E-05	0.001507
Bnip3	0.665398	5.00E-05	0.001507
Fam174b	0.672003	5.00E-05	0.001507

Table S4 cont.

Ctsf	0.634518	5.00E-05	0.001507
Crocc2	0.436705	5.00E-05	0.001507
Zfp703	0.50537	5.00E-05	0.001507
Pou3f1	0.361919	5.00E-05	0.001507
Tbx3	0.651274	1.00E-04	0.002828
Lama4	0.532802	1.00E-04	0.002828
Tshr	0.410897	1.00E-04	0.002828
Hcn1	0.632014	1.00E-04	0.002828
Srbd1	0.661536	1.00E-04	0.002828
Traf5	0.454969	1.00E-04	0.002828
Trp53inp1	0.603727	1.00E-04	0.002828
Bhlhe40	0.569946	1.00E-04	0.002828
Cdo1	0.77683	1.00E-04	0.002828
Fam214a	0.62893	1.00E-04	0.002828
Fam110c	0.302289	1.00E-04	0.002828
Capn3	0.034987	1.00E-04	0.002828
Mbnl2	0.744057	0.00015	0.004063
Zfpm2	0.689684	0.00015	0.004063
Zeb2	0.605712	0.00015	0.004063
Flcn	0.722392	0.00015	0.004063
Arap1	0.556395	0.00015	0.004063
Rbm46	0.630865	0.00015	0.004063
Ssc5d	0.553635	0.00015	0.004063
Tgfbi	0.759057	0.00015	0.004063
Fnip1	0.679019	0.00015	0.004063
Ak5	0.4633	0.00015	0.004063
Kdm7a	0.663098	0.00015	0.004063
Upk3b	0.766757	0.00015	0.004063
Tmem119	0.760711	0.00015	0.004063
Susd2	0.533964	2.00E-04	0.005219
C1qtnf1	0.282214	2.00E-04	0.005219
Sh3yl1	0.660999	2.00E-04	0.005219
Prickle2	0.631427	0.00025	0.00633
Fah	0.491877	0.00025	0.00633
Ip6k1	0.736736	0.00025	0.00633
Ndp	0.36009	0.00025	0.00633
Jun	0.779192	0.00025	0.00633
mt-Nd4	0.760276	0.00025	0.00633
Arhgef25	0.755466	3.00E-04	0.007321
Hs1bp3	0.698519	3.00E-04	0.007321

Table S4 cont.

Cygb	0.434245	3.00E-04	0.007321
Aldh6a1	0.679051	3.00E-04	0.007321
Nr1d2	0.648773	3.00E-04	0.007321
Arhgdib	0.645955	3.00E-04	0.007321
Sbspon	0.377828	3.00E-04	0.007321
Myrf	0.791847	3.00E-04	0.007321
Ypel5	0.689612	3.00E-04	0.007321
Efna5	0.757469	3.00E-04	0.007321
B3gnt7	0.615403	3.00E-04	0.007321
Mr1	0.363851	0.00035	0.008289
Plekha5	0.758161	0.00035	0.008289
Tmem252	0.401616	0.00035	0.008289
Foxd1	0.686793	0.00035	0.008289
Nr4a1	0.638617	4.00E-04	0.009335
Tagln2	0.720813	4.00E-04	0.009335
Nrep	0.793483	4.00E-04	0.009335
Eva1b	0.715302	4.00E-04	0.009335
App	0.795774	0.00045	0.010332
Fam114a1	0.724822	0.00045	0.010332
Usp11	0.787519	0.00045	0.010332
Ephb1	0.644585	0.00045	0.010332
Fhad1	0.209694	0.00045	0.010332
Timp2	0.796047	5.00E-04	0.011318
Net1	0.786614	5.00E-04	0.011318
Cth	0.741269	5.00E-04	0.011318
Dzip1	0.754044	5.00E-04	0.011318
Tubg2	0.497159	5.00E-04	0.011318
Lrig3	0.77063	0.00055	0.012234
Glipr2	0.746268	0.00055	0.012234
Adgrb3	0.401402	0.00055	0.012234
Gns	0.7697	0.00055	0.012234
Arrdc3	0.755398	0.00055	0.012234
Scarf2	0.771843	6.00E-04	0.013208
Coch	0.485489	6.00E-04	0.013208
Rftn1	0.676542	6.00E-04	0.013208
Gm8399	0.717116	6.00E-04	0.013208
Dhrs3	0.641805	6.00E-04	0.013208
Btn1a1	0.441605	0.00065	0.014139
Fbxo32	0.650837	0.00065	0.014139
Olfml1	0.621576	0.00065	0.014139

Table S4 cont.

Thbd	0.732933	0.00065	0.014139
Pcsk5	0.699652	7.00E-04	0.014947
Nrp2	0.762786	7.00E-04	0.014947
Tpp1	0.764011	7.00E-04	0.014947
Sh3bgrl	0.766142	7.00E-04	0.014947
Aff3	0.695329	7.00E-04	0.014947
mt-Nd2	0.799119	7.00E-04	0.014947
Vim	0.688287	0.00075	0.01583
Dact1	0.803136	0.00075	0.01583
Kcnb2	0.575457	0.00075	0.01583
Alx1	0.709721	8.00E-04	0.016693
Vstm4	0.647107	8.00E-04	0.016693
Gm26617	0.53279	8.00E-04	0.016693
Tfpi	0.707625	0.00085	0.017508
Negr1	0.202976	0.00085	0.017508
Gm13456	0.773629	0.00085	0.017508
Maged2	0.810245	9.00E-04	0.018361
Igfbp5	0.809481	9.00E-04	0.018361
Boll	0.011093	0.00095	0.019077
Wnt2b	0.598741	0.00095	0.019077
Npr2	0.62063	0.00095	0.019077
Otud1	0.648294	0.00095	0.019077
mt-Cytb	0.779592	0.00095	0.019077
Dcn	0.736381	0.001	0.019864
Sorbs1	0.726196	0.001	0.019864
Leprot	0.777416	0.001	0.019864
Arhgap24	0.522562	0.00105	0.020665
Hbp1	0.737015	0.0011	0.021418
Ptger3	0.490315	0.0011	0.021418
Foxc1	0.792368	0.0011	0.021418
Myo6	0.580056	0.00115	0.022057
Mfap4	0.630086	0.00115	0.022057
Snai1	0.755254	0.00115	0.022057
Flrt2	0.734266	0.00115	0.022057
Pex26	0.606094	0.00115	0.022057
Apcdd1	0.696973	0.00115	0.022057
Cldn1	0.622781	0.0012	0.022845
Adam33	0.18176	0.0012	0.022845
Parm1	0.755782	0.0012	0.022845
Washc3	0.708054	0.00125	0.023621

Table S4 cont.

Sntg2	0.392037	0.00125	0.023621
Ttc28	0.684175	0.0013	0.024386
Hist3h2a	0.691153	0.0013	0.024386
Ypel3	0.734582	0.00135	0.025067
P4ha1	0.798247	0.0014	0.025771
Grina	0.67406	0.0014	0.025771
Arntl2	0.306604	0.0014	0.025771
Mxra8	0.732333	0.00145	0.026615
Mest	0.786743	0.0015	0.027415
Gstm6	0.130622	0.0015	0.027415
Enpep	0.548953	0.00155	0.028168
Zfhx3	0.781919	0.00155	0.028168
Calcr	0.538101	0.0016	0.028832
Arhgap6	0.366938	0.0016	0.028832
Hemk1	0.523932	0.0016	0.028832
Egln3	0.629568	0.0016	0.028832
Pnpla8	0.748754	0.0016	0.028832
Rab11b	0.581459	0.00165	0.029608
Lmo4	0.709265	0.0017	0.030377
Ugdh	0.814392	0.0017	0.030377
Erbin	0.792398	0.00175	0.030926
Clasp2	0.751903	0.00175	0.030926
Tril	0.816001	0.00175	0.030926
Malat1	0.718961	0.00175	0.030926
Prss12	0.55495	0.0019	0.033255
Lamp2	0.785641	0.00195	0.033991
Tdrd1	0.620975	0.002	0.034487
Kcnq4	0.547491	0.002	0.034487
Sspn	0.682747	0.002	0.034487
Cpt1c	0.739653	0.00205	0.035113
Btd	0.623455	0.00205	0.035113
Itgb5	0.753204	0.00205	0.035113
Qpct	0.423481	0.00205	0.035113
Twsg1	0.822107	0.0021	0.035826
Mid1	0.445248	0.0021	0.035826
Chrm2	0.394758	0.0021	0.035826
Sh3rf1	0.766449	0.0022	0.037136
Pdlim2	0.569354	0.00225	0.037781
Rnf19a	0.801266	0.00225	0.037781
Rtl3	0.654428	0.00225	0.037781

Table S4 cont.

Pabpc4l	0.7025	0.00225	0.037781
Epb41l2	0.810243	0.00235	0.039306
Cd99l2	0.643338	0.0024	0.039934
Rps6ka5	0.693468	0.00245	0.04045
Tppp	0.324322	0.00245	0.04045
Nexn	0.657028	0.0025	0.041064
Camk1g	0.699087	0.0026	0.042435
Carmn	0.661231	0.00265	0.043141
Tmem45a	0.407197	0.0027	0.043677
Ldlrad4	0.517744	0.0027	0.043677
Jund	0.815904	0.0027	0.043677
Rab35	0.705141	0.0028	0.045011
Ubl3	0.803755	0.0029	0.046444
Tmem8b	0.528541	0.0029	0.046444
Enox1	0.727562	0.003	0.047687
Cnrip1	0.705518	0.003	0.047687
Atg14	0.780527	0.00305	0.048243
Nfam1	0.565289	0.0031	0.048913
Tgfbr2	0.717937	0.0032	0.049998
Fstl4	0.624958	0.0032	0.049998

Table S5. Genes with *Osr1*-dependent expression gradient from SHF to OFT.

Gene symbol	p-value	Gene symbol	p-value
Rnf138	1.77E-05	Champ1	0.025967
Tdp2	3.17E-05	Exosc3	0.026165
E2f5	6.35E-05	Zfp385a	0.026509
A030001D20Rik	0.000116	Dhx15	0.026669
Caap1	0.00013	Nsun3	0.026874
Gt(ROSA)26Sor	0.000238	Exosc4	0.026898
Dnajc30	0.000531	Zfp775	0.026916
Poldip2	0.000546	Gm11273	0.026954
Pi4k2b	0.000547	Tmem245	0.027031
Prpf39	0.000559	Gm49336	0.027047
Saxo2	0.000672	Tanc1	0.027069
4933417C20Rik	0.000722	Esyt2	0.027238
Chmp1b	0.000738	Tgfbrap1	0.027369
Qdpr	0.000794	Zfp975	0.027398
Sec62	0.00082	Tmem143	0.02743
Hspa1l	0.000829	Jagn1	0.027504
Zfyve19	0.00099	Tctex1d2	0.027532
4-Sep	0.001083	Gan	0.027593
Snrnp27	0.001093	Adsl	0.027624
Cd2ap	0.001168	Fbxw5	0.02765
Zdhhc7	0.00125	Mfsd12	0.027658
Lsm5	0.001254	Fam133b	0.027713
1110059G10Rik	0.001322	Cript	0.027733
Mtpn	0.001354	Ybey	0.027804
Ier5	0.001359	Zbtb1	0.027818
Sumo1	0.001509	Gpalpp1	0.027824
Orc4	0.001581	Timm44	0.02783
Dr1	0.001723	Xiap	0.027859
Zfp994	0.001785	Rasa3	0.027862
Sfi1	0.001986	Commd7	0.027969
Trim59	0.002051	Acp6	0.028036
Fam185a	0.002137	Cers6	0.02812
Pdrg1	0.002251	Mrps6	0.028213
Frmd8	0.002285	Ralgapa2	0.028301
Commd8	0.002418	AI314180	0.028325
Vwa8	0.002494	Dbp	0.028337
Npepps	0.002537	Plcl2	0.028657
Haus6	0.002762	Zfp850	0.028889
C230062I16Rik	0.002806	Gm7832	0.028921

Table S5 cont.

Bet1	0.003148	Rbm8a	0.028922
Thoc2	0.003174	Etaa1	0.028931
Tgfbr3	0.003265	Tjap1	0.028992
Cyb5rl	0.003522	1700096K18Rik	0.028995
Trmu	0.003613	Acat1	0.029017
Vps26a	0.00363	Nudt16l1	0.02908
Mga	0.00367	Gm14399	0.029214
Gm8177	0.00367	Zfp788	0.029225
Papolg	0.003762	Svip	0.029235
Cdkn2aip	0.003974	Ccdc71l	0.02934
Ech1	0.004062	Scoc	0.029351
Macrod2	0.004111	Nosip	0.029661
Uhrf2	0.004205	Abcb8	0.029677
Terf1	0.004248	Pmpcb	0.029882
Aldh4a1	0.004299	Gm37422	0.029895
Hist1h3c	0.004303	Xkr8	0.030017
Chd8	0.004316	9330151L19Rik	0.030019
Sirt1	0.00444	Tcp1l1	0.030058
R3hdm1	0.00455	Gm45731	0.030068
Elavl1	0.004562	Hist1h3d	0.030128
Surf1	0.004574	Zfp758	0.030191
Sfr1	0.004577	Mms22l	0.030245
Trim23	0.004612	Agk	0.030283
Rwdd3	0.004637	Maea	0.030296
Dpy19l4	0.004689	Usp33	0.030311
Ndufaf3	0.004698	Yipf4	0.030438
Tank	0.004792	Nt5c3b	0.030478
Pdpr	0.004916	Tmem33	0.030521
Gm6063	0.004943	Ube4a	0.030666
Fgfr1op	0.004983	Ptrh1	0.030728
Slbp	0.005009	Cenpq	0.030795
Ivd	0.005012	Tmem201	0.03103
AU040320	0.005409	Ankrd39	0.031132
Set	0.005441	Snrnp48	0.031237
Nr6a1	0.005537	Gm10033	0.031312
Katnbl1	0.005635	Disp1	0.031381
Ssb	0.005671	Tmem41a	0.03157
Zbtb40	0.005686	Poll	0.031664
Klhl18	0.005698	Nubpl	0.031974
Dennd6b	0.005866	Agl	0.032034

Table S5 cont.

Zdhhc4	0.00597	Dctd	0.032102
Lin7c	0.006027	Chd4	0.032237
Fam103a1	0.00642	Bnip1	0.032269
Clasp1	0.006686	Zfp944	0.032279
Pcnp	0.006839	Fign	0.032287
Plekhm3	0.006933	2810021J22Rik	0.032327
Lhpp	0.006947	Ndufaf5	0.032463
Tmem55a	0.006971	4932442E05Rik	0.032593
Mgmt	0.006972	E530011L22Rik	0.032695
Pi4ka	0.007029	Mfsd4b4	0.032781
Rbm7	0.007103	Gm15559	0.032914
Ttc38	0.007111	Ankrd17	0.032919
Smcr8	0.007149	Slc25a22	0.033152
Kpna4	0.007186	Perp	0.033184
Zfp943	0.007193	Mgrn1	0.033292
Mir17hg	0.007296	Xpnpep3	0.033384
Ptges2	0.007448	Ythdc2	0.033397
Vars2	0.007485	Bphl	0.033444
Crls1	0.007625	Pdcd7	0.033674
Nagpa	0.007848	3830406C13Rik	0.033757
Lin9	0.0079	Slc15a4	0.033763
Fam76b	0.008016	C8g	0.034029
Stard3	0.008088	2610005L07Rik	0.034078
5330438D12Rik	0.008092	Xpo6	0.034091
Tcea1	0.008154	Jmjd7	0.034118
4931414P19Rik	0.008191	Frg1	0.03422
Gm26582	0.008207	Sash1	0.034236
Pecr	0.008438	Gm16973	0.034289
Cobll1	0.00856	Gm48673	0.034359
Ints8	0.008649	Adck5	0.034437
Trmt13	0.009064	B3gnt3	0.034585
Qrsl1	0.009077	Fam160b2	0.034612
Lmf1	0.009111	Tmem203	0.034643
Fitm2	0.009112	Atl3	0.034733
Atp9b	0.00912	Cops2	0.034748
Polr3k	0.009254	Smc6	0.034912
Gm43178	0.009329	Fam49b	0.035098
Hist1h2ac	0.009891	Tnik	0.035174
Heatr5b	0.009934	Zfp691	0.035232
Sh3kbp1	0.010072	Comtd1	0.035277

Table S5 cont.

Thada	0.01011	Srpk2	0.035837
Npepl1	0.010179	Meioc	0.03597
Ireb2	0.010456	Gm43654	0.036007
Kpna3	0.010484	Naa50	0.036019
Gm43597	0.010615	Slc25a33	0.036143
Rsbn1l	0.010932	Smyd4	0.036313
D10Jhu81e	0.011068	Zfp3	0.03637
Csnk1g1	0.01117	Ubxn6	0.036378
Dcaf4	0.011205	Gne	0.036438
Gm5620	0.011252	Pde4dip	0.036534
Dcaf12l1	0.011254	Ankzf1	0.036831
Glud1	0.011321	Polg2	0.036859
Ing5	0.01141	Ubxn2b	0.036877
Tada2b	0.011548	Ppm1l	0.036907
Apc2	0.011771	Rwdd2b	0.036933
Thap4	0.011868	Arhgap39	0.037138
Efnb3	0.011906	2510002D24Rik	0.037185
Slc3a1	0.011934	Glcci1	0.037228
2310009B15Rik	0.012289	Gmeb1	0.037512
Star	0.012328	Pvt1	0.03754
Psmg3	0.012391	Ddx5	0.037673
Ppp4r3a	0.012408	Rsad1	0.037871
Sh3glb2	0.012536	Abcc10	0.037921
Nudt8	0.012637	Cryzl2	0.03803
Serhl	0.012722	Swt1	0.038065
Tceal8	0.012896	Dmap1	0.038098
Adar	0.013007	Rnpc3	0.03818
Abtb2	0.013263	4930503L19Rik	0.038274
Gpatch2l	0.013274	Ydjc	0.038374
Gcn1l1	0.013292	Gm28048	0.038384
Pqlc1	0.013506	Pycard	0.038414
Dffa	0.013526	Smyd2	0.038556
Prcp	0.013632	Rnf115	0.038576
Scap	0.01389	Kif1b	0.038666
Ptpn2	0.013954	Catsper2	0.038691
Ddt	0.014037	Ick	0.038785
Clk4	0.014272	Ddhd2	0.038791
1300014J16Rik	0.014335	Rubcn	0.038843
Ptpn12	0.014378	Fdx1	0.038849
Chmp5	0.01484	Ccdc28b	0.038958

Table S5 cont.

Thoc1	0.015001	Lias	0.038967
Rab9	0.01508	Angel1	0.038994
Pafah2	0.015284	Ndufaf6	0.039012
Acbd5	0.01533	Haus3	0.039065
Rab10	0.015413	Fyco1	0.039107
7-Sep	0.015522	Engase	0.039382
Gm43593	0.015631	Snapc5	0.039681
Cdkn1c	0.01567	Stard7	0.039812
Ano1	0.015676	Gm26909	0.040176
Tonsl	0.015732	Slc18a1	0.040226
Nav3	0.015785	Mon1b	0.040238
Sp2	0.015983	Gm26530	0.040261
Prss36	0.016206	Atp11b	0.040332
Gosr1	0.016274	Mvd	0.040436
Sirt5	0.016359	Pmm2	0.040514
Gatsl2	0.016524	Usp20	0.040545
Tomm20	0.01667	Rgp1	0.040801
Acad8	0.016674	Stk39	0.040968
Sde2	0.016692	Snupn	0.041016
Ppp1r9a	0.016773	Zfp870	0.041019
Dhodh	0.0169	Map4k4	0.04103
Dhtkd1	0.016903	Papola	0.04114
Sla2	0.016938	Rom1	0.041156
Eepd1	0.016965	Ccdc171	0.041213
Zfp507	0.016979	Stx17	0.041275
Mis18a	0.016981	Wdr91	0.041394
Dnajc4	0.016999	Snx12	0.041433
Ankhd1	0.017045	Fkrp	0.041513
Gm20163	0.017081	Mapk8ip3	0.04168
1110065P20Rik	0.017223	Dip2b	0.041698
Cnot1	0.017227	Gm6863	0.041768
A130010J15Rik	0.017267	Apip	0.041779
Dck	0.01728	Csnk2b	0.041811
Dusp11	0.017363	Plekha7	0.041942
Bdh1	0.017674	Dus2	0.041959
Miga2	0.017815	Pphln1	0.04196
Rdh13	0.017945	Pgk1	0.042022
Ccnl1	0.017948	Wdr92	0.042126
Golga4	0.017954	Gm15283	0.042155
Zcchc10	0.018039	Gstm4	0.042162

Table S5 cont.

Depdc1a	0.018194	Lipt1	0.042208
Foxred1	0.018353	Tpx2	0.042351
Plpp7	0.018446	Wbp11	0.04241
Ptges3	0.018491	Hif1an	0.042481
Mccc1	0.018502	Zbtb6	0.042627
Tmx3	0.018616	Gm37677	0.042651
Depdc5	0.0187	Pkn1	0.042742
Adck1	0.018842	Flvcr2	0.042786
Dguok	0.018849	Taz	0.042901
Pias4	0.018855	Sdr39u1	0.042965
Nfkb2	0.018941	Slc43a3	0.043029
8-Sep	0.019141	Alyref	0.043051
Mrps27	0.019284	Ppif	0.043123
Galt	0.019415	Polr2g	0.043174
Alg13	0.019522	Gpbp1	0.043186
Nhsl1	0.019542	Got2	0.043212
Elmod2	0.019559	0610012G03Rik	0.043393
Rab8b	0.019695	Gm26819	0.043439
2810039B14Rik	0.019721	Gm45205	0.043601
Acad11	0.019768	Mrpl48	0.043712
Drp2	0.019769	Sgk3	0.044338
Mpv17	0.019778	Rock1	0.044671
Atp11c	0.01988	Nmnat1	0.044713
Cpsf2	0.020197	Gm48551	0.044714
Gm28901	0.020219	Grb10	0.04476
Tecpr2	0.020369	Eed	0.044818
Ankrd24	0.020396	Tmem183a	0.044823
Mtmr14	0.020442	Coprs	0.04484
Sdhaf1	0.020534	Amdhd2	0.044851
Rundc1	0.02056	Pth1r	0.044994
Pacsin3	0.020835	Eef1akmt2	0.045086
Ube2d-ps	0.02085	Zfp839	0.045212
Lats1	0.020879	Rbbp8	0.045242
Snx30	0.020935	Cish	0.045359
Smoc1	0.020964	Mlec	0.045377
Tef	0.021038	Dnd1	0.045393
Lrch1	0.021058	Cdkn1a	0.045415
Spryd4	0.021113	Ppp5c	0.04542
Abcd1	0.021256	Gm20661	0.045487
Pctp	0.021265	Sat2	0.045558

Table S5 cont.

Rangrf	0.021659	Prdx5	0.045696
Usp46	0.021664	Txnl4b	0.045706
Tor1a	0.021683	Mest	0.045764
Bri3bp	0.02172	Smg1	0.045835
Ntpcr	0.021723	Cd3eap	0.045904
Nemp1	0.02193	Vbp1	0.046019
AA465934	0.021963	Lins1	0.046099
Ppp6c	0.021989	Fgf13	0.046147
Rbm39	0.022012	Rhobtb2	0.046351
Irf7	0.022059	Abhd14a	0.046413
Birc6	0.022165	Mmab	0.046484
Ipo4	0.022194	Actr1a	0.046649
Gm6159	0.022244	As3mt	0.046716
Fam168a	0.022264	0610037L13Rik	0.046795
Rsph3a	0.022477	Tom1l2	0.046799
Dedd	0.022672	Nt5m	0.046803
Gm11960	0.022687	Dhrs7b	0.04691
Sco2	0.0227	Gm10110	0.047234
Gpd2	0.022907	Hsd17b4	0.047284
Rabgap1l	0.022911	Coq7	0.047301
Ppid	0.022994	Gm38431	0.047587
Dnah14	0.023051	Rassf3	0.047611
Gm43292	0.023187	Tbc1d10b	0.047681
Slc29a2	0.023245	Slc25a11	0.047763
Son	0.023271	Acad12	0.047801
Zeb1	0.023292	Elovl6	0.047954
Twnk	0.023368	Phka1	0.048045
Cnep1r1	0.023579	Lcat	0.048157
Rpn1	0.023598	Gchfr	0.048283
Zfp429	0.023633	Ttc7b	0.048295
Chchd5	0.023647	Sirt3	0.048366
Stk11ip	0.023794	Eny2	0.048377
1810043G02Rik	0.023804	Elf1	0.048389
Upf3b	0.023848	Gm47138	0.0485
Srsf9	0.023965	Lnpk	0.048569
Wars2	0.024008	Btbd10	0.048583
Dennd4b	0.02415	Gm10277	0.048721
Hpf1	0.024207	Rogdi	0.048792
Cdk11b	0.024213	Lin52	0.048794
BC031181	0.024273	Hint2	0.048805

Table S5 cont.

Tmem177	0.024292	Cpt2	0.048826
Slx1b	0.024307	Gm11423	0.048839
Ddx3x	0.024465	Glb1	0.048862
Mapkbp1	0.024615	Pnma1	0.049024
Gm16374	0.025004	Ccl27a	0.049064
Wdr41	0.02535	Klf10	0.049176
Acad9	0.02535	Spty2d1	0.049221
Mlycd	0.02536	Yod1	0.049267
Fam3a	0.025542	9330020H09Rik	0.049284
Plek	0.025604	Esco1	0.049357
Bpnt1	0.02563	Mrpl41	0.049471
Ndufb5	0.025835	Dnajc5	0.049473
Atpaf1	0.025849	Srsf10	0.049609
Gabarapl2	0.02585	Gm3200	0.049901
Zzz3	0.025897	Tmem106c	0.049936
Klf15	0.02592	BC037034	0.049994

REFERENCES

Abbey, D., and Seshagiri, P.B. (2013). Aza-induced cardiomyocyte differentiation of P19 EC-cells by epigenetic co-regulation and ERK signaling. Gene *526*, 364–373.

Abe, M., Ruest, L., and Clouthier, D.E. (2007). Fate of cranial neural crest cells during craniofacial development in endothelin-A receptor-deficient mice. Int J Dev Biol *51*, 97–105.

Adachi, I., Seale, A., Uemura, H., McCarthy, K.P., Kimberley, P., and Ho, S.Y. (2009). Morphologic spectrum of truncal valvar origin relative to the ventricular septum: Correlation with the size of ventricular septal defect. J. Thorac. Cardiovasc. Surg. *138*, 1283–1289.

Ahmad, S.M. (2017). Conserved Signaling Mechanisms in Drosophila Heart Development. Dev. Dyn. *246*, 641–656.

Van den Akker, N.M.S., Winkel, L.C.J., Nisancioglu, M.H., Maas, S., Wisse, L.J., Armulik, A., Poelmann, R.E., Lie-Venema, H., Betsholtz, C., and Gittenberger-de Groot, A.C. (2008). PDGF-B signaling is important for murine cardiac development: Its role in developing atrioventricular valves, coronaries, and cardiac innervation. Dev. Dyn. *237*, 494–503.

Anderson, R., Webb, S., Brown, N., Lamers, W., and Moorman, A. (2003). Development of the heart: (2) Septation of the atriums and ventricles. Heart *89*, 949–958.

Ansel, K.M., Harris, R.B.S., Cyster, J.G., Francisco, S., and Hall, D. (2002). CXCL13 Is Required for B1 Cell Homing , Natural Antibody Production , and Body Cavity Immunity. Immunity *16*, 67–76.

Bajolle, F., Zaffran, S., Kelly, R.G., Hadchouel, J., Bonnet, D., Brown, N.A., and Buckingham, M.E. (2006). Rotation of the myocardial wall of the outflow tract is implicated in the normal positioning of the great arteries. Circ. Res. *98*, 421–428.

Bax, N.A.M., Bleyl, S.B., Gallini, R., Wisse, L.J., Hunter, J., Van Oorschot, A.A.M., Mahtab, E.A.F., Lie-Venema, H., Goumans, M.-J., Betsholtz, C., et al. (2010). Cardiac malformations in Pdgfrα mutant embryos are associated with increased expression of WT1 and Nkx2.5 in the second heart field. Dev. Dyn. *239*, 2307–2317.

Benjamin, E.J., Virani, S.S., Callaway, C.W., Chang, A.R., Cheng, S., Chiuve, S.E., Cushman, M., Delling, F.N., Deo, R., de Ferranti, S.D., et al. (2018). Heart Disease and Stroke Statistics—2018 Update: A Report From the American Heart Association.

Bird, A.P., and Wolffe, A.P. (1999). Methylation-Induced Repression— Belts, Braces, and Chromatin. Cell *99*, 451–454.

Bloomekatz, J., Singh, R., Prall, O.W., Dunn, A.C., Harvey, R.P., Yelon, D., Vaughan, M., and Loo, C.-S. (2017). Platelet-derived growth factor (PDGF) signaling directs cardiomyocyte movement toward the midline during heart tube assembly. Elife *6*, 1–23.

Briggs, L.E., Burns, T.A., Lockhart, M.M., Phelps, A.L., Van den Hoff, M.J.B., and Wessels, A. (2016). Wnt/β-catenin and sonic hedgehog pathways interact in the regulation of the development of the dorsal mesenchymal protrusion. Dev. Dyn. *245*, 103–113.

Buckingham, M., Meilhac, S., and Zaffran, S. (2005). Building the mammalian heart from two sources of myocardial cells. Nat. Rev. Genet. *6*, 826–835.

Buenrostro, J., Wu, B., Chang, H., and Greenleaf, W. (2015). ATAC-seq: A Method for Assaying Chromatin Accessibility Genome-Wide. Curr Protoc Mol Biol *109*, 21.29.1-21.29.9.

Buenrostro, J.D., Giresi, P.G., Zaba, L.C., Chang, H.Y., and Greenleaf, W.J. (2013). Transposition of native chromatin for fast and sensitive epigenomic profiling of open chromatin, DNA-binding proteins and nucleosome position. Nat. Methods *10*, 1213–1218.

Cai, C.L., Liang, X., Shi, Y., Chu, P.H., Pfaff, S.L., Chen, J., and Evans, S. (2003). Isl1 identifies a cardiac progenitor population that proliferates prior to differentiation and contributes a majority of cells to the heart. Dev. Cell *5*, 877–889.

Camenisch, T.D., Biesterfeldt, J., Brehm-Gibson, T., Bradley, J., and McDonald, J.A. (2001). Regulation of cardiac cushion development by hyaluronan. Exp. Clin. Cardiol. *6*, 4–10.

Chamberlain, A.A., Lin, M., Lister, R.L., Maslov, A.A., Wang, Y., Suzuki, M., Wu, B., Greally, J.M., Zheng, D., and Zhou, B. (2014). DNA methylation is developmentally regulated for genes essential for cardiogenesis. J. Am. Heart Assoc. *3*, 1–20.

Chang, C.-P., and Bruneau, B.G. (2012). Epigenetics and Cardiovascular Development. Annu. Rev. Physiol. *74*, 41–68.

Collet, R., and Edwards, J. (1949). Persistent truncus arteriosus: a classification according to anatomical types. Surg. Clin. North Am. *29*, 1245–1270.

Coulter, D.E., and Wieschaus, E. (1988). Gene activities and segmental patterning in Drosophila: analysis of odd-skipped and pair-rule double mutants. Genes Dev. *2*, 1812–1823.

Coulter, D.E., Swaykus, E.A., Beran-Koehn, M.A., Goldberg, D., Wieschaus, E., and Schedl, P. (1990). Molecular analysis of odd-skipped , a zinc finger encoding segmentation gene with a novel pair-rule expression pattern. Embo J. *8*, 3795–3804.

Decaillot, F.M., Kazmi, M.A., Lin, Y., Ray-saha, S., Sakmar, T.P., and Sachdev, P. (2011). CXCR7/CXCR4 Heterodimer Constitutively Recruits beta-Arrestin to Enhance Cell Migration. J. Biol. Chem. *286*, 32188–32197.

Duchek, P., Somogyi, K., Jekely, G., Beccari, S., and Rørth, P. (2001). Guidance of Cell Migration by the Drosophila PDGF/VEGF Receptor. Cell *107*, 1–10.

Dyer, L.A., and Kirby, M.L. (2009). Sonic hedgehog maintains proliferation in secondary heart field progenitors and is required for normal arterial pole formation. Dev. Biol. *330*, 305–317.

Dyer, L.A., Makadia, F.A., Scott, A., Pegram, K., Hutson, M.R., and Kirby, M.L. (2010). BMP signaling modulates hedgehog-induced secondary heart field proliferation. Dev. Biol. *348*, 167–176.

Fantauzzo, K.A., and Soriano, P. (2016). PDGFRβ regulates craniofacial development through homodimers and functional heterodimers with PDGFRα. Genes Dev. *30*, 2443–2458.

Fujita, N., Watanabe, S., Ichimura, T., Tsuruzoe, S., Shinkai, Y., Tachibana, M., Chiba, T., and Nakao, M. (2003). Methyl-CpG binding domain 1 (MBD1) interacts with the Suv39h1-HP1 heterochromatic complex for DNA methylation-based transcriptional repression. J. Biol. Chem. *278*, 24132–24138.

Galli, D., Domínguez, J.N., Zaffran, S., Munk, A., Brown, N.A., and Buckingham, M.E. (2008). Atrial myocardium derives from the posterior region of the second heart field , which acquires left-right identity as Pitx2c is expressed. Development *135*, 1157–1167.

Gao, Y., Lan, Y., Liu, H., and Jiang, R. (2011). The zinc finger transcription factors Osr1 and Osr2 control synovial joint formation. Dev. Biol. *352*, 83–91.

Garg, V., Yamagishi, C., Hu, T., Kathiriya, I.S., Yamagishi, H., and Srivastava, D. (2001). Tbx1, a DiGeorge syndrome candidate gene, is regulated by sonic hedgehog during pharyngeal arch development. Dev. Biol. *235*, 62–73.

Gilboa, S.M., Devine, O.J., Kucik, J.E., Oster, M.E., Riehle-Colarusso, T., Nembhard, W.N., Xu, P., Correa, A., Jenkins, K., and Marelli, A.J. (2016). Congenital Heart Defects

in the United States: Estimating the Magnitude of the Affected Population in 2010. Circulation *134*, 101–109.

Gilsbach, R., Preissl, S., Grüning, B.A., Schnick, T., Burger, L., Benes, V., Würch, A., Bönisch, U., Günther, S., Backofen, R., et al. (2014). Dynamic DNA methylation orchestrates cardiomyocyte development, maturation and disease. Nat. Commun. *5*.

Goddeeris, M.M., Schwartz, R., Klingensmith, J., and Meyers, E.N. (2007). Independent requirements for Hedgehog signaling by both the anterior heart field and neural crest cells for outflow tract development. Development *134*, 1593–1604.

Gowher, H., Liebert, K., Hermann, A., Xu, G., and Jeltsch, A. (2005). Mechanism of stimulation of catalytic activity of Dnmt3A and Dnmt3B DNA-(cytosine-C5)-methyltransferases by Dnmt3L. J. Biol. Chem. *280*, 13341–13348.

Han, L., Xu, J., Grigg, E., Slack, M., Chaturvedi, P., Jiang, R., and Zorn, A.M. (2017). Osr1 functions downstream of Hedgehog pathway to regulate foregut development. Dev. Biol. *427*, 72–83.

Hang, C.T., Yang, J., Han, P., Cheng, H.L., Shang, C., Ashley, E., Zhou, B., and Chang, C.P. (2010). Chromatin regulation by Brg1 underlies heart muscle development and disease. Nature *466*, 62–67.

Hayashi, S., and McMahon, A.P. (2002). Efficient recombination in diverse tissues by a tamoxifen-inducible form of Cre: A tool for temporally regulated gene activation/inactivation in the mouse. Dev. Biol. *244*, 305–318.

Heinz, S., Benner, C., Spann, N., Bertolino, E., Lin, Y.C., Laslo, P., Cheng, J.X., Murre, C., Singh, H., and Glass, C.K. (2010). Simple combinations of lineage-determining transcription factors prime cis-regulatory elements required for macrophage and B cell identities. Mol. Cell *38*, 576–589.

High, F.A., Jain, R., Stoller, J.Z., Antonucci, N.B., Min, M.L., Loomes, K.M., Kaestner, K.H., Pear, W.S., and Epstein, J.A. (2009). Murine Jagged1/Notch signaling in the second heart field orchestrates Fgf8 expression and tissue-tissue interactions during outflow tract development. J. Clin. Invest. *119*, 1986–1996.

Hoffmann, A.D., Peterson, M.A., Friedland-Little, J.M., Anderson, S.A., and Moskowitz, I.P. (2009). Sonic Hedgehog Is Required in Pulmonary Endoderm for Atrial Septation. Development *136*, 1761–1770.

Huck-Hui, N., and Bird, A. (1999). DNA methylation and chromatin modification. Curr. Opin. Genet. Dev. *9*, 158–163.

Hutson, M.R., and Kirby, M.L. (2003). Neural crest and cardiovascular development: A

20-year perspective. Birth Defects Res. Part C - Embryo Today Rev. *69*, 2–13.

Kelly, R.G., and Buckingham, M.E. (2002). The anterior heart-forming field: Voyage to the arterial pole of the heart. Trends Genet. *18*, 210–216.

Kelly, R.G., Brown, N.A., Buckingham, M.E., and Kingdom, U. (2001). The Arterial Pole of the Mouse Heart Forms from. Dev. Cell *1*, 435–440.

Kim, D., Langmead, B., and Salzberg, S.L. (2015). HISAT: A fast spliced aligner with low memory requirements. Nat. Methods *12*, 357–360.

Kimbrell, D.A., Hice, C., Bolduc, C., Kleinhesselink, K., and Beckingham, K. (2002). The Dorothy Enhancer Has Tinman Binding Sites and Drives hopscotch -Induced Tumor Formation. Genesis *34*, 23–28.

Krueger, F., and Andrews, S.R. (2011). Bismark: A flexible aligner and methylation caller for Bisulfite-Seq applications. Bioinformatics *27*, 1571–1572.

Lan, Y., Liu, H., Ovitt, C.E., and Jiang, R. (2011). Generation of Osr1 conditional mutant mice. Genesis *49*, 419–422.

Landt, S.G., Marinov, G.K., Kundaje, A., and Kheradpour, P. (2012). ChIP-seq guidelines and practices of the ENCODE and modENCODE consortia. Genome Res. *22*, 1813–1831.

de Lange, F.J., Moorman, A.F.M., Anderson, R.H., Männer, J., Soufan, A.T., De Gier-De Vries, C., Schneider, M.D., Webb, S., Van Den Hoff, M.J.B., and Christoffels, V.M. (2004). Lineage and morphogenetic analysis of the cardiac valves. Circ. Res. *95*, 645–654.

Le-Drean, B.S., Nasiadka, A., Dong, J., and Krause, H.M. (1998). Dynamic changes in the functions of Odd-skipped during early Drozophila embryogenesis. Development *125*, 4851–4861.

Lickert, H., Takeuchi, J.K., Von Both, I., Walls, J.R., McAuliffe, F., Adamson, S.L., Henkelman, R.M., Wrana, J.L., Rossant, J., and Bruneau, B.G. (2004). Baf60c is essential for function of BAF chromatin remodelling complexes in heart development. Nature *432*, 107–112.

Lin, C.-J., Lin, C.-Y., Chen, C.-H., Zhou, B., and Chang, C.-P. (2012). Partitioning the heart: mechanisms of cardiac septation and valve development. Development *139*, 3277–3299.

Lin, L., Bu, L., Cai, C.L., Zhang, X., and Evans, S. (2006). Isl1 is upstream of sonic hedgehog in a pathway required for cardiac morphogenesis. Dev. Biol. *295*, 756–763.

Lin, L., Cui, L., Zhou, W., Dufort, D., Zhang, X., Cai, C.-L., Bu, L., Yang, L., Martin, J., Kemler, R., et al. (2007). β-Catenin directly regulates Islet1 expression in cardiovascular progenitors and is required for multiple aspects of cardiogenesis. Proc. Natl. Acad. Sci. *104*, 9313–9318.

Liu, H., Lan, Y., Xu, J., Chang, C.-F., Brugmann, S.A., and Jiang, R. (2013). Odd-skipped related-1 controls neural crest chondrogenesis during tongue development. Proc. Natl. Acad. Sci. *110*, 18555–18560.

Mae, S.I., Shono, A., Shiota, F., Yasuno, T., Kajiwara, M., Gotoda-Nishimura, N., Arai, S., Sato-Otubo, A., Toyoda, T., Takahashi, K., et al. (2013). Monitoring and robust induction of nephrogenic intermediate mesoderm from human pluripotent stem cells. Nat. Commun. *4*.

Martinez, S.R., Gay, M.S., and Zhang, L. (2015). Epigenetic mechanisms in heart development and disease. Drug Discov. Today *20*, 799–811.

Martins, P., and Castela, E. (2008). Transposition of the great arteries. Orphanet J. Rare Dis. *3*, 1–10.

Maurano, M.T., Wang, H., John, S., Shafer, A., Canfield, T., Lee, K., and Stamatoyannopoulos, J.A. (2015). Role of DNA Methylation in Modulating Transcription Factor Occupancy. Cell Rep. *12*, 1184–1195.

Mjaatvedt, C.H., Nakaoka, T., Moreno-Rodriguez, R., Norris, R.A., Kern, M.J., Eisenberg, C.A., Turner, D., and Markwald, R.R. (2001). The outflow tract of the heart is recruited from a novel heart-forming field. Dev. Biol. *238*, 97–109.

Mommersteeg, M.T.M., Soufan, A.T., De Lange, F.J., Van Den Hoff, M.J.B., Anderson, R.H., Christoffels, V.M., and Moorman, A.F.M. (2006). Two distinct pools of mesenchyme contribute to the development of the atrial septum. Circ. Res. *99*, 351–353.

Moorman, A., Webb, S., Brown, N., Lamers, W., and Anderson, R. (2003). Development of the Heart: (1) Formation of the Cardiac Chambers and Arterial Trunks. Heart *89*, 806–814.

Mugford, J.W., Sipilä, P., McMahon, J.A., and McMahon, A.P. (2008). Osr1 expression demarcates a multi-potent population of intermediate mesoderm that undergoes progressive restriction to an Osr1-dependent nephron progenitor compartment within the mammalian kidney. Dev. Biol. *324*, 88–98.

Neeb, Z., Lajiness, J.D., Bolanis, E., and Conway, S.J. (2013). Cardiac outflow tract anomalies. Wiley Interdiscip. Rev. Dev. Biol. *2*, 499–530.

Nüsslein-volhard, C., and Wieschaus, E. (1980). Mutations affecting segment number

and polarity in drosophila. Nature *287*, 795–801.

Obler, D., Juraszek, A.L., Smoot, L.B., and Natowicz, M.R. (2008). Double outlet right ventricle: Aetiologies and associations. J. Med. Genet. *45*, 481–497.

Ohtani, K., and Dimmeler, S. (2011). Epigenetic regulation of cardiovascular differentiation. Cardiovasc. Res. *90*, 404–412.

Okamoto, N., Akimoto, N., Hidaka, N., Shoji, S., and Sumida, H. (2010). Formal genesis of the outflow tracts of the heart revisited: Previous works in the light of recent observations. Congenit. Anom. (Kyoto). *50*, 141–158.

Okano, M., Bell, D.W., Haber, D.A., and Li, E. (1999). DNA Methyltransferases Dnmt3a and Dnmt3b Are Essential for De Novo Methylation and Mammalian Development. Cell *99*, 1–11.

Peng, Y., Yan, S., Chen, D., Cui, X., and Jiao, K. (2017). Pdgfrb is a direct regulatory target of TGFβ signaling in atrioventricular cushion mesenchymal cells. PLoS One *12*, 1–14.

Pertea, M., Kim, D., Pertea, G.M., Leek, J.T., and Salzberg, S.L. (2016). Transcript-level expression analysis of RNA- seq experiments with HISAT , StringTie and Transcript-level expression analysis of RNA-seq experiments with HISAT , StringTie and Ballgown. Nat. Protoc. *11*, 1650–1667.

Plageman, T.F., and Yutzey, K.E. (2006). Microarray analysis of Tbx5-induced genes expressed in the developing heart. Dev. Dyn. *235*, 2868–2880.

Quinlan, A.R., and Hall, I.M. (2010). BEDTools: a flexible suite of utilities for comparing genomic features. Bioinformatics *26*, 841–842.

Ramsdell, A.F. (2005). Left-right asymmetry and congenital cardiac defects: Getting to the heart of the matter in vertebrate left-right axis determination. Dev. Biol. *288*, 1–20.

Rana, M.S., Horsten, N.C.A., Tesink-Taekema, S., Lamers, W.H., Moorman, A.F.M., and Van Den Hoff, M.J.B. (2007). Trabeculated right ventricular free wall in the chicken heart forms by ventricularization of the myocardium initially forming the outflow tract. Circ. Res. *100*, 1000–1007.

Reed, B.H., Mcmillan, S.C., and Chaudhary, R. (2009). The Preparation of Drosophila Embryos for Live-Imaging Using the Hanging Drop Protocol. J Vis Exp *25*.

Restivo, A., Piacentini, G., Placidi, S., Saffirio, C., and Marino, B. (2006). Cardiac outflow tract: A review of some embryogenetic aspects of the conotruncal region of the heart. Anat. Rec. - Part A Discov. Mol. Cell. Evol. Biol. *288*, 936–943.

Riahi, R., Sun, J., Wang, S., Long, M., Zhang, D.D., and Wong, P.K. (2015). Notch1-Dll4 signalling and mechanical force regulate leader cell formation during collective cell migration. Nat. Commun. *6*, 1–11.

Ruest, L.B., and Clouthier, D.E. (2009). Elucidating timing and function of endothelin-A receptor signaling during craniofacial development using neural crest cell-specific gene deletion and receptor antagonism. Dev. Biol. *328*, 94–108.

Saxonov, S., Berg, P., and Brutlag, D.L. (2006). A genome-wide analysis of CpG dinucleotides in the human genome distinguishes two distinct classes of promoters. Proc. Natl. Acad. Sci. *103*, 1412–1417.

Schmittgen, T.D., and Livak, K.J. (2008). Analyzing real-time PCR data by the comparative CT method. Nat. Protoc. *3*, 1101–1108.

Serra-Juhé, C., Cuscó, I., Homs, A., Flores, R., Torán, N., and Pérez-Jurado, L.A. (2015). DNA methylation abnormalities in congenital heart disease. Epigenetics *10*, 167–177.

Sim, C.B., Ziemann, M., Kaspi, A., Harikrishnan, K.N., Ooi, J., Khurana, I., Chang, L., Hudson, J.E., El-Osta, A., and Porrello, E.R. (2015). Dynamic changes in the cardiac methylome during postnatal development. FASEB J. *29*, 1329–1343.

Smith, Z.D., and Meissner, A. (2013). DNA methylation: Roles in mammalian development. Nat. Rev. Genet. *14*, 204–220.

Smoak, I.W., Byrd, N.A., Abu-Issa, R., Goddeeris, M.M., Anderson, R., Morris, J., Yamamura, K., Klingensmith, J., and Meyers, E.N. (2005). Sonic hedgehog is required for cardiac outflow tract and neural crest cell development. Dev. Biol. *283*, 357–372.

Snarr, B.S., Wirrig, E.E., Phelps, A.L., Trusk, T.C., and Wessels, A. (2007). A spatiotemporal evaluation of the contribution of the dorsal mesenchymal protrusion to cardiac development. Dev. Dyn. *236*, 1287–1294.

So, P.L., and Danielian, P.S. (1999). Cloning and expression analysis of a mouse gene related to Drosophila odd-skipped. Mech. Dev. *84*, 157–160.

Song, L., and Crawford, G.E. (2010). DNase-seq: A high-resolution technique for mapping active gene regulatory elements across the genome from mammalian cells. Cold Spring Harb. Protoc. *5*, 1–12.

Soriano, P. (1999). Generalized lacZ expression with the ROSA26 Cre reporter strain. Nat. Genet. *21*, 70–71.

Swygert, S.G., and Peterson, C.L. (2014). Chromatin dynamics: Interplay between remodeling enzymes and histone modifications. Biochim. Biophys. Acta - Gene Regul.

Mech. *1839*, 728–736.

Taguchi, A., Kaku, Y., Ohmori, T., Sharmin, S., Ogawa, M., Sasaki, H., and Nishinakamura, R. (2014). Redefining the in vivo origin of metanephric nephron progenitors enables generation of complex kidney structures from pluripotent stem cells. Cell Stem Cell *14*, 53–67.

Takeuchi, J.K., and Bruneau, B.G. (2009). Directed transdifferentiation of mouse mesoderm to heart tissue by defined factors. Nature *459*, 708–711.

Tao, Y., and Schulz, R.A. (2007). Heart development in Drosophila. Semin. Cell Dev. Biol. *18*, 3–15.

Trapnell, C., Roberts, A., Goff, L., Pertea, G., Kim, D., Kelley, D.R., Pimentel, H., Salzberg, S.L., Rinn, J.L., and Pachter, L. (2012). Differential gene and transcript expression analysis of RNA-seq experiments with TopHat and Cufflinks. Nat. Protoc. *7*, 562–578.

Vallaster, M., Vallaster, C.D., and Wu, S.M. (2012). Epigenetic mechanisms in cardiac development and disease. Acta Biochim. Biophys. Sin. (Shanghai). *44*, 92–102.

Vallecillo-García, P., Orgeur, M., Vom Hofe-Schneider, S., Stumm, J., Kappert, V., Ibrahim, D.M., Börno, S.T., Hayashi, S., Relaix, F., Hildebrandt, K., et al. (2017). Odd skipped-related 1 identifies a population of embryonic fibro-adipogenic progenitors regulating myogenesis during limb development. Nat. Commun. *8*.

Veevers-Lowe, J., Ball, S.G., Shuttleworth, A., and Kielty, C.M. (2011). Mesenchymal stem cell migration is regulated by fibronectin through 5 1-integrin-mediated activation of PDGFR- and potentiation of growth factor signals. J. Cell Sci. *124*, 1288–1300.

Verzi, M.P., McCulley, D.J., De Val, S., Dodou, E., and Black, B.L. (2005). The right ventricle, outflow tract, and ventricular septum comprise a restricted expression domain within the secondary/anterior heart field. Dev. Biol. *287*, 134–145.

Vilkaitis, G., Suetake, I., Klimašauskas, S., and Tajima, S. (2005). Processive methylation of hemimethylated CpG sites by mouse Dnmt1 DNA methyltransferase. J. Biol. Chem. *280*, 64–72.

van Vliet, P.P., Lin, L., Boogerd, C.J., Martin, J.F., Andelfinger, G., Grossfeld, P.D., and Evans, S.M. (2017). Tissue specific requirements for WNT11 in developing outflow tract and dorsal mesenchymal protrusion. Dev. Biol. *429*, 249–259.

Waldo, K., Miyagawa-Tomita, S., Kumiski, D., and Kirby, M.L. (1998). Cardiac neural crest cells provide new insight into septation of the cardiac outflow tract: Aortic sac to ventricular septal closure. Dev. Biol. *196*, 129–144.

Waldo, K.L., Kumiski, D.H., Wallis, K.T., Stadt, H.A., Platt, D.H., and Kirby, M.L. (2001). Conotruncal myocardium arises from a secondary heart field. Development *128*, 3179–3188.

Waldo, K.L., Hutson, M.R., Ward, C.C., Zdanowicz, M., Stadt, H.A., Kumiski, D., Abu-Issa, R., and Kirby, M.L. (2005a). Secondary heart field contributes myocardium and smooth muscle to the arterial pole of the developing heart. Dev. Biol. *281*, 78–90.

Waldo, K.L., Hutson, M.R., Stadt, H.A., Zdanowicz, M., Zdanowicz, J., and Kirby, M.L. (2005b). Cardiac neural crest is necessary for normal addition of the myocardium to the arterial pole from the secondary heart field. Dev. Biol. *281*, 66–77.

Wamstad, J.A., Alexander, J.M., Truty, R.M., Shrikumar, A., Li, F., Eilertson, K.E., Ding, H., Wylie, J.N., Pico, A.R., Capra, J.A., et al. (2012). Dynamic and coordinated epigenetic regulation of developmental transitions in the cardiac lineage. Cell *151*, 206–220.

Wang, Q., Lan, Y., Cho, E.S., Maltby, K.M., and Jiang, R. (2005). Odd-skipped related 1 (Odd1) is an essential regulator of heart and urogenital development. Dev. Biol. *288*, 582–594.

Ward, E.J., and Skeath, J.B. (2000). Characterization of a novel subset of cardiac cells and their progenitors in the Drosophila embryo. Development *127*, 4959–4969.

Watt, F., and Molloy, P.L. (1988). Cytosine methylation prevents binding to DNA of a HeLa cell transcription factor required for optimal expression of the adenovirus major late promoter. Genes Dev. *2*, 1136–1143.

Wessels, A., Anderson, R.H., Markwald, R.R., Webb, S., Brown, N.A., Viragh, S., Moorman, A.F.M., and Lamers, W.H. (2000). Atrial development in the human heart: An immunohistochemical study with emphasis on the role of mesenchymal tissues. Anat. Rec. *259*, 288–300.

Xie, L., Hoffmann, A.D., Burnicka-Turek, O., Friedland-Little, J.M., Zhang, K., and Moskowitz, I.P. (2012). Tbx5-Hedgehog Molecular Networks Are Essential in the Second Heart Field for Atrial Septation. Dev. Cell *23*, 280–291.

Yamagishi, H., Maeda, J., Hu, T., McAnally, J., Conway, S.J., Kume, T., Meyers, E.N., Yamagishi, C., and Srivastava, D. (2003). Tbx1 is regulated by tissue-specific forkhead proteins through a common Sonic hedgehog-responsive enhancer. Genes Dev. *17*, 269–281.

Yelbuz, T.M., Waldo, K.L., Kumiski, D.H., Stadt, H.A., Wolfe, R.R., Leatherbury, L., and Kirby, M.L. (2002). Shortened outflow tract leads to altered cardiac looping after neural crest ablation. Circulation *106*, 504–510.

Yu, G., Wang, L.-G., Han, Y., and He, Q.-Y. (2012). clusterProfiler: an R Package for Comparing Biological Themes Among Gene Clusters. Omi. A J. Integr. Biol. *16*, 284–287.

Yu, G., Wang, L.G., and He, Q.Y. (2015). ChIPseeker: An R/Bioconductor package for ChIP peak annotation, comparison and visualization. Bioinformatics *31*, 2382–2383.

Yuan, Y., Gao, Y., Wang, H., Ma, X., Ma, D., and Huang, G. (2014). Promoter methylation and expression of the VANGL2 gene in the myocardium of pediatric patients with Tetralogy of Fallot. Birth Defects Res. Part A - Clin. Mol. Teratol. *100*, 973–984.

Zaret, K. (2005). Micrococcal Nuclease Analysis of Chromatin Structure. Curr. Protoc. Mol. Biol. 1–17.

Zemunik, T. (2014). The OSR1 rs12329305 Polymorphism Contributes to the Development of Congenital Malformations in Cases of Stillborn/Neonatal Death. Med. Sci. Monit. *20*, 1531–1538.

Zhang, K.K., Xiang, M., Zhou, L., Liu, J., Curry, N., Heine Suñer, D., Garcia-Pavia, P., Zhang, X., Wang, Q., and Xie, L. (2015). Gene network and familial analyses uncover a gene network involving Tbx5/Osr1/Pcsk6 interaction in the second heart field for atrial septation. Hum. Mol. Genet. *25*, 1140–1151.

Zhang, X.M., Ramalho-Santos, M., and McMahon, A.P. (2001). Smoothened mutants reveal redundant roles for Shh and Ihh signaling including regulation of L/R asymmetry by the mouse node. Cell *105*, 781–792.

Zhang, Y., Liu, T., Meyer, C.A., Eeckhoute, J., Johnson, D.S., Bernstein, B.E., Nussbaum, C., Myers, R.M., Brown, M., Li, W., et al. (2008). Model-based analysis of ChIP-Seq (MACS). Genome Biol. *9*.

Zhou, L., Liu, J., Olson, P., Zhang, K., Wynne, J., and Xie, L. (2015). Tbx5 and Osr1 interact to regulate posterior second heart field cell cycle progression for cardiac septation. J. Mol. Cell. Cardiol. *85*, 1–12.

Zhou, L., Liu, J., Xiang, M., Olson, P., Guzzetta, A., Zhang, K., Moskowitz, I.P., and Xie, L. (2017). Gata4 potentiates second heart field proliferation and Hedgehog signaling for cardiac septation. Proc. Natl. Acad. Sci. *114*, E1422–E1431.

Zhou, Y., Kim, J., Yuan, X., and Braun, T. (2011). Epigenetic modifications of stem cells: A paradigm for the control of cardiac progenitor cells. Circ. Res. *109*, 1067–1081.